Phase Behavior and Applications of Glycerol-Monooleate/Water/Polymer Ternary Systems

Thesis Submitted to AcSIR for the Award of
the Degree of
DOCTOR OF PHILOSOPHY
in Chemical Sciences

By

Manoj Kumar
Reg. No.10CC11A26037

Under the Guidance of
Dr. Guruswamy Kumaraswamy

CSIR-National Chemical Laboratory,
Pune-411008, India, 2017

सीएसआयआर–राष्ट्रीय रासायनिक प्रयोगशाला
(वैज्ञानिक तथा औद्योगिक अनुसंधान परिषद)
डॉ. होमी भाभा मार्ग, पुणे – 411 008. भारत
CSIR-NATIONAL CHEMICAL LABORATORY
(Council of Scientific & Industrial Research)
Dr. Homi Bhabha Road, Pune - 411008. India

CERTIFICATE

This is to certify that the work incorporated in this Ph.D. thesis entitled **"Phase Behavior and Applications of Glycerol Monooleate/Water/Polymer Ternary Systems"** submitted by **Mr. Manoj Kumar** to Academy of Scientific and Innovative Research (AcSIR) in fulfilment of the requirement for the award of the Degree of **Doctor of Philosophy**, embodies original research work under my guidance. We further certify that this work has not been submitted to any other University or Institution in part or full for the award of any degree of diploma. Research material obtained from other sources has been duly acknowledged in the thesis. Any text, illustration, table etc., used in the thesis from other sources have been duly cited and acknowledged.

Manoj Kumar

Reg. No. **10CC11A26037**

Dr. Guruswamy Kumaraswamy

(Research Supervisor)

Date: 18 May 2017
Place: Pune

Communications Channels
NCL Level DID : 2590
NCL Board No. : +91-20-25902000
Four PRI Lines : +91-20-25902000
FAX
Director's Office : +91-20-25902601
COA's Office : +91-20-25902660
SPO's Office : +91 20 25902664
WEBSITE
www.ncl-india.org

DECLARATION BY RESEARCH SCHOLAR

I hereby declare that the thesis entitled **"Phase Behavior and Applications of Glycerol Monooleate/Water/Polymer Ternary Systems"** submitted by me for the Degree of Doctor of Philosophy to Academy of Scientific & Innovative Research (AcSIR) is the record of work carried out by me at Polymer Sciences & Engineering Division (PSE), CSIR-National Chemical Laboratory, Pune - 411008, India, under the supervision of Dr. Guruswamy Kumaraswamy (research supervisor). The work is original and has not formed the basis for the award of any degree, diploma, associateship, and fellowship titles in this or any other university or other institute of higher learning. I further declare that the material obtained from other resources has been duly acknowledged in the thesis.

Manoj Kumar

Polymer Science & Engineering
CSIR-National Chemical Laboratory
Dr. Homi Bhabha Road, Pashan
Pune – 411008
Maharashtra, India

Dedicated to.....

Maa, Papa

Acknowledgement

This thesis is the outcome of several people's contribution by encouraging, helping, supporting, criticising and finally believing in me. The thesis is incomplete without acknowledging their efforts. First and foremost, I thank to my parents who always stood and supported me to pursue my ambitions and gave me a freedom to choose my career. I express my deepest appreciation to my research guide and mentor ***Dr. Guruswamy Kumaraswamy (CSIR-NCL****). I am greatly inspired by his principles, ethics, scientific temperament, and discipline to perform high value science. I enjoyed discussions (both scientific and general) with him, and his teaching during the course-work. He helped me to improve my skills of presentations, in choosing scientific problem, data analysis, and to think out of the box. He provided me all possible platforms to flourish scientifically and non-scientifically. Overall, I really enjoyed this journey with him and became more passionate towards research.*

I would like to thank my Doctoral Advisory Committee members ***Dr. Ashish K. Lele (CSIR-NCL), Dr. Suresh K. Bhat (CSIR-NCL),*** *and* ***Dr. Pankaj Poddar (CSIR-NCL)*** *for their critical comments and suggestions. I am also grateful to* ***Dr. Amy S. Blum (McGill University, Montreal)*** *and her group for helping me to learn protein purification. I am also thankful to* ***Dr. Sudip Roy, Dr. Ashootosh V. Ambade (CSIR-NCL), Dr. Arun Banpurkar (Pune University)*** *whom I have collaborated for carrying out my thesis work. I also thank* ***Dr. Raghunathan (RRI-Bangalore)*** *for helping me to learn electron density analysis for scattering. I would also like to thank* ***Dr. V. Premnath and Dr. Anuya Nisal*** *who have been there when I needed their help. I appreciate Gaurav Chaudhary's effort for providing GMO (glycerol-monooleate) a key material in my research.*

Now, I also take an opportunity to thank ***Dr. Venugopal Edakkal*** *for teaching me experimental techniques (X-ray scattering, optical microscopy, light scattering) and helping me to study phase diagram. I would like to thank* ***Dr. Chandan Chaudhary, Nagnath, Puneet, Mayuresh Kulkarni, Fayis, Aakash Sharma*** *for helping me to carry out my thesis work. I thank to* ***Dr. Sreenivas, Dr. Jijjo, Dr. Deepak Chand, Anil Nagraj, Anand, Sameer Huprikar, Yashpal Yadav, Arun Dadwal, Arun Torris and Manu*** *for scientific discussions. I would like to thank summer interns* ***Shashank,***

Parul Makaar, Prannay Sastry, CG Narendiran *for their help in my research work and to spend good time with me.*

My special thanks to friends, Deepak Kumar, Ravi Jhangir, Arun Dadwal, Deepak Chand, Yashpal, Shakuntala, Anil, Khiru who were always there to help me in all difficult and distressed situations to bring a smile on my face. I enjoyed with them especially, Sunday dinner/movies/cricket. I greatly enjoyed time with my table tennis and cricket friends Gunwant, Anup, Arun, Monika, Deepak, Yashpal, Debu, Deva (hilarious player), Yuvraj, Pinka, Deepak, Shahebaaz, Pinka, and Rajan.

I would also like to thank my seniors and friends Dr. Samruddhi Kamble, Parshant, Dhana, Aniket, Amruta Kulkarni, Dr. Mohan, Kundan, Anju, Kiran MK Tiwari, Yogesh, Ashwini, Sujeet, Shiva, Saibal, Prajitha, Parvin Devadi, Santosh, Amit, Manzoor, Wahid, Saleem, Roby, Inderapal, Subhadarshinee, Dr. Atul Thakur, Dr. Rami, Chetannya, Deepanjan, Trinadh, Brijesh, Dr. Anup for their help.

I am indebted to many of friends and teachers for their motivation and constant support especially, Dr. Sharadwatapan, Dr. Samjeet Thakur, Yashwant, Dr. Arijit Malik, Milap Attri, Prof. M. S. Chauhan, Prof. S. Chauhan, Prof. G. S. Chauhan, Dr. Chirag. Finally, I am also grateful to my labmates Soumyajyoti Chatterjee (for being my best critics), Dr. Anees khan, Karthika, Bipul, Aakash, Saurabh, Professor, Sudhakar. I sincerely acknowledge the financial support from UGC (New Delhi), and CSIR-NCL (Pune).

Manoj Kumar

Abstract

Organized lipid/water assemblies are encountered in Nature, and find applications as delivery agents in pharmaceutics, as templates for materials synthesis, as matrices for membrane protein crystallisation, etc. Here, we focus on a bio-derived, food-grade lipid, glycerol monooleate (GMO). GMO self-assembles with water to form several well-defined ordered mesophases at room temperature, including lamellar and cubic (Ia3d, Pn3m & Im3m) phases. Cubic phases are especially interesting due to their bicontinuous architecture, with non-intersecting oil and water channels. The bicontinuous nature of the cubic phases allows them to solubilize either hydrophobic or hydrophilic molecules or a combination of the two. The solubilized molecules are, thus, encapsulated and stabilized against enzymatic degradation. The cubic Pn3m mesophase coexists with excess water, affording the possibility of preparing low viscosity water based lipid nanoparticle dispersions. The GMO-water binary system does not readily form high curvature structures, like the reverse hexagonal (H_{II}) and reverse micellar cubic Fd3m mesophases. This has been attributed to the severe packing frustration imposed on the lipid tails in these high curvature phases. High curvature inverse phases are of significant interest since they are relevant to many biophysical processes, including enzymatic catalysis. In material science, high curvature mesophases can be used as sustained delivery vehicles for hydrophilic drugs.

In the first part of this thesis, we show an unusual pathway for GMO/water reorganization from a bicontinuous mesophase to a discontinuous reverse micellar assembly, directed by the inclusion of polar macromolecules as a ternary component in the system. This pathway is very different from those reported earlier, where the Fd3m phase formed only upon addition of apolar oils. Experiments and molecular dynamics simulations indicate that hydrophilic ternary additives capable of inducing discontinuous phase formation must (i) interact strongly with the monoolein head group and, (ii) have a compact molecular architecture. We present a detailed investigation that contrasts a GMO/water system containing polyamidoamine (PAMAM) dendrons with one containing their linear analogs. The Fd3m phase forms only on addition of PAMAM dendrons but not their linear analogs. Thus, the dendritic architecture of PAMAM plays an important role in determining lipid mesophase behavior. Both dendrons and their linear analogs interact strongly with GMO, through their amine groups. However, while linear polymers adsorb and spread on GMO,

dendrons form aggregates that interact with the lipid. Dendrons induce formation of an intermediate reverse hexagonal phase, which subsequently restructures into the Fd3m phase. Finally, we demonstrate that other additives that have compact structures and that are known to interact with monoolein, such as branched polyethylenimine and polyhedral silsesquioxane cages, also induce formation of the Fd3m phase.

Next, we investigate the effect of molecular size of PAMAM dendrons on the phase behaiour of GMO/water. We prepare ternary GMO/water/PAMAM systems containing a fifth generation dendron (G5) and investigate the phase behaviour as a function of G5 concentration and temperature. Addition of 1% G5 in a 85/15 GMO/water system induces a transition from the L_α to Ia3d phase. Further increase in G5 concentration to above 2% induces the formation of a very unusual mesophase with $P4_332$ symmetry. This is completely different from the effect of incorporation of lower generation PAMAM dendrons (G2 – G4) in GMO/water, where the formation of the reverse micellar Fd3m phase was observed. The $P4_332$ mesophase can be considered an intermediate phase between the bicontinuous Ia3d and discontinuous micellar mesophases. In this unusual phase, every third rod junction of the Ia3d mesophase is replaced with a spherical micelle. PAMAM dendrons of all generations, G2 – G5, bear terminal amine groups that interact with the GMO head group. The compact molecular architecture of the dendrons and these attractive interactions induce bending of the GMO bilayer structure. For smaller dendrons, G2 – G4, this results in the formation of the Fd3m phase. However, the large size of the G5 dendron precludes this and a rare intermediate phase between the Ia3d and discontinuous micellar phase, the $P4_332$ mesophase forms instead.

In Chapter 4, we show that addition of a branched polymer, polyethyleneimine, as a ternary component, significantly alters the organization of a glycerol monooleate (GMO) lipid–water system. We present detailed data over a wide range of compositions (water content from 10 to 40%, relative to GMO and, PEI fractions from 0 to 4%) and temperatures (25–80 °C). The effect of PEI molecular weight is examined using polymers over a range from 0.8 to 25 kDa. Addition of PEI induces the formation of high curvature reverse phases. In particular, PEI induces the formation of the Fd3m phase: a discontinuous phase comprising reverse micelles of two different sizes stacked in a cubic AB_2 crystal. The formation of the Fd3m phase at room temperature, upon addition of polar, water soluble PEI is unusual, since such phases typically are formed only upon addition of apolar oils. The largest stability window for the Fd3m phase is

observed for PEI with a molecular weight = 2 kDa. We discuss the influence of PEI on the formation and stability of high curvature phases.

In Chapter 5, we compare the release of the small hydrophilic drug molecules from bicontinuous (Pn3m) and discontinuous (Fd3m) mesophases of glycerol-monooleate (GMO). Bicontinuous Pn3m mesophases are formed in the binary GMO/water system while the discontinuous Fd3m mesophase is formed when PEI to the GMO-water system at a concentration of 2%. We model the diffusion of a model hydrophilic drug that is encapsulated in the mesophases using the 1-D Higuchi model. We demonstrate that the apparent diffusion rate obtained from the Higuchi model is not a characteristic of the mesophase symmetry. When the cooling rate for sample preparation is altered, the same mesophase forms – however, the release rate (and consequently, the apparent diffusion rate from the Higuchi model) vary. Therefore, we present an alternate model that incorporates the effect of mesophase domain size. We obtain estimates for the domain size distribution in the Fd3m phase from polarized optical microscopy and show that our model provides a good fit to the release data. The diffusion rates obtained from our model for samples cooled at different rates are the same, suggesting that these values might be representative of the mesophase structure.

Finally, we study the wetting of hydrophobic and superhydrophobic surfaces using aqueous dispersions of GMO nanoparticles, with bicontinuous Pn3m symmetry. Efficient delivery of aqueous sprays to hydrophobic surfaces is the key technological challenge in a wide variety of applications, including pesticide delivery to plants. To account for losses due to bouncing of pesticide sprays off hydrophobic leaf surfaces, large excess of pesticide is typically employed, resulting in environmentally hazardous run-offs that contaminate soil and ground water. We demonstrate that aqueous dispersions of GMO nanoparticles, called cubosomes, wet hydrophobic and superhydrophobic surfaces and adhere to them. Cubosomes comprise GMO lipid molecules self-assembled into a double diamond cubic phase and sterically stabilized using amphiphilic Pluronic block copolymer. We use high speed imaging to monitor the spreading and retraction of aqueous drops impinged on model hydrophobic substrates and on superhydrophobic lotus leaves. We show that cubosomes diffuse to hydrophobic substrates and reorganize to form a thin, ≈ 2 nm adsorbed lipid layer during the millisecond time scales that characterize drop impact. This adsorbed film drastically reduces the water contact angle, transforming the hydrophobic surface to hydrophilic, thus facilitating retention of the aqueous drop on the surface. Aqueous drops of cubosomes impinged at low

velocities on inclined natural superhydrophobic lotus leaf surfaces do not roll off, unlike drops of water or surfactant solutions. When sprayed on inclined lotus leaves, corresponding to the case of high velocity drop impingement, cubosome dispersions form a continuous wetting film. Our results have important implications for efficient, environment friendly delivery of pesticide sprays.

CONTENTS

List of Figures

fit passes through the origin indicating that the system forms a structure with the Fd3m space group symmetry with lattice parameter (a) 162±1 Å for G2 (b) 166±2 Å for G3 and, (c) 173±1 Å for G4.

Figure 2.7: Equilibrium phase behavior of GMO/water system at room temperature with variation of G2, G3 and G4 content, Φ and for the variation of water fraction (f_w).

Figure 2.8: In a system containing GMO/water/G4 in the ratio 50/50/4, by weight, we observe a reverse hexagonal phase (peak ratio: 1:√3) at 5-10 days, that subsequently reorganizes to form an Fd3m phase that is observed after about 20 days of equilibration. Note that a cubic phase with Pn3m symmetry coexists with excess water for a binary 50:50 GMO/water system.

Figure 2.9: Lattice parameter for Fd3m phase in GMO/water/G4 PAMAM (Φ = 4%) system, as a function of water content.

Figure 2.10: Kinetics of phase transformation: we observe structural changes for the 80:20:4 GMO/water/G4 systems as a function of equilibration time. This system forms the H_{II} phase in 4 days. We observe a coexistence of the H_{II} and Fd3m phases after about 4.5 days and finally, the Fd3m phase is observed after 15 days of equilibration.

Figure 2.11: Snapshots from MD simulations of G4 dendron-GMO/water systems (top) and linear analog-GMO/water systems (bottom). Snapshots on the left represent starting configurations, while right represents structure after 100 ns (G4) and 200 ns (linear analogs).

Figure 2.12: GMO/Water/G4-PEG-PAMAM system formed coexisting-Pn3m phase in 80:20:6 compositions (preferably Pn3m). Here, we modify the 1^o ammine at the surface of G4 dendron with 5-mer PEG-chains, and it transforms the Ia3d phase in GMO/water (80/20) system into Pn3m phase.

Figure 2.13: SAXS data for the (a) 80/20 GMO/water containing bPEI ternary additive. Φ represents the amount of bPEI in GMO/water. (b) GMO/water (80/20) containing POSS. Φ represents the amount of POSS in GMO/water system.

$P4_332/Ia3d \rightarrow P4332/H_{II} \rightarrow H_{II} \rightarrow L_2$. (B) POM image shows cone type textures at T = 50 °C characteristic of the H_{II} mesophase.

Figure 3.8: (A) SAXS data for ternary GMO/water/PAMAM-G5 (85/15/2) at Φ = 2% & f_w = 15% on heating from 25 °C to 65 °C. (B) SAXS data for ternary GMO/water/PAMAM-G5 (85/15/4) at Φ = 4% & f_w = 15% on heating from 25 °C to 45 °C.

Figure 3.9: (A) SAXS data for ternary GMO/water/PAMAM-G5 (80/20/0.5) at Φ = 0.5% & f_w = 20% on heating from 25 °C to 95 °C. At low q, some peaks corresponding to unknown structures are observed and are marked with (*). (B) SAXS data for ternary GMO/water/PAMAM-G5 (80/20/1) at Φ = 1% & f_w = 20% on heating from 25 °C to 90 °C.

Figure 3.10: (A) SAXS data for ternary GMO/water/PAMAM-G5 (80/20/2) at Φ = 2% & f_w = 20% on heating from 25 °C to 95 °C. (B) SAXS data for ternary GMO/water/PAMAM-G5 (80/20/4) at Φ = 4% & f_w = 20% on heating from 25 °C to 80 °C.

Figure 4.1: (1a) Structure of GMO; (1b) 3D structure of GMO; (2) A schematic representation of branched PEI containing primary, secondary and tertiary amines.

Figure 4.2: (a) SAXS for GMO/water/2 kDa PEI systems (f_w = 15%) as a function of PEI fraction (Φ). Data for ternary systems containing HP-GMO is also shown. Optical micrograph between crossed polarizers for the ternary system at (b) Φ = 0% (L_α phase) and (c) Φ = 1% (H_{II} phase).

Figure 4.3: A plot of the peak reciprocal spacing, q ($Å^{-1}$) as a function of $P= (h^2+k^2+l^2)^{1/2}$ is a straight line through the origin.

Figure 4.4: (a) Ternary GMO/H_2O/2 kDa PEI phase diagram as a function of f_w, Φ and temperature. Slices of the phase diagram showing the phase behaviour at (b) T = 25 ^oC; (c) Φ= 1, 2 and 4%.

Figure 4.5: Phase behaviour of the ternary system GMO/water/0.8 kDa PEI at T = 25 °C

Figure 4.6: Phase behaviour of the ternary system GMO/water/25 kDa PEI at T = 25 °C

Figure 6.7: (a) Ellipsometry was performed at angles ranging from 60 to 80^o and using light of wavelength ranging from 200 to 1000 nm. The substrate was a hydrophobic silicon wafer on which a drop of aqueous 1% dispersion of lipid nanoparticle was impinged, as described in the manuscript. The data was fitted using a Cauchy model to estimate a thickness of about 2 nm for the adsorbed film (details in Supporting Information: Ellipsometry). Contact angle (AOC) of a water drop (5 μl) on a hydrophobized silicon surface (b) as prepared and (c) after formation of the adsorbed lipid film during the drop impact experiment.

Figure 6.8: The plot shows the retraction of lipid nanoparticle drop impinged on a hydrophobic surface. The point where retraction stops is termed as stagnation point, D_s, whereas the time corresponds to D_s, known as stagnation time, τ_s.

Figure 6.9: (a) Drop area at the stagnation varies linearly with the cubosomes concentration (b) Comparision between reciprocal of adsorption rate $(r_{BD})^{-1}$ and the experimental stagnation time.

Figure 6.10: The cumulative adsorbed volume of cubosomes obtained from multiple simulation runs for cubosome concentration, Φ=0.9%. The adsorbed volume of cubosomes varies linearly with time. The adsorption rate, r_{BD}, is obtained as the slope of this data. Similar data was obtained for simulations at different cubosome concentrations.

Figure 6.11: (a) The rate of nanoparticle diffusion across the bottom face, r_{BD} is plotted for different nanoparticle concentration, Φ. We observe that r_{BD} is linear in Φ. (b) We obtain the rate for nanoparticle adsorption to form a film, as described in the Simulation Methods, r'_{BD}. We adjust the fitting parameter, k, so that the Φ –dependence of r'^{-1}_{BD} matches that of τ_s, obtained from experiments.

Figure 6.12: Shape adopted on a horizontal lotus leaf of a 5μl drop of (a) water (b) 1% Tween 20 and (c) 1% aqueous cubosome dispersion. Images are taken 5 minutes after drop deposition on the leaf surface. (d) The contact angle for the water drop remains constant at ≈155^o over 10 minutes, while that for cubosomes decreases continuously with time until the drop flattens on the lotus leaf surface.

Figure 6.13: Motion along an inclined lotus leaf (as described in the main text) of a drop of (a) water; (b) 1% aqueous Tween 20 and (c) 1% aqueous cubosomes. We show the position of the drop as soon as it is placed on the leaf surface (t = 0 ms), and after approximately 30

and 60 ms. (d) The displacement of the center of the drop along the inclined leaf surface is plotted for water, 1% Tween 20 and 1% cubosome drops.

Figure 6.14: Sequence of images shows the spreading of a drop of water (top layer), 1% Tween 20 (middle layer), and 1% cubosomes (lipid nanoparticle dispersion) when impinged on a lotus leaf. The images show the behaviour of the drop before impact (first panel, t = 0; $D_o = 2.20 \pm 0.02$ mm) and at t= 1.9, 8.9 and 23 ms (after impact). The arrow in the middle panel indicates a pinned droplet.

Figure 6.15: Photographs showing the surface of an inclined lotus leaf that is sprayed with water (left panel); 1% aqueous Tween 20 (middle panel) and 1% cubosome dispersion (right panel). Data is presented as a function of time after spraying.

Figure 6.16: Photographs showing the lotus leaf that is sprayed with APSA-80 commercial surfactant (left panel); 1% aqueous Tween 20 (middle panel) and 1% cubosome dispersion (right panel). We observed the effect of spray before and after the spray.

List of Tables

Chapter 1

Introduction

1.1 Introduction

The study of thermodynamics of lipid self-assembly is of great technical and fundamental importance. Consider, for example, the structural transformations which occur during cell membrane-protein interactions. These structural transformations hold the key to several biologically important processes ranging from digestion[1] to disease.[2] This provides strong motivation to address a fundamental question, viz. what structural changes occur when a lipid membrane interacts with proteins? Specifically, how does curvature develop in lipid membranes as a consequence of such interactions and what are the transient structures that form during such structural transitions? Self-assembled lipid structures are also ubiquitous in the fields of materials,[3-5] foods,[6-8] pharmaceutics,[9] cosmetics etc. The functionality of lipid assemblies in these applications is governed by their structure. Therefore, understanding structure formation in lipid assemblies and understanding structural transitions is also of significant technological importance.

In this thesis, we explore the thermodynamics of self-assembly of a commercially important lipid, glycerol monooleate (GMO) in the presence of polymers as a ternary component in a lipid-water system. Specifically, our work highlights the role of polymer architecture in accessing different structures in self-assembled lipids. We show that highly curved organised lipid structures can form, mediated by polymer-lipid interactions. The formation of such high curvature structures determines material properties, such as diffusion of hydrophilic molecules through the lipid assemblies. Finally, we study how self-assembled lipid nanoparticles can dramatically transform the wetting of hydrophobic and superhydrophobic surfaces, with implications for agrochemical delivery.

1.2 Curvature in Biology

Membrane curvature is a physical bending of the lipid bilayer to generate sub-cellular compartments which provide a complex architecture to the cell (Figure 1.1). Lipid membranes are characterized by a spontaneous curvature, and their fluctuations are determined by elastic moduli that resist membrane deformation. Interactions of proteins with lipid membranes can influence the spontaneous curvature, and can induce local or global changes in membrane shape. Membranes can have either positive or negative curvature with respect to the cytoplasm.[10] During membrane fusion, lipid bilayer membranes can undergo a temporary local structural destabilisation and show high curvature in some regions.[10]

Recently, in membrane biology, the influence of membrane curvature on many dynamic and static processes has become a hot topic of research. A cell is the fundamental unit of life. This is bounded by a cell membrane that encloses a complex structure (Figure1.1). The cell has organelles which are bound by membranes to create an isolated environment to carry out organelle-specific reactions and metabolic activities and also to store genetic material.[11]

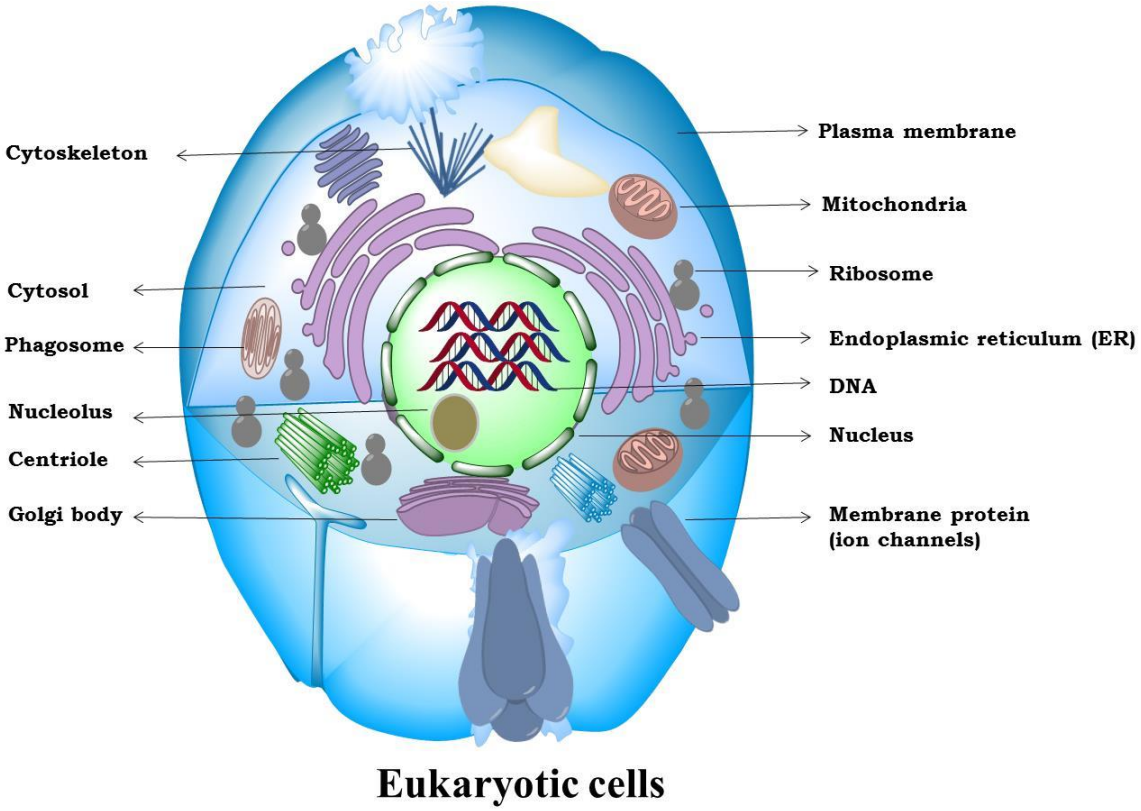

Figure 1.1: The Eukaryotic cell with curvature in its various compartments.

The biological membrane that forms the cell surface is one of the important determinants of the shape of the cell.[12] The dynamic shapes adopted by organelles in eukaryotic cells influences the cell physiology.[10] Intracellular organelles such as Golgi, endosomes, vesicles and endoplasmic reticulum (ER) also have dynamic curved membrane structures that facilitate vesicle trafficking. Membrane shapes produced by the dynamic assemblies of lipid and proteins have a significant role in physiological processes.

1.3 Why is it important to study lipid curvature?

Many biological functions such as cell signalling and trafficking are facilitated by bilayer membranes and are controlled by membrane curvature.[12] Here, we discuss various biophysical processes that are significantly influenced by membrane curvature. Curvature in membranes acts as a "sensor" for drugs, enzymes, proteins, helping them bind to the membrane surface and/or enhancing their activity. For example, protein kinase has higher activity at a curved membrane surface compared with at a flat membrane.[13] High membrane curvature enhances binding of amyloid-β protein and can promote aggregation and fibril formation.[14] Negative curvature accelerates the nucleation of endosomal sorting complex which plays a role in signalling transport (ESCST).[15] Membrane curvature also helps to sense the amphipathic helix (AH) such as the ALPSA motif; AH are present in helical conformation only on curved membrane surfaces whereas it remains in unfolded form in solution.[16] Recently, it has been observed that Sar1 GTPase binds strongly at the curved membranes and this regulates its activity.[17] Therefore, clearly, membrane curvature plays an important role in controlling a wide variety of physiologically important cellular processes.

Further, curved transient double-membrane organelles are formed by bending of membranes and play an important role in processes such as reproduction, autophagy, and viral infection. Proteins induce morphological transition to generate organelle curvature. However, the mechanisms by which protein-membrane interactions generate curvature are not well understood.[18] It is worth mentioning that the compartmentalisation observed in biological cells[19,20] has also inspired bio-mimetic design of complex mesoporous shapes in materials science.[21]

1.4 Factors controlling curvature in biological membranes

In cell biology, investigations show that curvature results due to physical forces that arise from a complex interplay between lipids and membrane proteins.[12]Membranes are primarily comprised of lipids and therefore change in lipid composition and chemical structure can alter membrane curvature. The chemistry of lipids, such as the size of their head group relative to the acyl chain tail determines the packing and the shape of the lipid assemblies. For examples, lipids whose head groups effectively occupy similar volume as their acyl chain tails form flat assemblies. Decreasing the size of the polar head group induces negative curvature by bending the lipid monolayer towards the head groups. Conversely,

lipids with larger head groups exhibit positive curvature by bending away from the head group in a monolayer.[12,22] Additionally, the packing of the lipids is also influenced by the nature of acyl chain. For example, the presence of a double bond induces a kink along the chain, changing the volume ratio of the head group and acyl chain.[23,24]

Many membrane proteins have a tendency to oligomerise, resulting in local scaffolding of the membrane.[25] Clustering of transmembrane proteins results in protein crowding that affects the local rigidity of the membrane and can influence membrane curvature.[26] Another route to influencing membrane curvature is by generation of cytoskeleton scaffolding. The cell membrane curvature is supported through scaffolding by a cytoskeleton comprising networks of microtubules, actin and intermediate filaments. These are present in intracellular organelles such as ER or Golgi.[27]

1.5 Structures of self-assembled lipid systems: Packing parameter

In general, amphiphilic molecules such as surfactants self-assemble into various micellar structures in solvents. The type of assembly (type 1: oil in water or type 2: water in oil depends on the relative volume of hydrophilic and hydrophobic parts of the amphiphilic molecule (and is parameterized by the hydrophilic-lipophilic balance or the HLB value) (Figure 1.2). Lipids have an amphiphilic nature like surfactants. Typically, lipids have smaller head groups relative to their tails and therefore, organise into type 2 (inverse, w/o) micellar structures (Figure 1.2). The packing parameter, γ, is a dimensionless geometrical parameter, also known as the critical packing parameter or ratio and is a simple measure that indicates the structures and shape formed by lipid assemblies.[28]

$$\gamma = V/a_g l_c$$

where l_c represents the length of the hydrocarbon tail, a_g is the effective surface area of the head group and V is the volume of the molecule. The shape of the self-assembled structure depends upon the packing parameter which, in turn, is influenced by the interactions between the tail regions and head group in the aggregate. Preferred structures at different values of packing parameters, classified into type 1 (positive curvature, normal) and type 2 (negative curvature, inverse) are summarised below (Figure 1.2):

Type 1:

If $\gamma \leq 1/3$: spherical micelles;

$1/3 < \gamma < 1/2$: non-spherical ellipsoidal; $\gamma \approx 1/2$: cylindrical/rod-like micelles

$1/2 < \gamma < 1$: interconnected structures

$\gamma = 1$: flat bilayer (lamellar)

Type 2:

$\gamma > 1$: inverse micelles

Lipids self-assemble in the presence of water to form 1D, 2D and 3D structures that correspond to lamellar (L_α), reverse hexagonal (H_{II}) and reverse cubic mesophases (Q_{II}).[29] Ordered surfactant and lipid assemblies are termed mesophases. The reverse hexagonal mesophase (H_{II}) is formed by reverse cylindrical micelles packed in a hexagonal lattice. Bicontinuous reverse cubic mesophases can also form in gyroid (Ia3d), double diamond (Pn3m), and primitive (Im3m) symmetries.[30,31] These mesophases are characterised by the space group symmetry, as indicated. These cubic mesophases are bicontinuous with continuous non-intersecting oil and water channels. The junction of continuous channels is different for the various mesophases. The Ia3d mesophase has a junction of three connected channels at 120°, Pn3m has a junction of four connected channels at 109.5°, and Im3m forms a junction of six connected channels at 90° (shown in figure 1.3). Lipids also form cubic discontinuous structures, such as, for example the cubic reverse micellar Fd3m mesophase. The Fd3m mesophase contains two different size inverse micelles packed in an FCC lattice.[32-34] Lipids like glycerol monooleate readily form lamellar, Ia3d, Pn3m mesophases. The H_{II} and Fd3m mesophases have also been reported to form under specific conditions (temperature, pressure or addition of ternary component).[35-37]

There are several inverted structures that have been observed in lipid assemblies including, inverted bicontinuous structures (Q_{II}), reverse hexagonal (H_{II}), reverse micellar cubic (I_2), reverse micellar (L_2), etc. The curvature modulus associated with inverted mesophases is higher and the negative mean curvature increases from $Q_{II} \rightarrow H_{II} \rightarrow I_2 \rightarrow L_2$ (Figure 1.4). In an inverted mesophase, amphiphilic molecules are organized to form cylindrical or spherical micelles that are packed in a hexagonal or cubic lattice.[38]

Mesophases can be identified using small angle X-ray scattering (SAXS). Anisotropic mesophases also exhibit distinct textures in polarised optical microscopy (POM). The SAXS patterns of the mesophases can be used to identify their structure based on characteristic Bragg peak positions, as summarised in Table 1.1. Polarised microscopy is an alternative technique where mesophases can be identified through their texture under cross-polarisation. All cubic mesophases are isotropic – therefore, no texture can be observed between crossed-polarizers whereas the reverse hexagonal and lamellar mesophase form fan and cone type textures, respectively.

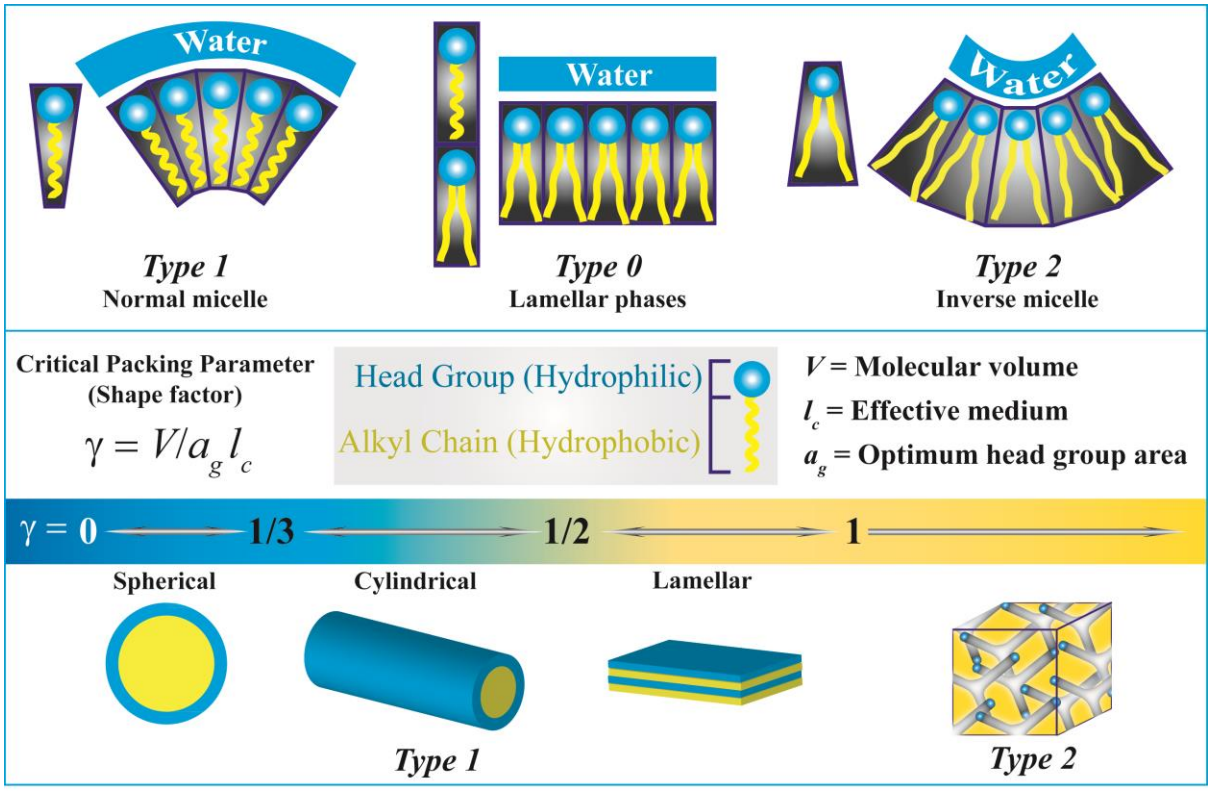

Figure 1.2: Different self-assembled mesophase structures in surfactants or lipids.

Mesophase	Reciprocal peak Spacing, S_{hkl}	Peak ratios
Lamellar (1D), L_α	$S_l = l/d$	1: 2 : 3: 4…..
Hexagonal (2D), H_{II}	$S_{hk} = \frac{2\sqrt{(h^2+k^2-hk)}}{\sqrt{3}a}$	$\sqrt{1} : \sqrt{3} : \sqrt{4} : \sqrt{7} : \sqrt{9} : \sqrt{12} : \sqrt{13}$ …..
Cubic (3D), Q_{II}		
Ia3d		$\sqrt{6} : \sqrt{8} : \sqrt{14} : \sqrt{16} : \sqrt{20} : \sqrt{22} : \sqrt{24}$ …..
Pn3m	$S_{hkl} = \frac{\sqrt{(h^2+k^2+l^2)}}{a}$	$\sqrt{2} : \sqrt{3} : \sqrt{4} : \sqrt{6} : \sqrt{8} : \sqrt{9} : \sqrt{10}$ …..
Im3m		$\sqrt{2} : \sqrt{4} : \sqrt{6} : \sqrt{8} : \sqrt{10} : \sqrt{12} : \sqrt{14}$ …..
Fd3m		$\sqrt{3} : \sqrt{8} : \sqrt{11} : \sqrt{12} : \sqrt{16} : \sqrt{19} : \sqrt{24}$ …..

Table 1.1: Characteristic peak ratios for different mesophases. h, k, l represent the Miller indices of X-rays peaks; 'a' represents the lattice parameter and d is the interplanar spacing.

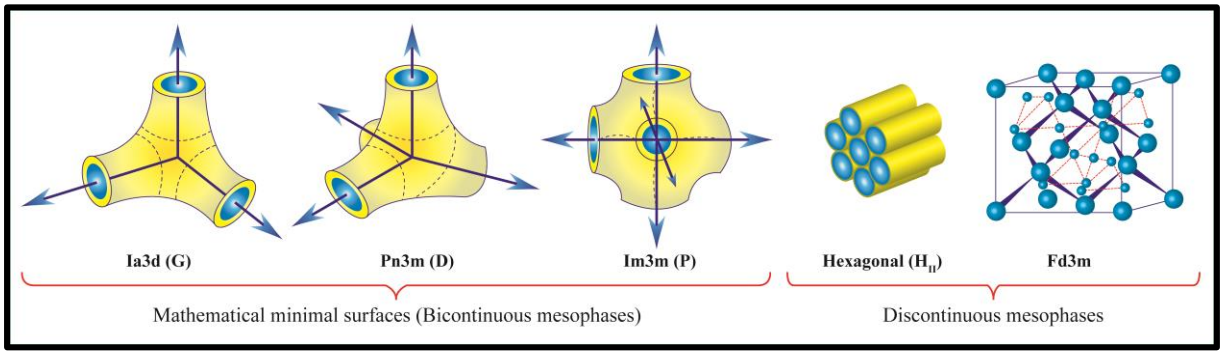

Figure 1.3: Bicontinuous inverse cubic mesophases (Ia3d, Pn3m & Im3m) and discontinuous reverse (H_{II}) hexagonal and reverse micellar cubic (Fd3m) mesophases.

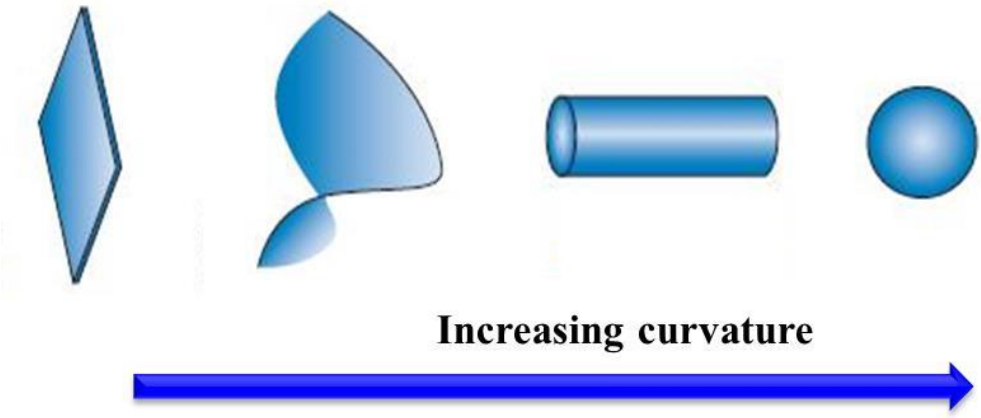

Figure 1.4: The interfacial mean curvature increases from right to left when the lipid bilayer undergoes a transition from lamellar to reverse micellar mesophase (adapted from Kozlov, 2006). [12]

1.6 Physical Parameters that influence Curvature

The total free energy associated with the formation of lipid mesophases with different geometries is related to membrane elasticity and packing frustration. The packing of lipids in a flat bilayer takes place under various interactions that are acting on the different part of the molecule e.g repusive interactions between the head group (hydration/electrostatic/steric), attractive interactions at the oil-water interface (interfacial interactions), and the repulsive interactions between the hydrocarbon chanis. The increase of conformational disorder between the hydrocarbon tails induces curvature that drives phase transitions. To form an inverse non-lamellar mesophases with high curvature, membrane elasticity and packing frustration are two important factors that play a significant role.[38,39]

1.6.1 Curvature associated with different structures

Self-assembled lipid bilayers are models for biological membranes. The sheet-like morphology of membranes can undergo shape changes due to physical and chemical changes in the membrane. Commonly encountered membrane shapes include flat sheets, spherical shapes, cylindrical, and saddle-like shapes which differ in their curvature. The membrane elastic moduli, including bilayer bending modulus, k and Gaussian curvature modulus, $\bar{k}$

determine the energy required to bend the membrane away from its spontaneous shape. [41, 42]Thus, the curvature elastic energy of a membrane is given by combining both bending and Gaussian moduli in the Helfrich expresion:[41]

$$E_{bend,Helfrich} = \frac{1}{2}k(c_1 + c_2 - c_o)^2 + \bar{k}c_1c_2$$

$$= \frac{1}{2}k(K - c_o)^2 + \bar{k}K_G$$

where c_o is the spontaneous curvature, c_1 and c_2 are the principal curvatures, k is the bending modulus, $\bar{k}$ is the elastic modulus, $K_G = c_1c_2$ is the Gaussian curvature and, $K = c_1 + c_2$ is the spontaneous curvature.

The spontaneous curvature (mean curvature) K, changes when the bilayer bends whereas the Gaussian curvature K_G does not change unless the bilayer is stretched. The formation of different structures is occasioned by change in membrane curvature.[30, 43] For a flat bilayer (lamellar structure) there is no curvature: both mean and Gaussian (K & K_G) curvatures are zero since principal curvatures, c_1 and c_2 are zero. For spherical micelles the Gaussian curvature is positive. In the case of cylindrical lipid assemblies (hexagonal phase), one of the principal curvatures is zero. Thus, the Gaussian curvature is also zero and the surface has a parabolic point. For saddle shaped bilayer surface, the principal curvatures have opposite sign, resulting in zero mean curvature and negative Gaussian curvature to give a surface with hyperbolic geometry. Such a surface is called a minimal surface, since it locally minimizes its surface area. Infinite periodic minimal surfaces include the Gyroid surface, the Schwarz P-surface and the Schwarz D-surface.[44,45]

1.6.2 Energetics of Spontaneous curvature formation:

The energy associated with the cylindrical shape of the membrane is given by:

$$E_{cyl} = \pi \cdot L \cdot k \left(\frac{1}{R} - 2K\right)$$

where R and L represent the radius and length of the cylinder, k is the bending modulus of the bilayer, K represents the spontaneous curvature of the bilayer. If $E_{cyl} = 0$, the spontaneous

curvature of the bilayer will be, $K = 1/(2R)$ and the lipids naturally organize into a cylindrical shape. The lipid bilayer can be induced to form a cylindrical assembly by strong interactions of the lipid membrane with proteins or polymers.

For lipids to organize into spherical micelles, a strongly curved lipid assembly is required. The energy associated with a spherical lipid assembly with radius, R is given by:

$$E_{sp} = 8\pi[(k + \frac{1}{2\bar{k}}) - kRK)$$

For lipids that organize spontaneously into spherical assemblies, $E_{sp} = 0$ and $K = \frac{1}{R}(1 + \frac{1}{2} \cdot \frac{\bar{k}}{k})$. Thus, K depends upon the bending modulus, k and the Gaussian curvature modulus $\bar{k}$.[12,41] Similar to the cylindrical shape, formation of a spherical shape requires a high energy penalty that can become available under unusual conditions/compositions, such as, for example, lipid – protein interactions.

1.6.3 Packing frustration

Packing of inverse cylindrical or spherical micelles into hexagonal or cubic lattices results in structures with packing fractions less than 1, with voids between packed micellar structures. This void volume must be filled with solvent so that the large spontaneous interfacial curvature can be maintained in the micellar assemblies. Thus, in such assemblies, there is competition between the forces that seek to maintain the interfacial curvature of the interface and those that result from hydrocarbon tails filling out the void volume. The stretching of the hydrocarbon chains to fill out the void volume costs an energy penalty and results in packing frustration. Higher interfacial curvature generates more void volume and introduces more tension in the hydrocarbon chain and results in increased packing frustration in the system. This can be clearly seen in the case of inverse hexagonal (H_{II}) and inverse micellar cubic mesophases (Fd3m). The inverse hexagonal mesophase has a packing fraction of 0.907 ($= \pi/\sqrt{12}$) with $\sim$9% void volume, while the FCC (face centered cubic) packing of the spherical micelles has a packing fraction of 0.71 with remaining 29% as void volume.[33,46,47] Thus, the increased void volume in transitioning from hexagonal to cubic symmetry introduces enormous packing frustration as the lipid tails are required to stretch to almost double to their average length along the vertices of the cube. Such packing frustration can be relieved by solubilising the lipid tails using non-polar solvents, such as alkanes or apolar oils

or by mixing lipids with dissimilar tail lengths.[47-50] The amount of the hydrophobic solvent required to maintain a particular interfacial curvature represents the extent of packing frustration.[51,52] Khoo et al. have shown that the progressive addition of alkanes to the monoglycerides allows a series of phase transitions (Q_{II}→ H_{II}→ Fd3m→ L_2) by relieving packing frustration and enabling the system to access assemblies with increasing reverse interfacial curvature.[52]In my thesis, we explore the role of attractive interactions of lipids with hydrophilic ternary components as a novel strategy to relieve packing frustration. This biomimetic strategy is inspired by biological lipid –protein interactions, ubiquitous in Nature.

1.7 Glycerol Monooleate

Several investigations have been carried out to understand the origin of curvature in biological membranes. One approach is to examine self-assembly of model lipid-water systems in the presence of hydrophilic ternary components. There are several literature reports on the encapsulation of hydrophilic proteins in organized lipid-water structures. Several studies focus on proteins encapsulated in a cubic bicontinuous mesophase of glycerol-monooleate (GMO). GMO is a simple molecule with many advantages for the experimentalist due to its ability to self-assemble into various complex structures. Here,we use GMO as a model lipid for the investigation of curvature formation in lipid-water-polymer ternary systems.

GMO is also technologically important since it has diverse applications. This is apparent from the large (and increasing) number of publications that investigate GMO. Further, until 2011, more than 2200 US patents referred to this molecule.[31] Glycerol-monooleate (also known as monoolein) is an amphiphilic molecule comprising a non-polar oleic acid chain that forms a monoester with polar glycerol. GMO is characterized by a density of 0.94 g/cm^3, refractive index 1.46, boiling point of 238-240 °C and melting point of 36 °C.[31,53] It is insoluble in water (solubility in water = 10^{-6} mol/dm^{-3}) but highly soluble in organic solvents such as alcohol, chloroform, ether etc.[54] GMO is a non-ionic lipid that, upon mixing with water, forms several ordered mesophases at room temperature. As the water fraction is varied, it forms the inverse bicontinuous cubic Ia3d and Pn3m mesophases, and the lamellar (L_α) mesophase.[55,56] These organised structures have been used as matrices for protein crystallisation,[57-59] in tissue engineering, and for delivery of nutrients and drugs, etc.[60-63] Proteins encapsulated in complex three-dimensional (3D) cubic bilayer structures retain their native activity. Therefore, such cubic structures have also been suggested as

media for enzyme encapsulation for applications in biofuel cells and as biosensors.[64-72] GMO also finds commercial use as a food emulsifying agent [9] and has been used in many industrial applications[73] It is a biocompatible, non-toxic, and biodegradable material, and has been used as a drug carrier in pharmaceutical applications.[31,74,75]

1.8 Glycerol Monooleate/Water/Polymer Ternary Mixtures

Encapsulation of proteins in lipid bilayers can reveal their role in changing the bilayer curvature, mediated by protein-lipid interactions. There are several examples of water soluble proteins that have been incorporated in GMO cubic mesophases including, lysozyme, transferrin, myoglobin, immunoglobin, glucose oxidase, ovalbumin, cytochrome c, etc (at least nineteen proteins have been encapsulated).[67,76-89] The addition of these proteins into the GMO mesophase does not always result in structural transitions by inducing a change in membrane curvature. Several of these proteins induce transitions between the bicontinuous Ia3d, Pn3m and Im3m cubic mesophases. Such transitions between bicontinuous structures do not require a significant change in bilayer curvature. A few proteins, such as FITC-ovalbumin, glucose-oxidase have been reported to transform the bicontinuous cubic Ia3d structure to a reverse hexagonal (H_{II}) structure[79, 85,87] In the presence of hydrophilic proteins, these bicontinuous cubic-cubic and bicontinuous cubic-H_{II} transitions happen due to dehydration of the GMO lipid head group, thus changing the effective packing parameter of the lipid.

Most of the aforementioned proteins are localized in the aqueous domains of the cubic mesophase. There is considerable literature on the encapsulation of lysozyme and the peripheral membrane protein, cytochrome c, in the GMO cubic mesophase. However, only cytochrome c induces a significant change in lipid bilayer curvature, resulting in a transition of the bicontinuous (Ia3d, Pn3m) mesophases to a cubic $P4_332$ micellar structure.[90-93] The high curvature $P4_332$ micellar structure in GMO-water system is thought to result from a strong attractive interaction between the lipid head group and the amine containing residues of cytochrome c. This indicates that attractive lipid-protein interactions could play an important role in stabilizing high curvature structures in lipid bilayers. High curvature structures form through the interplay between membrane elasticity and packing frustration of the lipid bilayer. Therefore, in GMO-water systems, high curvature phases like the H_{II} phase form only at high temperature (~80 °C).[56] At these temperatures, the head group is dehydrated and there is strong repulsion between alkyl tails. Even higher curvature structures

like Fd3m (packing fraction = 71%) form only when ternary components are added to stabilize the assembly, by reducing the packing frustration due to the large fraction of voids. We are interested in investigating structure formation in ternary systems comprising hydrophilic polymers that interact with the GMO head group. Such hydrophilic polymers represent model systems for proteins that access high curvature phases in lipid bilayers. Literature reports show that proteins containing several amine residues, viz. those incorporating amino acids such as lysine and arginine stabilize the high curvature $P4_332$ micellar mesophase in GMO-water system at ambient conditions.[90-93]

In the literature, amine containing polymers like polyethyleneimine (PEI) and poly-l-lysine (PAL) have been well studied as vehicles for the delivery of genes into cells.[94,95] PEI/PAL polycations form strong complexes with DNA and convey these into cell nuclei.[96] Further, polyethylenimine and poly-ε-lysine have a large number of functional groups available that can be chemically modified to achieve targeted delivery. Recently, Driever et al. and Deshpande et al. have shown the layer-by-layer coating of such multifunctional polymers on lipid nanoparticles (cubosomes) for bio-conjugation.[97,98] Encapsulated amine functionalised polymers in lipid mesophases are expected to influence the lipid bilayer curvature, as would be expected from reports of encapsulation of amine containing proteins inducing high curvature structures in GMO mesophases.

1.9 Role of Polymer Architecture in Inducing Curvature in Lipid Bilayers

In this thesis, we investigate the role ofpolymer architecture on the curvature induced in the lipid bilayer in ternary lipid/water/polymer systems. The role of the molecular shape of inclusions on determining lipid curvature has not been extensively investigated and a clear understanding of this is not available in the literature. There are only very few experimental and simulation reports in the literature that examine how molecular shape of inclusion determines bilayer curvature. In addition to molecular shape, the charge density, and size of the polymer chain also influence its interaction with lipid membranes and, subsequently influence membrane curvature. [99] Hong et al. experimentally investigated the interactions of polymers with different architecture viz. linear poly-ε-lysine, branched-PEI, and a ring containing diethyl aminoethyl-dextran (DEAE-DEX) with DAMC lipid bilayer. They showned that rigid and spheroidal polymers induce higher membrane curvature since they attach at a single point on the bilayer whereas flexible linear chains interact at multiple points, spread over the bilayer and do not induce bilayer bending. These results are consistent

with the simulations carried out by Lee et al. that compare the interactions of PAMAM-dendrimers and linear PAL with DAMC lipid bilayers.[100] However, a detailed, systematic study of the influence of polymer architecture and molecular weight on inducing curvature in lipid bilayers is currently not available. This is one of the themes that we explore in this thesis.

1.10 Lipid Mesophases Form Aqueous Dispersions of Lipid Nanoparticles

One of the major problems in working with lipid mesophases is their high viscosity. For example, the room temperature viscosity of the Pn3m mesophase is of the order of 10^5 Pa s. Therefore, it is difficult to process the bulk mesophase.

The GMO-water phase diagram shows a miscibility gap, and at high water concentrations, the bicontinuous Pn3m mesophase is in equilibrium with excess water.[55,56] Thus, the Pn3m bulk mesophase can be converted into dispersions of internally ordered nanoparticles by applying high energy homogenisation. These nanoparticles retain internal structural symmetry identical to the bulk cubic bicontinuous Pn3m. Such nanoparticles are known as *cubosomes.*[101-103] *Cubosomes* are kinetically stable formulations since they are stabilised using a triblock PEO-PPO-PEO copolymer (called Pluronic F127).[104] These dispersions are low viscosity formulations that can be used for aqueous based encapsulated delivery applications.[105-108]

The bicontinuous nature of cubosomes allows loading of both hydrophilic and hydrophobic molecules.[97] Cubosomes show a burst release of the hydrophilic guest molecules in aqueous matrices.[97,98] However, in aqueous medium cubosomes can solubilise hydrophobic molecules and deliver them with much slower rate compared with hydrophilic molecules.

1.11 Objective of Thesis:

In this work, we explore the role of polymer architecture in influencing the GMO-water phase behaviour. Our results have fundamental implications for understanding pathways of structural transformations and transient phase formation due to lipid-macromolecule interactions. Specifically, we investigate the influence of polymer architecture in forming high curvature structures like H_{II} and Fd3m phases. Such structures are desired for their use in sustained delivery of the hydrophilic molecules. We are motivated

to use amine functionalised polymers due to their strong attractive interactions with the GMO head group. Additionally, polymers like polyethyleneimine, poly-ε- lysine etc. are well-known examples of polymers that have been used for gene delivery. Finally, we also explore wetting of hydrophobic surfaces by impinging them with aqueous dispersions of lipid nanoparticles.

1.12 Outline of Thesis:

In this chapter (**Chapter 1),** we provide background literature to motivate our investigations of GMO-water-polymer ternary systems.

Chapter 2 explores the phase behaviour of GMO/water in the presence of hydrophilic poly-amidoamine (PAMAM) dendrons. We show, for the first time, that PAMAM dendrons promote the formation of high curvature stable mesophases viz. reverse hexagonal, H_{II} and the reverse micellar cubic, Fd3m mesophase at room temperature. Small angle X-ray scattering (SAXS) and polarised optical microscopy (POM) were used to identify the ordered lipid structures. We compare the influence of different generations of PAMAM-dendrons (G2-G4) with their linear analogues to explore the effect of molecular size and shape on forming high curvature phases.

Chapter 3 deals with the effect of the fifth generation PAMAM dendron on the phase behaviour of GMO-water system. With PAMAM-G5, we demonstrate the formation of a rare high curvature cubic micellar structure with $P4_332$ space group symmetry. We rationalize how large compact macromolecules induce the formation of such phases.

In **Chapter 4,** we discuss the phase behaviour of GMO-water systems containing commercial branched polymer polyethyleneimine (PEI) as a ternary component. We construct a phase diagram by varying both the composition and temperature in GMO-water-PEI ternary system and by varying PEI molecular weight from 0.8 kDa to 75 kDa. Our work provides thumb rules that can be used to predict the effect of polymer interactions and molecular shape on the formation of high curvature phases in GMO/water systems.

In **Chapter 5,** we model the diffusion of hydrophilic drug through the bicontinuous Pn3m and discontinuous Fd3m micellar phases, at room temperature. We demonstrate that diffusion of hydrophilic drug through the discontinuous Fd3m phase is significantly slower than through the bicontinuous Pn3m phase. We also demonstrate a novel approach to model

the diffusion of drug through bulk mesophases that is able to capture release data over the entire experimental time period.

In **Chapter 6,** we examine the spreading of aqueous dispersions of *cubosomes* on hydrophobic surfaces. We employ high speed video imaging to capture the spreading dynamics of 1% cubosome dispersions on hydrophobic surfaces and compare these with the behaviour of water and 1% Tween 20, as controls. We demonstrate the ability of the cubosome dispersions to wet hydrophobic and superhydrophobic natural surfaces like lotus leaves.

1.13 References

1. Patton, J. S.; Carey, M. C., Watching Fat Digestion. *Science* **1979**, *204*, 145-148.
2. Fantini, J.; Garmy, N.; Mahfoud, R.; Yahi, N., Lipid Rafts: Structure, function and Role in HIV, Alzheimer's and Prion Diseases. *Expert. Rev. Mol. Med.* **2002**, *4*, 1.
3. Braun, V. P.; Stupp, I. S. CdS Mineralization of Hexagonal, Lamellar, and Cubic Lyotropic Liquid Crystals. *Mater. Res. Bull.* **1999**, *34*, 463−469.
4. Wang, D.; Kou, R.; Choi, D.; Yang, Y.; Nie, Y.; Li, J.; Saraf, L. V.; Hu, D.; Zhang, J.; Graff, G. L.; Liu, J.; Pope, M. A.; Aksay, I. A. Ternary Self-assembly of Ordered Metal Oxide−Graphene Nanocomposites for Electrochemical Energy Storage. *ACS Nano* **2010**, *4*, 1587−1595.
5. Barauskas, J.; Johnsson, M.; Tiberg, F., Self-assembled Lipid Superstructures: Beyond Vesicles and Liposomes. *Nano Lett.* **2005**, *5*, 1615-1619.
6. Mezzenga, R.; Schurtenberger, P.; Burbidge, A.; Michel, M., Understanding Foods as Soft Materials. *Nat. Mater.***2005**, *4*, 729-740.
7. Sagalowicz, L.; Michel, M.; Blank, I.; Schafer, O.; Leser, M. E., Self-Assembly in Food: A Concept for Structure Formation Inspired by Nature. *Curr. Opin.Colloid Interface Sci.* **2017**.
8. Amar-Yuli, I.; Libster, D.; Aserin, A.; Garti, N., Solubilization of Food Bioactives within Lyotropic Liquid Crystalline Mesophases. *Curr. Opin. Colloid Interface Sci.* **2009**, *14*, 21-32.
9. Ganem-Quintanar, A.; Quintanar-Guerrero, D.; Buri, P., Monoolein: A Review of the Pharmaceutical Applications. *Drug Dev. Ind. Pharm.* **2000**, *26*, 809-820.
10. McMahon, H. T.; Gallop, J. L., Membrane Curvature and Mechanisms of Dynamic Cell Membrane Remodelling. *Nature* **2005**, *438*, 590-596.
11. Schrum, J. P.; Zhu, T. F.; Szostak, J. W., The Origins of Cellular Life. *Cold Spring Harb. Perspect. Biol.* **2010**, *2*, a002212.
12. Zimmerberg, J.; Kozlov, M. M., How Proteins Produce Cellular Membrane Curvature. *Nat. Rev. Mol. Cell Biol.* **2006**, *7*, 9-19.
13. Bhatia, V. K. l.; Hatzakis, N. S.; Stamou, D. In A Unifying Mechanism Accounts for Sensing of Membrane Curvature by BAR Domains, Amphipathic Helices and Membrane-Anchored Proteins. *Sem. Cell Develop. Biol.* **2010**, 381-390.

14. Sugiura, Y.; Ikeda, K.; Nakano, M., High Membrane Curvature Enhances Binding, Conformational Changes, and Fibrillation of Amyloid-β on Lipid Bilayer Surfaces. *Langmuir* **2015**, *31*, 11549-11557.
15. Lee, I. H.; Kai, H.; Carlson, L. A.; Groves, J. T.; Hurley, J. H., Negative Membrane Curvature Catalyses Nucleation of Endosomal Sorting Complex Required for Transport (ESCRT)-III Assembly. *Proc. Natl. Acad. Sci.* **2015**, *112*, 15892-15897.
16. Drin, G.; Casella, J. F.; Gautier, R.; Boehmer, T.; Schwartz, T. U.; Antonny, B., A General Amphipathic α-helical Motif for Sensing Membrane Curvature. *Nat. Struct. Mol. Biol.* **2007**, *14*, 138-146.
17. Hanna, M. G.; Mela, I.; Wang, L.; Henderson, R. M.; Chapman, E. R.; Edwardson, J. M.; Audhya, A., Sar1 GTPase Activity is Regulated by Membrane Curvature. *J. Biol. Chem.* **2016**, *291*, 1014-1027.
18. Knorr, R. L.; Dimova, R.; Lipowsky, R., Curvature of Double-Membrane Organelles Generated by Changes in Membrane Size and Composition. *PLoS One* **2012**, *7*, e32753.
19. Almsherqi, Z. A.; Landh, T.; Kohlwein, S. D.; Deng, Y., Chapter 6 Cubic Membranes: The Missing Dimension of Cell Membrane Organization. *Int. Rev. Cell Mol. Biol.*, Academic Press: **2009**, *274*, 275-342.
20. Lingwood, D.; Schuck, S.; Ferguson, C.; Gerl, M. J.; Simons, K., Generation of Cubic Membranes by Controlled Homotypic Interaction of Membrane Proteins in the Endoplasmic Reticulum. *J. Biol. Chem.* **2009**, *284*, 12041-12048.
21. Angelov, B.; Angelova, A.; Papahadjopoulos-Sternberg, B.; Lesieur, S.; Sadoc, J. F.; Ollivon, M.; Couvreur, P., Detailed Structure of Diamond-Type Lipid Cubic Nanoparticles. *J. Am. Chem. Soc.* **2006**, *128*, 5813-5817.
22. Chernomordik, L. V.; Kozlov, M. M., Protein-Lipid Interplay in Fusion and Fission of Biological Membranes. *Annu. Rev. Biochem.* **2003**, *72*, 175-207
23. Vanni, S.; Hirose, H.; Barelli, H. I.; Antonny, B.; Gautier, R., A Sub-nanometre View of How Membrane Curvature and Composition Modulate Lipid Packing and Protein Recruitment. *Nat. Commun.* **2014**, *5*.
24. Pinot, M.; Vanni, S.; Pagnotta, S.; Lacas-Gervais, S.; Payet, L. A.; Ferreira, T.; Gautier, R.; Goud, B.; Antonny, B.; Barelli, H. l., Polyunsaturated Phospholipids Facilitate Membrane Deformation and Fission by Endocytic Proteins. *Science* **2014**, *345*, 693-697.

25. Eckler, S. A.; Kuehn, R.; Gautam, M., Deletion of N-terminal Rapsyn Domains Disrupts Clustering and has Dominant Negative Effects on Clustering of Full-Length Rapsyn. *Neuroscience* **2005**, *131*, 661-670.
26. Stachowiak, J. C.; Schmid, E. M.; Ryan, C. J.; Ann, H. S.; Sasaki, D. Y.; Sherman, M. B.; Geissler, P. L.; Fletcher, D. A.; Hayden, C. C., Membrane Bending by Protein–Protein Crowding. *Nat. Cell Biol.* **2012**, *14*, 944-949.
27. Leduc, C.; Campàs, O.; Joanny, J. F.; Prost, J.; Bassereau, P., Mechanism of Membrane Nanotube Formation by Molecular Motors. *Biochim. Biophys. Acta, Biomemb.* **2010**, *1798*, 1418-1426.
28. J. Israelachvili, Intermolecular and Surface Forces, Academic Press, London, **1991**.
29. Fong, C.; Le, T.; Drummond, C. J., Lyotropic Liquid Crystal Engineering–Ordered Nanostructured Small Molecule Amphiphile Self-Assembly Materials by Design. *Chem. Soc. Rev.* **2012**, *41*, 1297-1322.
30. Seddon, J. M.; Templer, R. H., Polymorphism of Lipid-Water Systems. *Biol. Phys.* **1995**, *1*, 97-160.
31. Kulkarni, C. V.; Wachter, W.; Iglesias-Salto, G.; Engelskirchen, S.; Ahualli, S., Monoolein: A Magic Lipid? *Phys. Chem. Chem. Phys.* **2011**, *13*, 3004-3021.
32. Seddon, J. M.; and Cevc, G., Phospholipids Handbook, ed. G. Cevc, Marcel Dekker, Inc., **1993**, 403–454.
33. Seddon, J. M.; Robins, J.; Gulik-Krzywicki,T. ; Delacroix, H., Inverse Micellar Phases of Phospholipids and Glycolipids, Invited Lecture. *Phys. Chem. Chem. Phys.* **2000**, *2*, 4485–4493.
34. Nakano, M.; Teshigawara, T.; Sugita, A.; Leesajakul, W.; Taniguchi, A.; Kamo, T.; Matsuoka H.; Handa, T., Dispersions of Liquid Crystalline Phases of the Monoolein/Oleic acid/Pluronic F127 System. *Langmuir* **2002**, *18*, 9283–9288
35. Salentinig, S.; Yaghmur, A.; Guillot, S.; Glatter, O., Preparation of Highly Concentrated Nanostructured Dispersions of Controlled size. *J. Colloid Interface Sci.* **2008**, *326*, 211-220.
36. Caboi, F.; Amico, G. S.; Pitzalis, P.; Monduzzi, M.; Nylander, T.; Larsson, K., Addition of Hydrophilic and Lipophilic Compounds of Biological Relevance to the Monoolein/Water System. I. Phase Behavior. *Chem. Phys. Lipids* **2001**, *109*, 47-62.

37. Gulik-Krzywicki, T.; Larsson, K., An Electron Microscopy study of the L_2-Phase (microemulsion) in a Ternary System: Triglyceride/Monoglyceride/Water. *Chem. Phys. Lipids* **1984**, *35*,127-132.

38. Hyde, S. T., Identification of Lyotropic Liquid Crystalline Mesophases. *Appl.Surf. Colloid Chem.* **2001**, 299.

39. Shearman, G. C.; Tyler, A. I. I.; Brooks, N. J.; Templer, R. H.; Ces, O.; Law, R. V.; Seddon, J. M., Ordered Micellar and Inverse Micellar Lyotropic Phases. *Liq. Cryst.* **2010**, *37*, 679-694.

40. Rappolt, M., The Biologically Relevant Lipid Mesophases as "Seen" • by X-rays. Advances in Planar Lipid Bilayers and Liposomes**. 2006**, *5*, 253-283.

41. Helfrich, W., Elastic Properties of Lipid Bilayers: Theory and Possible experiments. *Z. Naturforsch. C* **1973**, *28*, 693-703.

42. Helfrich, W., Amphiphilic Mesophases Made of Defects. *Phys. Defects* **1981**, 716-

43. Hyde, S. T., Curvature and the Global Structure of Interfaces in Surfactant-Water Systems. *J. De Phys. Colloq.* **1990**, *51*, C7-209-C7-228.

44. Schoen, A. H., Infinite Periodic Minimal Surfaces without Self-Intersections NASA Technical Report TN D-5541. *Washington DC* **1970**.

45. Hyde, S.; Blum, Z.; Landh, T.; Lidin, S.; Ninham, B. W.; Andersson, S.; Larsson, K., The Language of Shape: The Role of Curvature in Condensed Matter: Physics Chemistry and Biology. *Elsevier* **1996**.

46. Rappolt, M.; Cacho-Nerin, F.; Morello, C.; Yaghmur, A., How the Chain Configuration Governs the Packing of Inverted Micelles in the Cubic Fd3m-Phase. *Soft Matter* **2013**, *9*, 6291.

47. Shearman, G. C.; Ces, O.; Templer, R. H.; Seddon, J. M., Inverse Lyotropic Phases of Lipids and Membrane Curvature. *J. Phys. Condens. Matter* **2006,** *18*, S1105.

48. Yaghmur, A.; Sartori, B.; Rappolt, M., Self-Assembled Nanostructures of Fully Hydrated Monoelaidin–Elaidic Acid and Monoelaidin–Oleic Acid Systems. *Langmuir* **2012**, *28*, 10105-10119.

49. Yaghmur, A.; Laggner, P.; Zhang, S.; Rappolt, M., Tuning Curvature and Stability of Monoolein Bilayers by Designer Lipid-like Peptide Surfactants. *PLoS One* **2007**, *2*, e479.

50. Alley, S. H.; Ces, O.; Barahona, M.; Templer, R. H., X-ray Diffraction Measurement of the Monolayer Spontaneous Curvature of Dioleoylphosphatidylglycerol. *Chem. Phys. Lipids* **2008**, *154*, 64-67.

51. Rand, R. P.; Fuller, N. L.; Gruner, S. M.; Parsegian, V. A., Membrane Curvature, Lipid Segregation, and Structural Transitions for Phospholipids Under Dual-Solvent Stress. *Biochem.* **1990**, *29*, 76-87.

52. Khoo, B. J., An Experimental examination of ideas in the curvature elasticity of lyotropic liquid crystals. Imperial College London (University of London), **1996**.

53. Wade et al., 1994, USP Convention-1990, Engström-**1990**, 13–15.

54 Food and Nutrition Board National Academy of Sciences, Food Chemicals Codex, 4th Ed. , National Academy Press, Washington, DC.

55. Qiu, H.; Caffrey, M., The Phase Diagram of the Monoolein/Water System: Metastability and Equilibrium Aspects. *Biomaterials* **2000**, *21*, 223-234.

56. Briggs, J.; Chung, H.; Caffrey, M., The Temperature-Composition Phase Diagram and Mesophase Structure Characterization of the Monoolein/Water System. *J. De Phys. II* **1996**, *6*, 723-751.

57. Cherezov, V.; Rosenbaum, D. M.; Hanson, M. A.; Rasmussen, S. G.; Thian, F. S.; Kobilka, T. S.; Choi, H. J.; Kuhn, P.; Weis, W. I.; Kobilka, B. K.; Stevens, R. C., High-Resolution Crystal Structure of an Engineered Human 2-Adrenergic G Protein-Coupled Receptor. *Science* **2007**, *318*, 1258−1265.

58. Caffrey, M.; Cherezov, V., Crystallizing Membrane Proteins Using Lipidic Mesophases. *Nat. Protoc.* **2009**, *4*, 706−731.

59. Zabara, A.; Mezzenga, R., Plenty of Room to Crystallize: Swollen Lipidic Mesophases for Improved and Controlled In-Meso Protein Crystallization. *Soft Matter* **2012**, *8*, 6535−6541.

60. Fong, W.; Hanley, T.; Boyd, B., Stimuli Responsive Liquid Crystals Provide 'on-demand' Drug Delivery in Vitro and in Vivo. *J. Control. Release* **2009**, *135*, 218−226.

61. Negrini, R.; Mezzenga, R., pH-Responsive Lyotropic Liquid Crystals for Controlled Drug Delivery. *Langmuir* **2011**, *27*, 5296− 5303.

62. Caboi, F.; Nylander, T.; Razumas, V.; Talaikyte, Z.; Monduzzi, M.; Larsson, K., Structural Effects, Mobility, and Redox Behavior of Vitamin K1 Hosted in the Monoolein/Water Liquid Crystalline Phases. *Langmuir* **1997**, *13*, 5476−5483.

63. Boyd, B. J.; Whittaker, D. V.; Khoo, S. M.; Davey, G., Lyotropic Liquid Crystalline Phases Formed from a Glycerate Surfactant as Sustained Release Drug Delivery System. *Int. J. Pharm.* **2006**, *309*, 218−226.

64. Sun, W.; Vallooran, J. J.; Zabara, A.; Mezzenga, R., Controlling Enzymatic Activity and Kinetics in Swollen Mesophases by Physical Nano-Confinement. *Nanoscale* **2014**, *6*, 6853−5859.

65. Sun, W.; Vallooran, J. J.; Mezzenga, R., Enzyme Kinetics in Liquid Crystalline Mesophases: Size Matter, But Also Topology. *Langmuir* **2015**, *31*, 4558−4565.

66. Razumas, V.; Kanapieniene, J.; Nylander, T.; Engstro ,S.; Larsson, K., Electrochemical Biosensors for Glucose, Lactate, Urea and Creatinine Based on Enzymes Entrapped in a Cubic Liquid Crystalline Phase. *Anal. Chim. Acta* **1994**, *289*, 155−162.

67. Nylander, T.; Mattisson, C.; Razumas, V.; Miezis, Y.; Hakansson, B., A Study of Entrapped Enzyme Stability and Substrate Diffusion in a Monoglyceride-Based Cubic Liquid Crystalline Phase. *Colloids Surf.*,**1996**, *114*, 311−320.

68. Nazaruk, E.; Bilewicz, R., Catalytic Activity of Oxidases Hosted in Lipidic Cubic Phases on Electrodes. *Bioelectrochemistry* **2007**, *71*, 8−14.

69. Nazaruk, E.; Bilewicz, R.; Lindblom, G.; Lindholm-Sethson, B., Cubic Phases in Biosensing Systems. *Anal. Bioanal. Chem.* **2008**, *391*, 1569−1578.

70. Li, D.; Caffrey, M., Lipid Cubic Phase as a Membrane Mimetic for Integral Membrane Protein Enzymes. *Proc. Natl. Acad. Sci. U. S. A.* **2011**, *108*, 8639−8644.

71. Nazaruk, E.; Landau, E. M.; Bilewicz, R., Membrane Bound Enzyme Hosted in Liquid Crystalline Cubic Phase for Sensing and Fuel Cells. *Electrochim. Acta* **2014**, *140*, 96−100.

72. Vallooran, J. J.; Handschin, S.; Pillai, S. M.; Vetter, B. N.; Rusch, S.; Beck, H. P.; Mezzenga, R., Lipidic Cubic Phases as Versatile Platform for the Rapid Detection of Biomarkers, Viruses, Bacteria and Parasites. *Adv. Funct. Mater.* **2016**, *26*, 181−190.

73. Kulkarni, C. V.; Ces, O.; Templer, R. H., Monoelaidin–Water Phase Behaviour with Temperature. *Eur. Biophys. J.* **2007**, *36*, S77.

74. Kulkarni, C. V.; Ces O.; Templer R. H., Presented in Part at the 23rd Conference of the *Eur. Colloid Interface Soci.* 06-11 Sept. 2009, Antalya, Turkey, **2009**.

75. Kulkarni, C. V.; Tang, T. Y.; Seddon, A. M.; Seddon, J. M.; Ces, O.; Templer, R. H., Engineering Bicontinuous Cubic Structures at the Nanoscale–the Role of Chain Splay. *Soft Matter* **2010**, *6*, 3191-3194.

76. Kraineva, J.; Narayanan, R. A.; Kondrashkina, E.; Thiyagarajan, P.; Winter, R., Kinetics of Lamellar-to Cubic and Inter Cubic Phase Transitions of Pure and Cytochrome c Containing Monoolein Dispersions Monitored by Time-Resolved Small-Angle X-ray Diffraction. *Langmuir* **2005**, *21*, 3559–3571.

77. Lendermann, J.; Winter R., Interaction of Cytochrome c with Cubic Monoolein Mesophases at Limited Hydration Conditions: The Effects of Concentration, Temperature and Pressure. *Phys. Chem. Chem. Phys.* **2003**, *5*, 1440–1450.

78. Misiunas, A.; Niaura, G.; Barauskas, J.; Meskys, R.; Rutkiene, R.; Razumas V.; Nylander, T., Horse Heart Cytochrome c Entrapped into the Hydrated Liquid-Crystalline Phases of Phytantriol: X-ray Diffraction and Raman Spectroscopic Characterization. *J. Colloid Interface Sci.* **2012**, *378*, 232–240.

79. Razumas, V.; Larsson, K.; Miezis Y.; Nylander, T., A Cubic Monoolein Cytochrome c Water Phase: X-ray Diffraction, FTIR, Differential Scanning Calorimetric, and Electrochemical Studies. *J. Phys. Chem.* **1996**, *100*, 11766–11774.

80. Buchheim, W.; Larsson, K., Cubic lipid–protein–water phases. *J. Colloid Interface Sci.***1987**, *117*, 582–583.

81. Razumas, V.; Talaikyte, Z.; Barauskas, J.; Larsson, K.; Miezis Y.; Nylander, T., Effects of Distearoyl Phosphatidylglycerol and Lysozyme on the Structure of the Monoolein–Water Cubic Phase: X-ray Diffraction and Raman Scattering Studies. *Chem. Phys. Lipids* **1996**, *84*, 123–138.

82. Tanaka, S.; Maki S.; Ataka, M., Structural Transitions of the Monoolein Bicontinuous Cubic Phase Induced by Inclusion of Protein Lysozyme Solutions. *Phys. Rev. E* **2006**, *73*, 061510.

83. Mezzenga, R.; Zabara, A.; Amar-Yuli, I., Tuning in Meso-Crystallized Lysozyme Polymorphism by Lyotropic Liquid Crystal Symmetry. *Langmuir*. **2011**, *27*, 6418–6425.

84. Clogston, J.; Caffrey, M., Controlling Release From the Lipidic Cubic Phase. Amino Acids, Peptides, Proteins and Nucleic Acids. *J. Control. Release* **2005**, *107*, 97–111.

85. Kraineva, J.; Nicolini, C.; Thiyagarajan, P.; Kondrashkina E.; Winter, R., Incorporation of Alpha-Chymotrypsin into the 3D Channels of Bicontinuous Cubic Lipid Mesophases. *Biochim. Biophys. Acta Proteins Proteomics* **2006**, *1764*, 424–433.

86. Leslie, S. B.; Puvvada, S.; Ratna B. R.; Rudolph, A. S., Encapsulation of Hemoglobin in a Bicontinuous Cubic Phase Lipid. *Biochim. Biophys. Acta, Biomemb.* **1996**, *1285*, 246–254.

87. Rizwan, S. B.; Hanley, T.; Boyd, B. J.; Rades T.; Hook, S., Liquid Crystalline Systems of Phytantriol and Glyceryl-Monooleate Containing a Hydrophilic Protein: Characterisation, Swelling and Release Kinetics. *J. Pharm. Sci.* **2009**, *98*, 4191– 4204.

88. Puvvada, S.; Qadri, S. B.; Naciri J.; Ratna, B. R., Ionotropic Gelation in a Bicontinuous Cubic Phase. *J. Phys. Chem.* **1993**, *97*, 11103–11107.

89. Barauskas, J.; Razumas V.; Nylander, T., Entrapment of Glucose Oxidase into the Cubic Q230 and Q224 Phases of Aqueous Monoolein. *Surf. Colloid Sci.***2001**, *116*, 16–20.

90. Ravindra, R.; Zhao, S.; Gies, H.; Winter, R., Protein Encapsulation in Mesoporous Silicate: The Effects of Confinement on Protein Stability, Hydration, and Volumetric Properties. *J. Am. Chem. Soc.* **2004,** *126*, 12224-12225.

91. Köhling, R.; Woenckhaus, J.; Klyachko, N. L.; Winter, R., Small-Angle Neutron Scattering Study of the Effect of Pressure on AOT–n-Octane–Water Mesophases and the Effect of α-Chymotrypsin Incorporation. *Langmuir* **2002,** *18*, 8626-8632.

92. Kraineva, J.; Smirnovas, V.; Winter, R., Effects of Lipid Confinement on Insulin Stability and Amyloid Formation. *Langmuir* **2007**, *23*, 7118-7126.

93. Kraineva, J.; Narayanan, R.; Kondrashkina, E.; Thiyagarajan, P.; Winter, R., Kinetics of Lamellar-to-Cubic and Inter cubic Phase Transitions of Pure and Cytochrome c Containing Monoolein Dispersions monitored by Time Resolved Small-angle X-ray diffraction. *Langmuir* **2005**, *21*, 3559– 3571.

94. Lee, C. H.; Ni, Y. H.; Chen, C. C.; Chou, C. K.; Chang, F. H., Synergistic Effect of Polyethylenimine and Cationic Liposomes in Nucleic acid Delivery to Human Cancer Cells. *Biochim. Biophys. Acta Biomemb.***2003**, *1611*, 55-62.

95. Godbey, W. T.; Barry, M. A.; Saggau, P.; Wu, K. K.; Mikos, A. G., Poly (ethylenimine)-Mediated Transfection: A New Paradigm for Gene Delivery. *J. Biomed. Mater. Research* **2000**, *51*, 321-328.

96. Godbey, W. T.; Wu, K. K.; Mikos, A. G., Tracking the Intracellular Path of Poly (ethylenimine)/DNA Complexes for Gene Delivery. *Proc. Natl. Acad. Sci.* **1999**, *96*, 5177-5181.

97. Deshpande, S.; Venugopal, E.; Ramagiri, S.; Bellare, J. R.; Kumaraswamy, G.; Singh, N., Enhancing Cubosome Functionality by Coating with a Single Layer of poly-ε-lysine. *ACS Appl. Mater. Interfaces* **2014**, *6*, 17126-17133.

98. Driever, C. D.; Mulet, X.; Johnston, A. P. R.; Waddington, L. J.; Thissen, H.; Caruso, F.; Drummond, C. J., Converging Layer-by-Layer Polyelectrolyte Microcapsule and Cubic Lyotropic Liquid Crystalline Nanoparticle Approaches for Molecular Encapsulation. *Soft Matter* **2011**, *7*, 4257-4266.

99. Hong, S.; Leroueil, P. R.; Janus, E. K.; Peters, J. L.; Kober, M. M.; Islam, M. T.; Orr, B. G.; Baker J, J. R.; Banaszak Holl, M. M., Interaction of Polycationic Polymers with Supported Lipid Bilayers and Cells: Nanoscale Hole Formation and Enhanced Membrane Permeability. *Bioconjug. Chem.* **2006**, *17*, 728-734.

100. Lee, H.; Larson, R. G., Lipid Bilayer Curvature and Pore Formation Induced by Charged Linear Polymers and Dendrimers: The Effect of Molecular Shape. *J. Phys. Chem. B* **2008**, *112*, 12279.

101. Spicer, P. T., Progress in Liquid Crystalline Dispersions: Cubosomes. *Curr. Opin. Colloid Interface Sci.* **2005**, *10*, 274-279.

102. Spicer, P. T.; Hayden, K. L.; Lynch, M. L.; Ofori-Boateng, A.; Burns, J. L., Novel Process for Producing Cubic Liquid Crystalline Nanoparticles (cubosomes). *Langmuir* **2001**, *17*, 5748-5756.

103. Barauskas, J.; Johnsson, M.; Joabsson, F.; Tiberg, F., Cubic Phase Nanoparticles (cubosomes): Principles for Controlling Size, Structure, and Stability. *Langmuir* **2005**, 21, 2569-2577.

104. Tilley, A. J.; Drummond, C. J.; Boyd, B. J., Disposition and Association of the Steric Stabilizer Pluronic® F127 in Lyotropic Liquid Crystalline Nanostructured Particle Dispersions. *J. Colloid Interface Sci.* **2013,** *392*, 288-296.

105. Mulet, X.; Boyd, B. J.; Drummond, C. J., Advances in Drug Delivery and Medical Imaging Using Colloidal Lyotropic Liquid Crystalline Dispersions. *J. Colloid Interface Sci.* **2013**, *393*, 1-20.

106. Pan, X.; Han, K.; Peng, X.; Yang, Z.; Qin, L.; Zhu, C.; Huang, X.; Shi, X.; Dian, L.; Lu, M., Nanostructed Cubosomes as Advanced Drug Delivery System. *Curr. Pharm. Des.* **2013**, *19*, 6290-6297.

107. Yaghmur, A.; Glatter, O., Characterization and Potential Applications of Nanostructured Aqueous Dispersions. *Adv. Colloid Interface Sci.* **2009**, *147*, 333-342.

108. Boyd, B. J., Characterisation of Drug Release from Cubosomes Using the Pressure Ultrafiltration Method. *Int. J. Pharm.* **2003**, *260*, 239-247.

Chapter 2

Compact Polar Moieties Induce Lipid-Water Systems to Form Discontinuous Reverse Micellar Phase

2.1 Introduction

Nature abhors voids. Ordered assemblies of oil-in-water micelles form readily since water occupies the interstitial spaces in such assemblies.[1,2] Formation of reverse (water-in-oil) micellar assemblies is, however, inhibited by packing frustration. Consider, for example, a reverse hexagonal (H_{II}) phase. Here, micellar cylinders are organized in a hexagonal lattice with a packing fraction of 91%. The 9% "void" space is filled, either by stretching hydrophobic lipid tails or by distorting the micellar cylinders towards a hexagonal cross-section.[1,3] Even more significant packing constraints are encountered by reverse micellar cubic assemblies. Curiously, the Fd3m phase[4] with a packing fraction of 71%, forms more readily than fcc or hcp phases (with higher packing fractions of 74%). The Fd3m phase is comprised of micelles of two distinct sizes organized in a cubic AB_2 lattice (Figure 2.1).

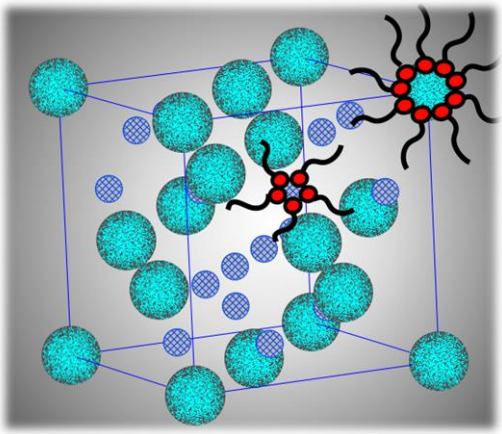

Figure 2.1: Schematic of the reverse micellar Fd3m phase with micelles of two different sizes arranged in an AB_2 lattice.

It has been suggested that preferential formation of the Fd3m phase relative to more densely packed cubic phases results from the lower free energy cost for stretching lipid tails in the Fd3m phase.[5] Fd3m phases have been reported[6,7] for lipid/water systems where the lipids have hydrocarbon tails that are long or branched. Packing frustration in the Fd3m phase can also be reduced by solvating lipid tails through addition of an apolar ternary component. Thus, for hydrophobic lipids such as monolinolein, phytantriol or monoolein, Fd3m phases form on adding hexadecane or tetradecane oil,[8-10] limonene[11] or vitamin E acetate.[12] Recently, the influence of apolar ternary additives on membrane curvature has been analysed

in detail[13,14] by accounting for the effect of the additive on membrane rigidity and on lipid tail solvation. Here, we report that a new pathway to the Fd3m phase can be opened, by addition of small quantities of polar, water soluble moieties to a monoolein/water system. We demonstrate that perfectly branched polyamidoamine (PAMAM) dendrons, branched polyethylenimine and silsesquioxane cages induce formation of the Fd3m reverse micellar phase in a monoolein/water system. Further, we contrast the behavior of PAMAM dendrons with their linear analogs (that do not induce Fd3m phase formation) to demonstrate that compact molecular architecture is critical in the formation of discontinuous phase. Introducing a third component into a lipid/water system can change the mesophase lattice parameter[15-17] or even induce order-order or order-disorder transitions.[18-20] These structural changes significantly affect mesophase properties. For example, transition from bicontinuous organization to a discontinuous micellar structure can retard the release of encapsulated molecules by an order of magnitude.[21] Therefore, a fundamental understanding of how ternary inclusions influence lipid/water systems is necessary for rational design of mesophase formulations. This is technologically important since ordered lipid/water mesophases have implications for a wide variety of areas, ranging from control of food texture,[22-24] to biological processes;[25] and from templated syntheses in materials science[26, 27] to protein crystallization[28] and delivery strategies for therapeutic applications.[29-35]

Ternary inclusions can relieve packing frustration, or can affect the local bilayer curvature by changing the effective packing ratio[36] of lipid molecules in the mesophase. In particular, polymeric inclusions strongly affect mesophase organization[37-43] and offer the added advantage of customization, by copolymerization or by varying molecular weight or chain architecture. Recent simulations[44] indicate that chain architecture of a polymer tethered to a bilayer membrane critically determines its curvature. Inspired by these results, we contrast the effect of poly (amidoamine) (PAMAM) dendrons and their matched linear analogs on the phase behaviour of the technologically important monoolein/water system. PAMAM dendritic structures have attracted attention for their potential in medical applications: PAMAM dendrimers are already in commercial use as high contrast MRI agents.[45] These synthetic constructs afford fractal structures with precise control over the number of functional groups at their periphery and preserve molecular shape across generations. We begin by describing the phase behaviour of ternary systems containing PAMAM dendrimers in monoolein/water and highlight the role of molecular architecture by contrasting this to monoolein/water containing a linear analog of PAMAM.

2.2 Experimental Section

2.2.1 Materials:

Glycerol monooleate (called GMO in this work, commercial trade name: Rylo MG 20 Pharma) was received as a generous gift from Danisco Corporation India. Distilled, deionised water, with a resistivity of 18 MΩ.cm, was used to prepare the samples. Branched polyethylenimine (bPEI) of $M_w \approx 2$ kDa, was obtained from Sigma Aldrich and was used as received. bPEI has a branched architecture and is reported to comprise 25% primary, 50% secondary and 25% tertiary amines. The structure of bPEI was characterized earlier[46] using NMR at different pH. Polysilsesquioxane hydrate-octakis tetramethylammonium substituted (POSS) was obtained from Sigma Aldrich and used as received. Reported procedures were used to synthesize poly-amidoamine (PAMAM) dendrons of various generations (G2, G3 and G4) and their linear analogues (L3, and L4).

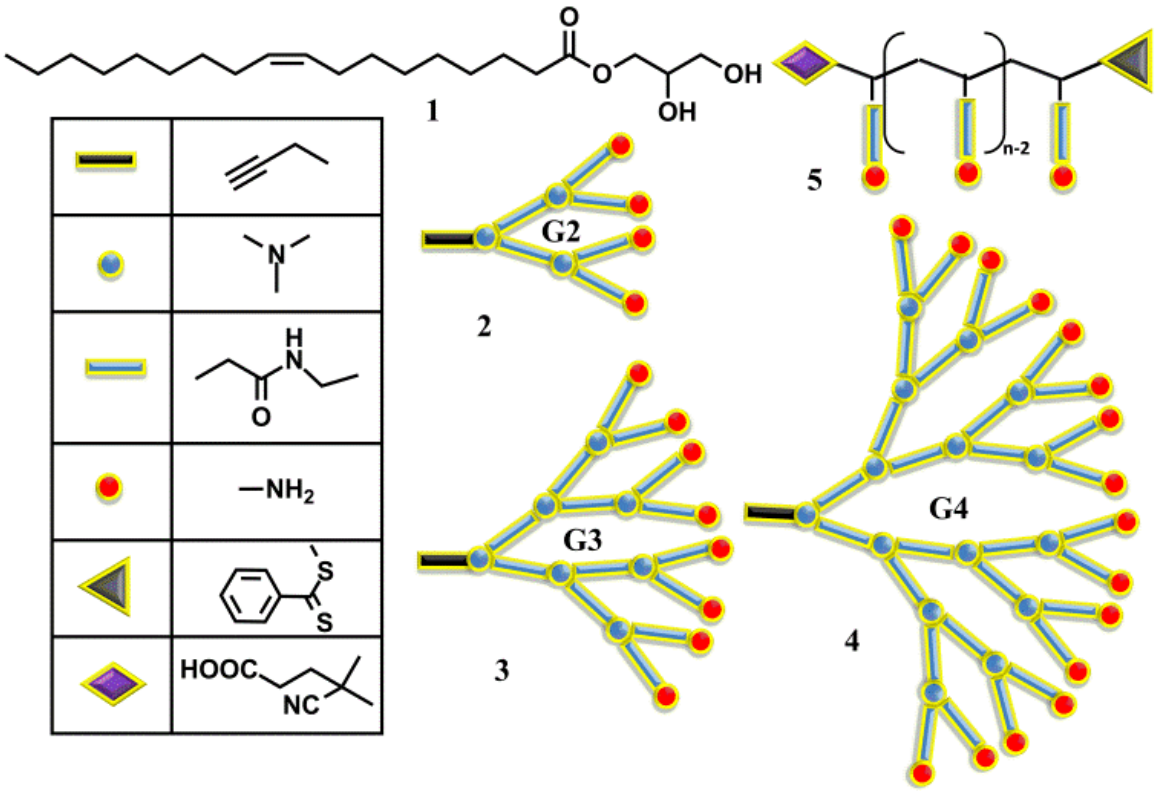

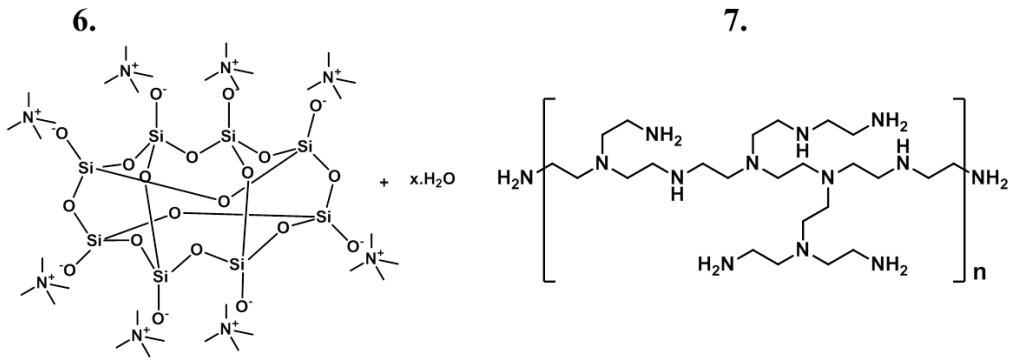

Figure 2.2: Schematics of (1) GMO; (2) – (4) G2 to G4 dendrons, respectively and (5) linear analog of the dendron, (6) Represents the chemical structure for the Polysilsesquioxane hydrate-octakis tetramethylammonium (POSS) molecule (7) represents the chemical structure for branched polyethylenimine (bPEI).

We gratefully acknowledge Dr. Ashootosh Ambade's group at CSIR-NCL for synthesizing these molecules and providing them to us. Detailed synthesis procedures are provided in the literature (Kumar et al.).[47] Chemical structures of all the molecules used in the experiments are shown in the schematics of Figure 2.2.

2.2.2 Sample Preparation:

100 mg of PAMAM dendron (G2, G3, or G4) was added to 100 μl of water to prepare a 50 wt% PAMAM/water stock solution. This stock solution was used to prepare GMO/water/PAMAM systems. For example, 500 mg of 80:20:4 GMO/water/G4 was prepared by mixing 384 mg of GMO with 96 mg of water and 40 mg of the PAMAM/water stock solution. This mixture was then heated to ~80 ^{o}C, and then cooled to room temperature. Samples were stored in a sealed Borosil vial for equilibration. Samples containing other additives or samples at other GMO/water ratios were prepared in a similar manner.

2.3 Characterisation

2.3.1 Small Angle X-ray Scattering (SAXS):

Small angle X-ray scattering (SAXS) experiments were carried out on a Bruker Nanostar machine equipped with a Cu rotating anode, with a tungsten filament

(filament size 0.1*1 mm^2). The SAXS was operated at a voltage of 45 kV and current of 20 mA. We used Cu K_α radiation (wavelength = 1.54 Å) and calibrated the detector with silver behenate. Samples were sandwiched between Kapton films and pasted on a metallic holder with a hole for X-rays to pass through. Scattering data were collected on a multiwire gas filled Hi-star 2D area detector and were reduced to 1D using the Bruker offline software.

2.3.2 Rheology:

Rheological experiments were performed to determine the mechanical properties of the mesophases. Experiments were carried on the MCR 301 (Anton Paar) using an 8 mm parallel plate assembly. Samples were carefully loaded on the plate after allowing several days for equilibration. All tests were carried out at 30 °C. Initially, we performed a stress ramp to determine the yield stress for the sample. We then loaded a fresh sample and conducted a creep test at a stress value significantly lower than the yield stress. The viscosity was calculated from the slope of the compliance curve. The yield stress, creep test parameters and viscosity are shown in Table 2.1.

2.3.3 Polarised Optical Microscopy Study (POM):

We performed optical microscopy between crossed polarizers on GMO–water–additive systems to visualise their textures and to identify phases. We used a Nikon Eclipse E600 POL with a conventional digital camera (Nikon) connected to a PC. Samples were mounted on a Linkam Shear cell CSS450 for controlled heating. The CSS450 stage is equipped with two heaters for the top and bottom plates. The sample was placed on the lower plate and sandwiched with a glass coverslip. The sample was heated at a rate of 5 °Cmin^{-1} up to ~80 °C and was subsequently cooled to ambient temperature. We identify the H_{II} phase based on characteristic focal conic textures and the L_α phase based on their streak-like textures. Polarized optical microscopy was used to assign the SAXS peaks to the H_{II} and L_α phases, since only a few peaks were observed for these phases. Fd3m and Ia3d phases are isotropic, and exhibit no texture under cross polarisation.

2.4 Results and Discussions

We were provided G2, G3 and G4 PAMAM dendrons that display terminal amine groups, synthesized using reported divergent procedures[48] (Figure 2.2; synthesis, characterization details; Schemes reported in the literature).[47] A linear analog of G4, that we term L4, with a matched number of amine groups on a methacrylate backbone was prepared using reported procedures[47,49] and was provided to us.

We use a commercial sample of monoolein (Rylo MG 20 Pharma, > 95% purity, henceforth referred to as GMO), that has been previously characterized.[35] Monoolein is widely used as a food emulsifier,[50] and more recently has found uses in pharmaceutical applications[51] and as a model lipid for thermodynamic investigations of phase behavior.[52,53]

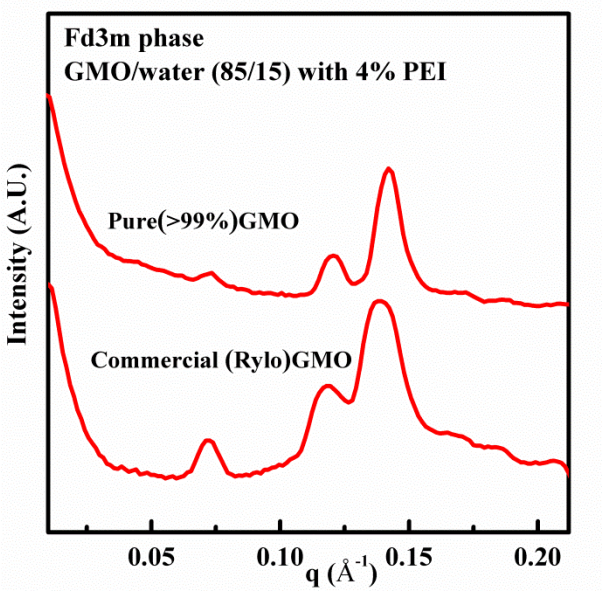

Figure 2.3: Control experiment comparing pure GMO (purity > 99%) and commercial GMO (Rylo) in ternary systems comprising GMO, water and a ternary polymeric additive (branched polyethyleneimine) in the ratio of 85:15:4, respectively.

An 80/20 (by weight) mixture of GMO/water forms a highly viscous phase, with room temperature creep viscosity on the order of 10^4 Pas (Table 2.1). With Φ = 2% G4 (viz., GMO: water: G4 = 80:20:2), the creep viscosity increases two-fold. For further addition of G4 (Φ = 4%, 6%), there is nearly a ten-fold increase in viscosity, to above 10^5 Pas (Figure 2.4 a). In contrast, for systems with Φ = 4% L4 (the linear analog of G4) there is a ~3-fold increase in viscosity that, for Φ =6% L4, decreases to a value similar to the neat GMO/water system (Figure 2.4 a). Thus, the effect of addition of G4 is qualitatively different when

compared with L4. We note that experiments repeated at a few selected compositions using high purity (≥99%) monoolein (Aldrich) showed identical results as with GMO (Figure 2.3), indicating the robustness of our results.

GMO/Water (80/20)

Composition stress ramp for creep test viscosity

(G4/L4)	**Yield stress (τ_y) Pa**		**Pa ($\tau < \tau_y$)**		**(η), Pa.s**	
Φ (w) %	**G4**	**L4**	**G4**	**L4**	**G4**	**L4**
0	**2.36**	**2.36**	**0.8**	**0.8**	10^4	10^4
2	**28.9**	------	**9**	-----	$2.5*10^4$	--------
4	**45.6**	**36.3**	**9**	**9**	$2*10^5$	$3.3*10^4$
6	**68.4**	**11.7**	**9**	**9**	$1.6*10^5$	$1.4*10^4$

Table 2.1: Creep viscosity measurement for GMO/water (80/20) system with G4 and L4 as a function of Φ.

The microstructural transformation that underlies this viscosity change is characterized using a combination of small angle X-ray scattering (SAXS) and optical microscopy. Phases are identified using SAXS peak positions: for the Ia3d phase, peaks at q values in the ratio of √6, √8, √14, are observed; at √2, √3, √4, √6, for Pn3m and √3, √8, √11, √12, for Fd3m. Samples are characterized after several days of equilibration at room temperature, when there is no further structural change.

The 80/20 GMO/water system shows a cubic bicontinuous phase with Ia3d symmetry, in accord with previous literature[51] (Figure 2.4 b). For systems with Φ =2% G4, we observe co-existence of Ia3d and reverse micellar hexagonal (H_{II}) phases (Figure 2.4 b, H_{II} phase characterized using optical microscopy: Figure 2.5). The discontinuous cubic Fd3m-reverse micellar phase is observed for 4 and 6% G4 (Figure 2.4 b, Figure 2.6).

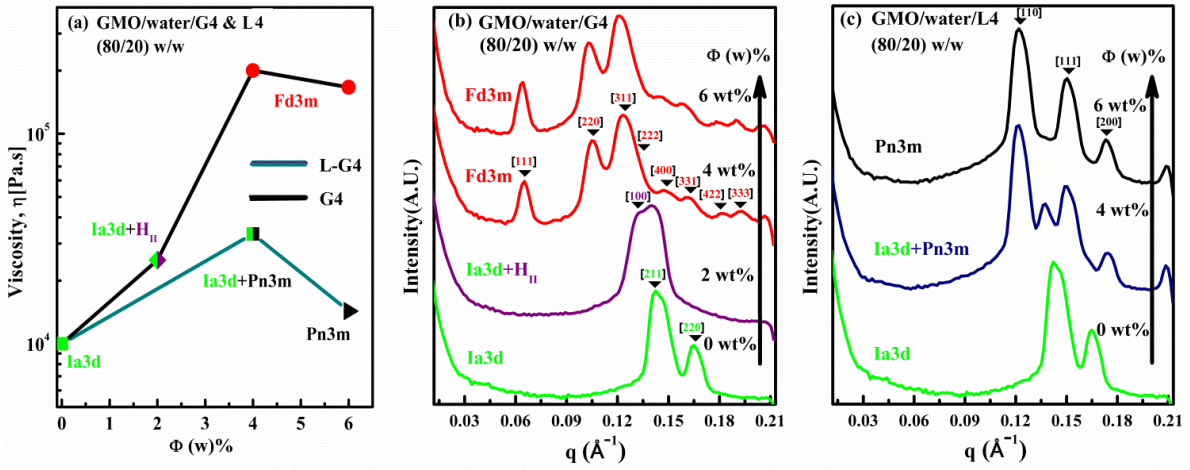

Figure 2.4: (a) Creep viscosity of the 80/20 GMO/water system containing the G4 dendron or its linear analog, L4, Φ represents the amount of the ternary inclusion. SAXS data for the 80/20 GMO/water system on addition of (b) G4 and (c) L4.

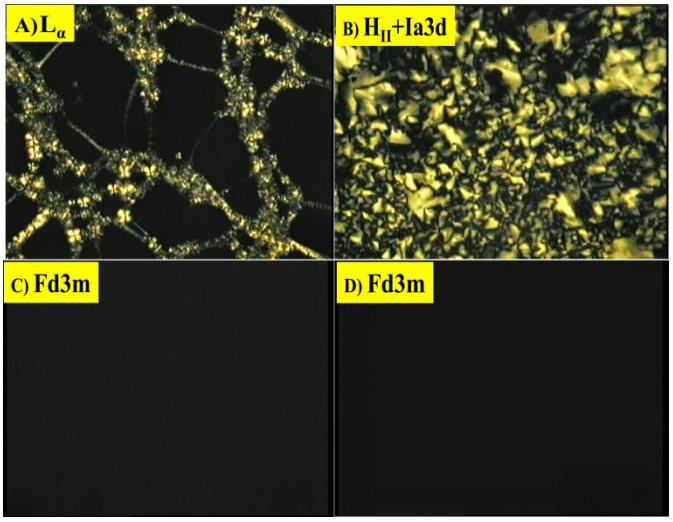

Fig. 2.5 Optical images for different liquid crystalline mesophases between crossed polarizers. (A) GMO/water/G4 (85/15/0) streak like features characteristic of the Lα phase are observed; (B) GMO/water/G4 (80/20/2) fan shaped structures characteristic of the H_{II} phase co-exist with Ia3d phase. (C) GMO/water/G4 (80/20/4); (D) GMO/water/G4 (80/20/6). The Fd3m phases identified from SAXS for (C) and (D) are isotropic, and appear dark between crossed polarisers.

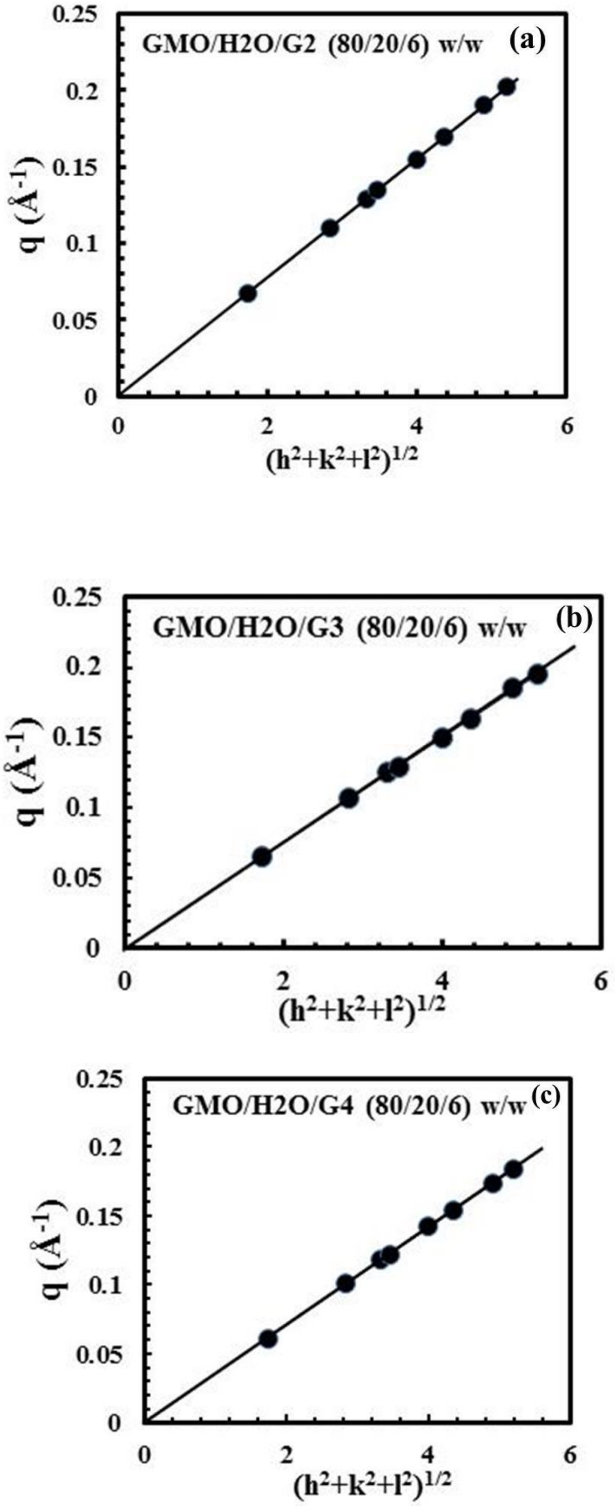

Figure 2.6: SAXS diffraction peaks for the GMO/water (80/20) w/w system in the presence of 6 wt.% G2, G3, and G4 are plotted as the peak spacing q_{hkl} *versus* $(h^2+k^2+l^2)^{1/2}$. The linear fit passes through the origin indicating that the system forms a structure with the Fd3m space group symmetry with lattice parameter (a) 162±1 Å for G2 (b) 166±2 Å for G3 and, (c) 173±1 Å for G4.

For systems with L4, we observe Ia3d and Pn3m co-existence at 4%, and a transformation into the Pn3m phase at 6% (Figure 2.4 c). Phase pure bicontinuous cubic phases (with Ia3d and Pn3m symmetry) have comparable high viscosities (~10^4 Pas). Regions of phase coexistence show a 2-3 fold increase in viscosity, while the discontinuous Fd3m micellar phase is associated with significantly higher viscosity, exceeding 10^5 Pas. Formation of an Fd3m phase by addition of hydrophilic molecules to the GMO/water system is unprecedented.

Our results indicate that the chain architecture of the polymeric additive is critical. Only the G4 dendron induces formation of the Fd3m phase, while its linear analog (L4) forms the Pn3m phase. Neat 80/20 and 75/25 GMO/water systems form a bicontinuous Ia3d phase while the 85/15 system forms a lamellar (L_α) phase (Figure 2.4 b). All three systems form the Fd3m phase at dendron loadings of 6% (Figure 2.7). At higher water concentration, for example 50/50 GMO/water, the cubic Pn3m phase co-exists with excess water. Due to the high viscosity of cubic phases, practical formulations utilize dispersions of Pn3m cubic phase particles in water, termed cubosomes.[54] We note that excess water Pn3m phases with 4% G4 dendrons also transform to discontinuous Fd3m micellar phases (Figure 2.8).

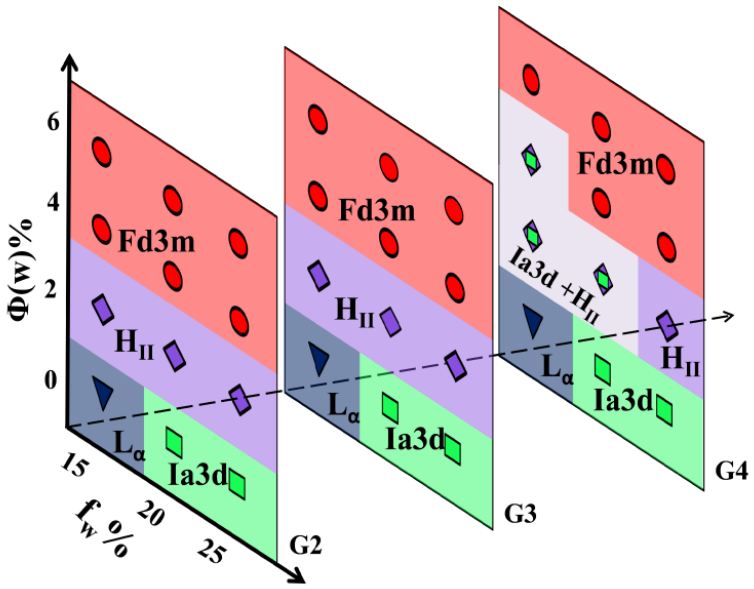

Figure 2.7: Equilibrium phase behavior of GMO/water system at room temperature with variation of G2, G3 and G4 content, Φ and for the variation of water fraction (f_w).

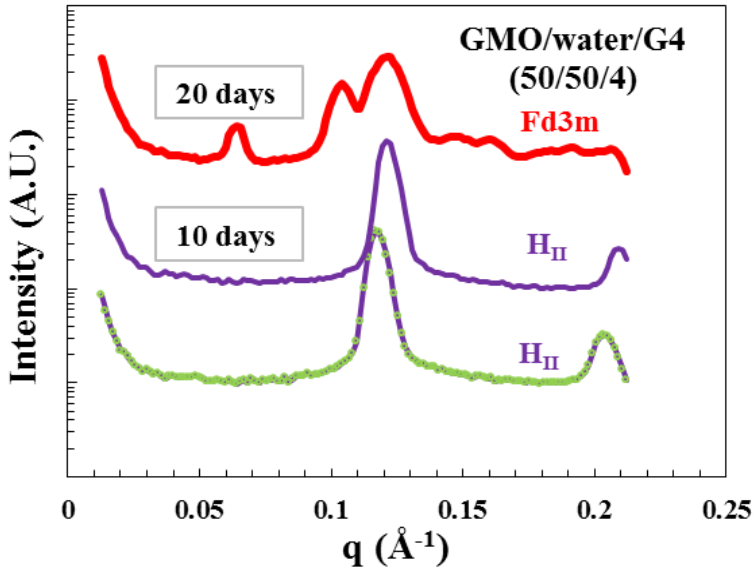

Figure 2.8: In a system containing GMO/water/G4 in the ratio 50/50/4, by weight, we observe a reverse hexagonal phase (peak ratio: 1:√3) at 5-10 days, that subsequently reorganizes to form an Fd3m phase that is observed after about 20 days of equilibration. Note that a cubic phase with Pn3m symmetry coexists with excess water for a binary 50:50 GMO/water system.

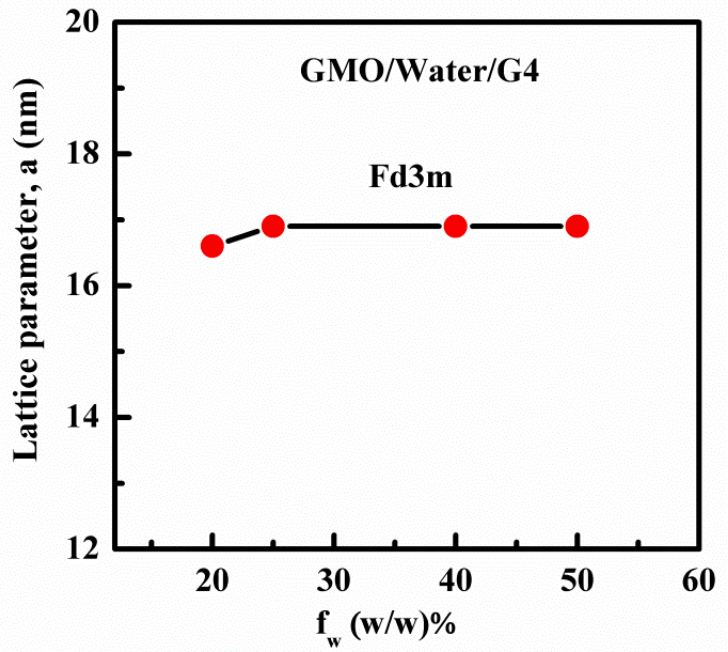

Figure 2.9: Lattice parameter for Fd3m phase in GMO/water/G4 PAMAM (Φ = 4%) system, as a function of water content.

For GMO/water/G4 (Φ = 4%), the Fd3m lattice parameter increases with water content, and saturates at 75/25 GMO/water (Figure 2.9). For higher water content, the Fd3m phase coexists with excess water. A discontinuous reverse micellar Fd3m phase also forms when second (G2) and third (G3) generation dendrons are added to the 80/20 GMO/water system (Figure 2.7. At 2% loading of G2 or G3, there is a transition to an H_{II} phase. At higher dendron concentrations (4% and 6%), we observe a transition to the Fd3m phase (Figure 2.7). This progression through the H_{II} phase, to the Fd3m is also observed at GMO/water ratios of 85/15 and 75/25. H_{II} or coexisting H_{II}/Ia3d phases are also observed for GMO/water with 2% G4.

Thus, at intermediate dendron concentrations, an H_{II} phase is observed as GMO/water systems transition to the Fd3m phase. In our experiments, samples are heated to high temperatures (≈ 80 ^{o}C), then cooled to room temperature and allowed to equilibrate over several days. The kinetics of Fd3m phase formation in GMO/water systems containing dendrons is a function of dendron generation.

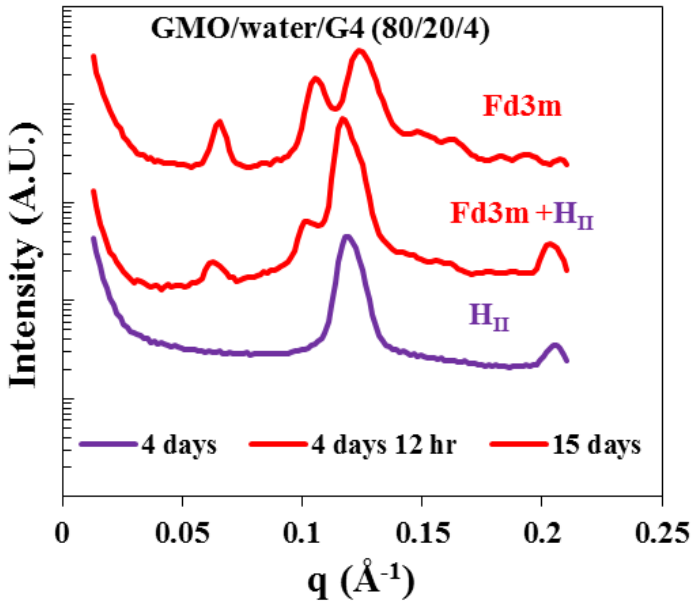

Figure 2.10: Kinetics of phase transformation: we observe structural changes for the 80:20:4 GMO/water/G4 systems as a function of equilibration time. This system forms the H_{II} phase in 4 days. We observe a coexistence of the H_{II} and Fd3m phases after about 4.5 days and finally, the Fd3m phase is observed after 15 days of equilibration.

The Fd3m phase forms relatively rapidly for G2 and G3 (~10 days) relative to the G4 (~15 days). In all cases, an intermediate H_{II} phase forms and is transformed into the Fd3m phase on equilibration (Figure 2.8 and 2.10). Hexagonal-cubic phase transitions have been reported[55] in block copolymer systems. In block copolymers, hexagonal cylinders pinch off to form a discontinuous body centered cubic phase.

In this context, we note that, for our GMO/water/dendron system, the lattice parameter characterizing the cubic Fd3m phase is always approximately $2\sqrt{2}$ times the H_{II} phase lattice parameter (Tables 2.2, 2.3, and 2.4). Thus, our observations suggest that, in analogy to the literature,[56-58] the formation of the Fd3m phase might happen through the breakup of micellar cylinders of the intermediate H_{II} phase. Transition pathways between bicontinuous cubic and H_{II} phases have been previously reported.[56-58] Our results suggest that the discontinuous Fd3m phase forms via an intermediate H_{II} phase for GMO/water/dendron systems.

GMO/water (85/15) w/w%			
Φ (w)%	**G2, a(Å)**	**G3, a(Å)**	**G4, a(Å)**
0	**39.8**	**39.8**	**39.8**
2	**52.0**	**54.8**	**-----**
4	**156.0**	**162.7**	**-----**
6	**159.3**	**166.2**	**169.9**

Table 2.2: Change in lattice parameters obtained from SAXS for the 85/15 GMO/water systems with variation of dendron (G2, G3, and G4) content, Φ. Different mesophases are obtained at different Φ, as detailed in Figures 2.4 and 2.7.

GMO/water (80/20) w/w%			
Φ (w)%	G2, a(Å)	G3, a(Å)	G4, a(Å)
0	108	108	108
2	54.2	59.2	-----
4	159.0	159.3	162
6	162	166.2	173

Table 2.3: Change in lattice parameters obtained from SAXS for the 80/20 GMO/water systems with variation of dendron (G2, G3, and G4) content, Φ.

GMO/water (75/25) w/w%			
Φ (w)%	G2, a(Å)	G3, a(Å)	G4, a(Å)
0	122.9	122.9	122.9
2	58.9	59.3	-----
4	159.0	162.7	169.9
6	162.7	166.2	------

Table 2.4: Change in lattice parameters obtained from SAXS for the 75/25 GMO/water systems with variation of dendron (G2, G3, and G4) content, Φ. Different mesophases are obtained at different Φ, as detailed in Figures 2.4 and 2.7.

We can derive insights from literature reports[47] of dendron-mediated mechanisms for formation of high curvature inverse micellar phases. Molecular Dynamics simulations carried out by Dr. Sudip Roy and Dr. Chandan Chaudhary at CSIR-NCL used a self-assembled GMO bilayer structure and introduced 9 G4 molecules (or 12 of their linear analogs, matching the 6% experimental concentration) at the interface of GMO bilayer head groups and water (Figure 2.11, taken from simulation data published in the literature). They have shown that G4 forms the aggregate in the

presence of water due to the intramolecular interactions of *t*-amine moiety with the amido–O. These G4 aggregate interacts with the bilayer (adopted Figure 2.11), interactions between the dendritic amine and GMO head group result in a peak in the distance distribution function at 0.35 nm.[47] This strong amine/GMO interaction drives the bilayer structure to bend, to maximize the number of GMO/amine contacts. The number of contacts between dendritic amine and GMO head-group oxygen increases with time, as does the bilayer curvature.[47] In contrast, the literature also shows the linear analog upon equilibration with the GMO bilayer, strong amine-GMO head-group interactions drive the linear molecule to spread on the bilayer to maximize amine-GMO interactions. These simulations suggest that strong attractive interactions between the GMO and amine groups play an important role in determining structure of the lipid assembly.

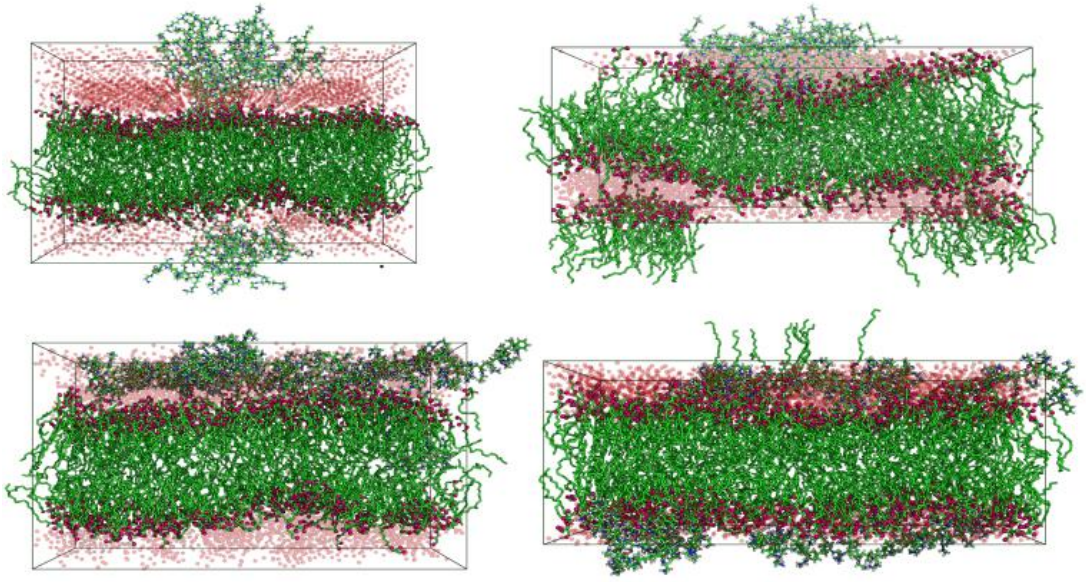

Figure 2.11: Snapshots from MD simulations of G4 dendron-GMO/water systems (top) and linear analog-GMO/water systems (bottom). Snapshots on the left represent starting configurations, while right represents structure after 100 ns (G4) and 200 ns (linear analogs) adapted from Kumar et al. 2015.[47]

In a control study to verify this, we investigated a ternary system of GMO/water/6% PAMAM G4-PEG, where the terminal primary amines are modified to present an oligomeric ethylene glycol moiety. These systems form only bicontinuous cubic phases and do not exhibit formation of an Fd3m phase (Figure 2.12), validating the role of GMO/amine interactions indicated by simulations.[47]

Simulation results[47] suggest how the structure of water soluble polymeric inclusions induces Fd3m phase formation. Clearly, addition of PAMAM dendrons does not mitigate packing frustration. Rather, strong interactions between the amine groups on the dendrons and the GMO head groups compensate for the increase in free energy due to the increased curvature of the discontinuous micellar phases. Dendrons have a compact molecular architecture. They aggregate to form clusters that interact with the GMO interface and bend it. Linear analogs of the dendrons can access a large number of conformational states. Therefore, these molecules can spread on the GMO surface when they adsorb while, this is not possible for dendrons. While synthesis of perfectly branched dendritic structures is well established, it is significantly easier to access randomly branched molecules, such as, for example, branched polyethylenimine (bPEI) (Schematic in Figure 2.2 (7)).

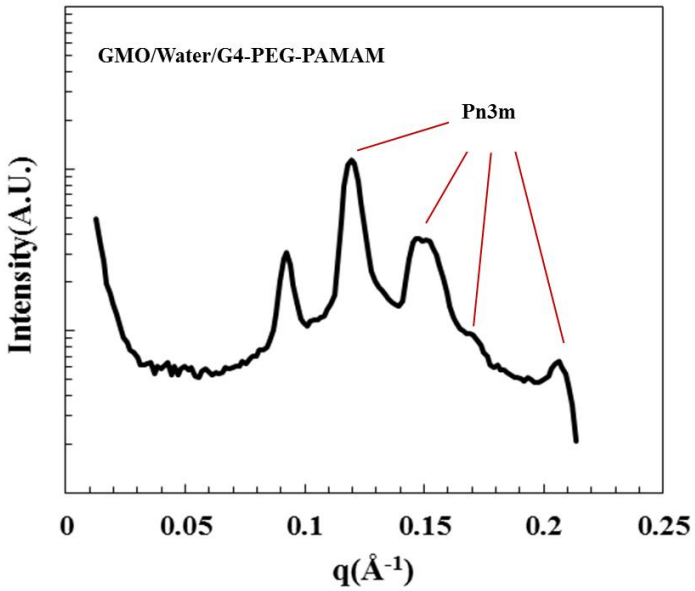

Figure 2.12: GMO/Water/G4-PEG-PAMAM system formed coexisting-Pn3m phase in 80:20:6 compositions (preferably Pn3m). Here, we modify the 1^{o} amine at the surface of G4 dendron with 5-mer PEG-chains, and it transforms the Ia3d phase in GMO/water (80/20) system into Pn3m phase.

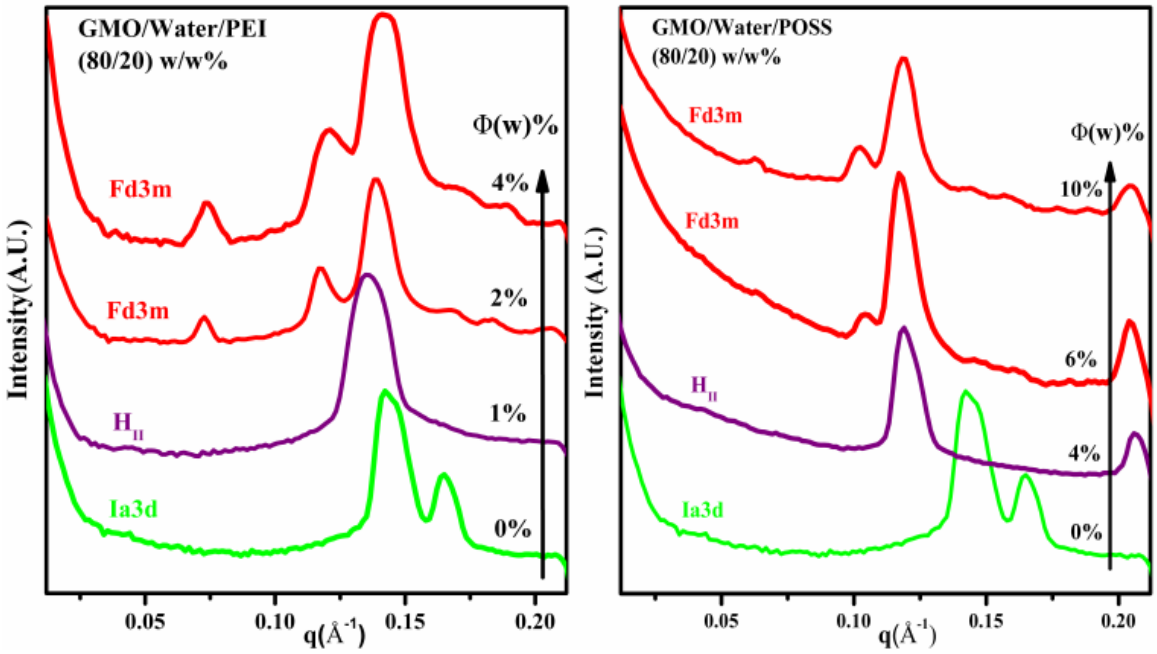

Figure 2.13: SAXS data for the (a) 80/20 GMO/water containing bPEI ternary additive. Φ represents the amount of bPEI in GMO/water. (b) GMO/water (80/20) containing POSS. Φ represents the amount of POSS in GMO/water system.

Branching of macromolecules results in a compact architecture, and, similar to PAMAM, bPEI presents primary amine groups (in addition to secondary and tertiary amines). Addition of Φ = 1% bPEI transforms 80/20 GMO/water from an Ia3d phase to an H_{II} phase. For higher bPEI content, Φ = 2, 4%, we observe the formation of an Fd3m phase (Figure 2.13 a). Further, we report that other moieties with functional groups that are very different from those present in PAMAM or bPEI, but that have compact molecular structures, and that interact with monoolein, also induce the formation of the Fd3m phase. It has been reported[59-61] that negatively charged silica nanoparticles interact with phytantriol, and are effective stabilizers for phytantriol dispersions. As the silica particles used in these reports were several tens of nanometers in size, we used a negatively charged silsequioxane cage as a molecular analog (POSS: Schematic in Figure 2.2 (6)). Remarkably, here too, we observed a transformation of an 80/20 monoolein water system from a bicontinuous Ia3d structure to an H_{II} phase (for POSS inclusion at Φ = 2, 4%) and to an Fd3m phase (at Φ = 6, 10%) (Figure 2.13 b). Our results suggest that addition of compact, interacting polar

macromolecular additives to monoolein/water open a new route to the Fd3m phase, through an intermediate H_{II} phase.

2.5 Summary

We demonstrate that the monoolein/water system can form a discontinuous reverse micellar Fd3m phase in ternary systems containing polar, water soluble macromolecular additives. Our results demonstrate a new pathway to the Fd3m phase through addition of polar molecules that is very different from previous reports where apolar oils were used as ternary components to access the Fd3m phase. We present selection rules for polar ternary additives that mediate the formation of the discontinuous reverse phase: additives with a compact molecular architecture and that have strong attractive interaction with the monoolein lipid induce formation of the Fd3m phase. We establish the general validity of these criteria by investigating monoolein/water systems containing three very different additives – that are all molecularly compact moieties that interact strongly with monoolein. Monoolein/water systems form Fd3m phases on addition of a few weight percent of PAMAM dendrons, branched PEI and silsesquioxane cages. Remarkably, while PAMAM dendrons induce Fd3m phase formations, their linear analogs with a matched number of amine groups do not. Formation of the Fd3m phase is always preceded by the formation of an intermediate reverse hexagonal phase. This work presents evidence for an unprecedented route to Fd3m phase formation in lipid/water systems. Our work has implications for fundamental understanding of the principles that guide lipid assembly.

2.6 References

1. Shearman, G.; Tyler, A.; Brooks, N.; Templer, R.; Ces, O.; Law, R.; Seddon, J., Ordered Micellar and Inverse Micellar Lyotropic Phases. *Liq. Cryst.* **2010**, *37*, 679-694.
2. Rappolt, M.; Cacho-Nerin, F.; Morello, C.; Yaghmur, A., How the Chain Configuration Governs the Packing of Inverted Micelles in the Cubic Fd3m-Phase. *Soft Matter* **2013**, *9*, 6291.
3. Shearman, G, C. ; Arwen, T, ; Nicholas J. B.; Richard, H. ; Templer, Oscar Ces, Robert V. Law, and John M. Seddon. A 3-D Hexagonal Inverse Micellar Lyotropic Phase. *J. Am. Chem. Soc.* **2009**, *131*, 1678-1679.
4. Luzzati, V.; Vargas, R.; Gulik, A.; Mariani, P.; Seddon, J. M.; Rivas, E., Lipid polymorphism: a correction. The Structure of the Cubic Phase of Extinction Symbol Fd--Consists of Two Types of Disjointed Reverse Micelles Embedded in A 3-D Hydrocarbon Matrix. *Biochemistry* **1992**, *31*, 279-285.
5. Duesing, P.; Seddon, J.; Templer, R.; Mannock, D., Pressure Effects on Lamellar and Inverse Curved Phases of Fully Hydrated Dialkyl Phosphatidylethanolamines and β-D-Xylopyranosyl-Sn-Glycerols. *Langmuir* **1997**, *13*, 2655-2664.
6. Seddon, J. M.; Zeb, N.; Templer, R. H.; McElhaney, R. N.; Mannock, D. A., An Fd3m Lyotropic Cubic Phase in a Binary Glycolipid/Water System. *Langmuir* **1996**, *12*, 5250-5253.
7. Seddon, J. M.; Robins, J.; Gulik-Krzywicki, T.; Delacroix, H., Inverse Micellar Phases of Phospholipids and Glycolipids. Invited Lecture. *Phys. Chem. Chem. Phys.* **2000,** *2*, 4485-4493.
8. Yaghmur, A.; De Campo, L.; Sagalowicz, L.; Leser, M. E.; Glatter, O., Emulsified Microemulsions and Oil-Containing Liquid Crystalline Phases. *Langmuir* **2005,** *21*, 569-577.
9. Yaghmur, A.; De Campo, L.; Salentinig, S.; Sagalowicz, L.; Leser, M. E.; Glatter, O., Oil-Loaded Monolinolein-Based Particles with Confined Inverse Discontinuous Cubic Structure (Fd3m). *Langmuir* **2005,** *22*, 517-521.
10. Chemelli, A.; Maurer, M.; Geier, R.; Glatter, O., Optimized Loading and Sustained Release of Hydrophilic Proteins from Internally Nanostructured Particles. *Langmuir* **2012,** *28*, 16788-16797.

11. Pouzot, M.; Mezzenga, R.; Leser, M. E.; Sagalowicz, L.; Guillot, S.; Glatter, O., Structural and Rheological Investigation of Fd3m Inverse Micellar Cubic Phases. *Langmuir* **2007**, *23*, 9618-9628.
12. Sagalowicz, L.; Guillot, S.; Acquistapace, S.; Schmitt, B.; Maurer, M.; Yaghmur, A.; De Campo, L.; Rouvet, M.; Leser, M.; Glatter, O., Influence of Vitamin E Acetate and Other Lipids on the Phase Behavior of Mesophases Based on Unsaturated Monoglycerides. *Langmuir* **2013**, *29*, 8222-8232.
13. Martiel, I.; Sagalowicz, L.; Mezzenga, R., Phospholipid-Based Nonlamellar Mesophases for Delivery Systems: Bridging The Gap Between Empirical and Rational Design. *Adv. Colloid Interface Sci.* **2014**, *209*, 127-143.
14. Martiel, I.; Sagalowicz, L.; Mezzenga, R., A Reverse Micellar Mesophase of Face-Centered Cubic $Fm\bar{3}m$ Symmetry in Phosphatidylcholine/Water/Organic Solvent Ternary Systems. *Langmuir* **2014,** 29, 15805-15812.
15. Angelov, B.; Angelova, A.; Ollivon, M.; Bourgaux, C.; Campitelli, A., Diamond-Type Lipid Cubic Phase with Large Water Channels. *J. Am. Chem. Soc.* **2003**, *125*, 7188-7189.
16. Angelov, B.; Angelova, A.; Papahadjopoulos-Sternberg, B.; Lesieur, S.; Sadoc, J. F.; Ollivon, M.; Couvreur, P., Detailed Structure of Diamond-Type Lipid Cubic Nanoparticles. *J. Am. Chem. Soc.* **2006**, *128*, 5813-5817.
17. Angelov, B.; Angelova, A.; Garamus, V. M.; Lebas, G.; Lesieur, S.; Ollivon, M.; Funari, S. S.; Willumeit, R.; Couvreur, P., Small-Angle Neutron And X-Ray Scattering From Amphiphilic Stimuli-Responsive Diamond-Type Bicontinuous Cubic Phase. *J. Am. Chem. Soc.* **2007**, *129*, 13474-13479.
18. Mezzenga, R.; Grigorov, M.; Zhang, Z.; Servais, C.; Sagalowicz, L.; Romoscanu, A. I.; Khanna, V.; Meyer, C., Polysaccharide-Induced Order-to-Order Transitions in Lyotropic Liquid Crystals. *Langmuir* **2005**, *21*, 6165-6169.
19. Rädler, J. O.; Koltover, I.; Salditt, T.; Safinya, C. R., Structure of DNA-Cationic Liposome Complexes: DNA Intercalation in Multilamellar Membranes in Distinct Interhelical Packing Regimes. *Science* **1997**, *275*, 810-814.
20. Bilalov, A.; Elsing, J.; Haas, E.; Schmidt, C.; Olsson, U., Embedding DNA in Surfactant Mesophases: The Phase Diagram of the Ternary System Dodecyltrimethylammonium–DNA/Monoolein/Water in Comparison to the DNA-Free Analogue. *J. colloid Interface Sci.* **2013**, *394*, 360-367.

21. Phan, S.; Fong, W. K.; Kirby, N.; Hanley, T.; Boyd, B. J., Evaluating the Link between Self-Assembled Mesophase Structure and Drug Release. *Int. J. Pharm.* **2011**, *421*, 176-182.
22. Mezzenga, R.; Schurtenberger, P.; Burbidge, A.; Michel, M., Understanding Foods as Soft Materials. *Nat. Mater.* **2005**, *4*, 729-740.
23. Vauthey, S.; Milo, C.; Frossard, P.; Garti, N.; Leser, M.; Watzke, H., Structured Fluids as Micro Reactors for Flavour Formation by the Maillard Reaction. *J. Agric. Food Chem.* **2000**, *48*, 4808-4816.
24. Krog, N. J., Food Emulsifiers and Their Chemical and Physical Properties. *Food Emulsions* **1997**
25. Patton, J. S.; Carey, M. C., Watching Fat Digestion. *Science*, **1979**, *204*, 145-148
26. Mann, S.; Ozin, G. A., Synthesis of Inorganic Materials with Complex Form. *Nature* **1996**, *382*, 313-318.
27. Archibald, D. D.; Mann, S., Template Mineralization of Self-Assembled Anisotropic Lipid Microstructures. *Nature* **1993**, *364*, 430-433.
28. Caffrey, M.; Li, D.; Dukkipati, A., Membrane Protein Structure Determination Using Crystallography and Lipidic Mesophases: Recent Advances and Successes. *Biochemistry* **2012,** *51*, 6266-6288
29. Larsson, K., Aqueous Dispersions of Cubic Lipid–Water Phases. *Curr. Opin. Colloid Interface Sci.* **2000**, *5*, 64-69.
30. Safinya, C. R., Structures of Lipid–DNA Complexes: Supra Molecular Assembly and Gene Delivery. *Curr. Opin. Struct. Biol.* **2001**, *11*, 440-448.
31. Fong, C.; Le, T.; Drummond, C. J., Lyotropic Liquid Crystal Engineering–Ordered Nanostructured Small Molecule Amphiphile Self-Assembly Materials by Design. *Chem. Soc. Rev.* **2012**, *41*, 1297-1322
32. Angelova, A.; Angelov, B.; Garamus, V. M.; Couvreur, P.; Lesieur, S., Small-Angle X-Ray Scattering Investigations of Biomolecular Confinement, Loading, and Release From Liquid-Crystalline Nanochannel Assemblies. *J. Phys. Chem. Lett.* **2012**, *3*, 445-457.
33. Barauskas, J.; Johnsson, M.; Tiberg, F., Self-Assembled Lipid Superstructures: Beyond Vesicles and Liposomes. *Nano Lett.* **2005**, *5*, 1615-1619
34. Danino, D.; Kesselman, E.; Saper, G.; Petrache, H. I.; Harries, D., Osmotically Induced Reversible Transitions in Lipid-DNA Mesophases. *Biophys. J.* **2009**, *96*, L43-L45.

35. Deshpande, S.; Venugopal, E.; Ramagiri, S.; Bellare, J. R.; Kumaraswamy, G.; Singh, N., Enhancing Cubosome Functionality by Coating with a Single Layer of Poly-ε-Lysine. *ACS Appl. Mater. Interfaces* **2014**, *6*, 17126-17133.
36. Israelachvili, J. N., *Intermolecular and Surface Forces. 2nd Edition*, Academic Press, New York, **2011**.
37. Warriner, H. E.; Idziak, S. H.; Slack, N. L.; Davidson, P.; Safinya, C. R., Lamellar Biogels: Fluid-Membrane-Based Hydrogels Containing Polymer Lipids. *Science* **1996**, *271*, 969-973.
38. Ligoure, C.; Bouglet, G.; Porte, G., Polymer Induced Phase Separation in Lyotropic Smectics. *Phys. Rev. Lett.* **1993**, *71*, 3600.
39. Radlinska, E.; Gulik-Krzywicki, T.; Lafuma, F.; Langevin, D.; Urbach, W.; Williams, C., Modification of the Lamellar Phase in C12E5/Water System by a Random Hydrophilic-Hydrophobic Polyelectrolyte. *J. De Phys. II* **1997**, *7*, 1393-1416
40. Pal, A.; Bharath, P.; Dastidar, S. G.; Raghunathan, V., Collapse and Coacervation of a Lamellar Phase by Inter-Headgroup Bridging. *Soft Matter* **2012**, *8*, 927-930.
41. Yang, Y.; Prudhomme, R.; McGrath, K.; Richetti, P.; Marques, C., Confinement of Polysoaps in Membrane Lyotropic Phases. *Phys. Rev. Lett.* **1998**, *80*, 2729-2732.
42. Nicot, C.; Waks, M.; Ober, R.; Gulik-Krzywicki, T.; Urbach, W., Squeezing of Oil-Swollen Surfactant Bilayers by a Membrane Protein. *Phys. Rev. Lett.* **1996**, *77*, 3485-3488.
43. Ramos, L.; Ligoure, C., Copolymer-Induced Stabilizing Effect of Highly Swollen Hexagonal Mesophases. *Langmuir* **2008**, *24*, 5221-5224.
44. Auth, T.; Gompper, G., Self-Avoiding Linear and Star Polymers Anchored to Membranes. *Phys. Rev. E: Stat. Nonlinear Soft Matter Phys.* **2003**, *68*, 051801.
45. Menjoge, A. R.; Kannan, R. M.; Tomalia, D. A., Dendrimer-Based Drug and Imaging Conjugates: Design Considerations for Nano medical Applications. *Drug Discov. Today* **2010**, *15*, 171-185.
46. Sharma, K. P.; Choudhury, C. K.; Srivastava, S.; Davis, H.; Rajamohanan, P.; Roy, S.; Kumaraswamy, G., Assembly of Polye thyleneimine in the Hexagonal Mesophase of Non Ionic Surfactant: Effect of pH and Temperature. *J. Phys. Chem. B* **2011**, *115*, 9059-9069.
47. Kumar, M.; Patil, N. G.; Choudhury, C. K.; Roy, S.; Ambade, A. V.; Kumaraswamy, G., Compact Polar Moieties Induce Lipid–Water Systems to form Discontinuous Reverse Micellar Phase. *Soft Matter* **2015**, *11*, 5417-5424.

48. Lee, J. W.; Kim, J. H.; Kim, H. J.; Han, S. C.; Kim, J. H.; Shin, W. S.; Jin, S. H., Synthesis of Symmetrical and Unsymmetrical PAMAM Dendrimers by Fusion Between Azide-and Alkyne-Functionalized PAMAM Dendrons. *Bioconjugate Chem.* **2007**, *18*, 579-584.
49. Wang, H.; Zhuang, J.; Thayumanavan, S., Functionalizable Amine-Based Polymer Nano Particles. *ACS Macro Lett.* **2013**, *2*, 948-951.
50. Rousseau, D., Fat Crystals and Emulsion Stability–A Review. *Food Res. Int.* **2000**, *33*, 3-14.
51. Ganem-Quintanar, A.; Quintanar-Guerrero, D.; Buri, P., Monoolein: A Review of The Pharmaceutical Applications. *Drug Dev. Ind. Pharma* **2000**, *26*, 809-820.
52. Kulkarni, C. V.; Wachter, W.; Iglesias-Salto, G.; Engelskirchen, S.; Ahualli, S., Monoolein: A Magic Lipid? *Phys. Chem. Chem. Phys.* **2011**, *13*, 3004-3021.
53. Qiu, H.; Caffrey, M., The Phase Diagram of The Monoolein/Water System: Metastability and Equilibrium Aspects. *Biomaterials* **2000**, *21*, 223-234.
54. Landh, T., Phase-Behavior In The System Pine Oil Monoglycerides-Poloxamer-407-Water at 20 °C. *J. Phys. Chem.* **1994**, *98*, 8453-8467.
55. Lee, H. H.; Jeong, W. Y.; Kim, J. K.; Ihn, K. J.; Kornfield, J. A.; Wang, Z. G.; Qi, S., Orientational Proliferation and Successive Twinning from Thermo reversible Hexagonal – Body Centered Cubic Transitions. *Macromolecules* **2002**, ***35***, 785-794.
56. Caffrey, M., The Study of Lipid Phase Transitions by Time-Resolved X-Ray Diffraction. *Biochemistry* **1987**, *26*, 6349-6363.
57. Caboi, F.; Amico, G. S.; Pitzalis, P.; Monduzzi, M.; Nylander, T.; Larsson, K., Addition of Hydrophilic and Lipophilic Compounds of Biological Relevance to the Monoolein/Water System. I. Phase Behaviour. *Chem. Phys. Lipids* **2001**, *109*, 47-62.
58. Marrink, S. J.; Tieleman, D. P., Molecular Dynamics Simulation of Spontaneous Membrane Fusion during a Cubic-Hexagonal Phase Transition. *Biophysical J.* **2002**, *83*, 2386-2392.
59. Salonen, A.; Muller, F.; Glatter, O., Dispersions of Internally Liquid Crystalline Systems Stabilized by Charged Disk like Particles as Pickering Emulsions: Basic Properties and Time-Resolved Behavior. *Langmuir* **2008**, *24*, 5306-5314
60. Dulle, M.; Glatter, O., Internally Self-Assembled Sub-Micrometer Emulsions Stabilized with a Charged Polymer with Silica Particles. *Langmuir* **2011**, *28*, 1136-1141

61. Salonen, A.; Muller, F.; Glatter, O., Internally Self-Assembled Sub Micrometer Emulsions Stabilized by Spherical Nano Colloids: Finding the Free Nano particles in the Aqueous Continuous Phase. *Langmuir* **2010**, *26*, 7981-7987

Chapter 3

Inclusion of 5th generation PAMAM Dendron in Lipid/Water System Induces Formation of unusual P4$_3$32 Mesophase

3.1 Introduction

Biological processes such as protein signalling and aggregation,[1] and the interaction of drugs and enzymes with cells, are regulated by the curvature in the cell membrane.[2-7]The shape adopted by a membrane depends on its intrinsic curvature, its bending rigidity and on its interactions with cellular components such as proteins.[8]Lipid membranes in cells can adopt a wide variety of shapes, including bicontinuous cubic gyroid phases present in the plasma membrane, Pn3m phases in the ER membrane, and G-type mesophases in the mitochondrial membrane.[9] During fat digestion in the gut, monoglycerides and fatty acids form a micellar cubic Q227 mesophase.[10,11]The biological significance of some these structures is not yet clear. However, it appears that Nature uses control of membrane curvature as a tool in regulating biological processes.

One of the factors that influences curvature in lipid membranes is the presence of proteins that interact with or that are embedded in the membrane. Therefore, it is important to study the interactions of proteins with lipid molecules that form membranes. Cytochrome c is a biologically important membrane binding protein that acts as an electron carrier in eukaryotes.[12]Given the importance of this protein, the thermodynamics of lipid/water systems containing Cytochrome c have been investigated in the literature.[13-15]Specifically, structural transitions in bicontinuous cubic lipid mesophases containing Cytochrome c have been investigated.[13,14]Mariani et al. have shown that Cytochrome c induces the formation of the cubic $P4_32$ mesophase in glycerol monooleate (GMO) lipid –water systems at room temperature.[15] Winter et. al. have also reported observation of the $P4_32$ mesophase during their investigations of the effect of temperature and pressure on GMO/water/Cytochrome c systems.[12,16]Cytochrome c is the only known example of a protein that can induce the formation of the $P4_32$ phase in GMO-water systems.[17]The $P4_32$ mesophase is a highly unusual phase. Structurally, it can be thought of as a cubic Ia3d mesophase where out of two networks of water channels, one is replaced by spherical micelles. Thus, the $P4_32$ phase structure comprises of both the continuous water channels and discontinuous micelles.

Recently, we have investigated the phase behaviour of the GMO–water system in the presence of PAMAM (Polyamidoamine) dendrons (G1-G4).[18]Our study reveals that hydrophilic polymeric ternary components can effectively change the curvature of the lipid bilayer. PAMAM dendrons induce the formation of stable reverse hexagonal (H_{II}) and cubic reverse micellar (Fd3m) mesophases at room temperature in the GMO/water system. The

formation of these phases is driven by strong attractive interactions between the polar head group of GMO and the dendron amines. Here, we demonstrate that inclusion of the 5th generation (G5) PAMAM dendron induces the formation of the $P4_332$ phase in GMO/water systems at room temperature. This is the first experimental demonstration of formation of the $P4_332$ phase by addition of a synthetic polymer to the GMO/water system.

3.2 Experimental Section

3.2.1 Materials:

The lipid, glycerol monooleate (commercial name: Rylo Pharma MG 20), was received as a generous gift from Danisco, India. Here, we refer to this as GMO. GMO was thoroughly characterised in our previous studies and has a purity >98%.[19,20] All experiments were carried out using the same batch of GMO. A 5th generation dendron based on polyamidoamine (called PAMAM-G5) was synthesised using a convergent approach, as reported in our previous work. Details of the synthetic protocol and characterization are provided in our previous work.[18] We used distilled deionized water for sample preparation, with a resistivity ≈ 18 MΩ/cm.

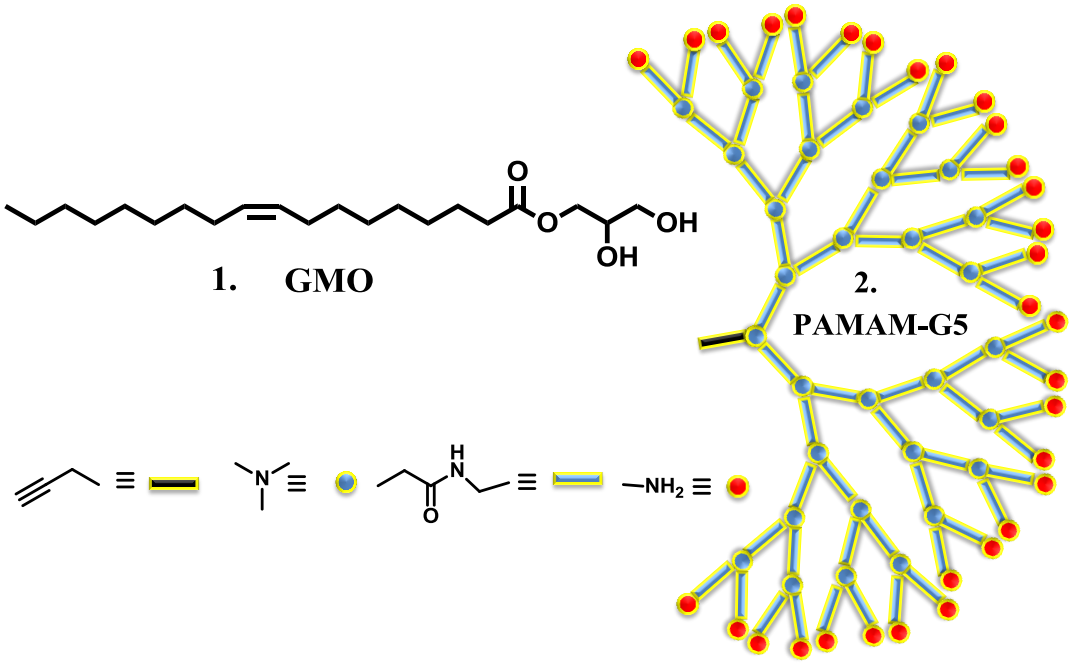

Figure 3.1: Schematics of (1) GMO; (2) Poly-amidoamine dendron (PAMAM-G5).

3.2.2 Sample Preparation:

GMO is a hydrophobic non-ionic lipid with an HLB value of 3.8, and is insoluble in water. It is a white solid at room temperature. We store GMO at -80°C to avoid degradation of the lipid. Before sample preparation, we melt GMO at 80°C. PAMAM-G5 was used as a 50% (w/w) stock solution in water. Samples were prepared by mixing the three components GMO, water and PAMAM-G5 in a closed vial. The weight fraction of the PAMAM-G5 in the final sample is represented as Φ. We report data for samples with GMO/water in the ratio of 85/15 and 80/20.To prepare 0.5 g of sample with GMO/water in the ratio of 85/15 and with Φ = 2%, 20 mg of PAMAM-G5 stock solution was thoroughly mixed with 63.5 mg of water and then added to 416.5 mg of GMO. Thorough mixing of the components was carried out by repeatedly heating to 80°C followed by vortexing. The samples were stored for 10-15 days to ensure equilibration. Similarly, we prepared samples with Φ = 0.5%, 1%, 2% and 4%.

3.3 Characterisation

3.3.1 Small Angle X-ray Scattering:

We characterized samples using polarized optical microscopy (POM) and Small Angle X-ray Scattering (SAXS). SAXS measurements were carried out using NANO-Viewer, Rigaku (Japan). The instrument is equipped with a microfocus point source (Cu rotating anode) and a three-pinhole collimation system. It operates at 40kV voltage and 30mA current. A Confocal Max Flux (CMF) mirror and three slit collimation system generates a monochromatic and collimated beam of X-rays. We exposed the sample to Cu K_α radiation of wavelength, λ=1.543 Å. The sample was placed between two Kapton® films that were separated with the help of an O-ring to maintain a 1mm gap, mounted in a Linkam HFSX-350-CAP stage placed in the X-ray beam path. Scattered radiation was collected on a HyPix-3000 2D semiconductor detector with pixel size of 100 microns x 100 microns (sample to detector distance = 738 mm). We calibrated the sample to detector distance using a silver behenate standard. The 2D image was integrated over a q-range 0.01 $Å^{-1}$ to 0.31 $Å^{-1}$ and converted to 1D data using offline Rigaku SAXS analysis software. Samples were loaded in X-ray capillaries and were heated to 90 °C and then cooled to room temperature to erase shear effects during sample loading. Temperature dependent measurements were performed by heating the sample at a rate of 2 °C/min. Once samples were heated to the desired temperature, they were held for 5 minutes before SAXS measurements were performed.

3.3.2 Polarised Optical Microscopy:

We characterized the phase of the sample using optical microscopy (Olympus BX-50, mounted with a Nikon camera). Samples were observed between crossed-polarizers and characteristic birefringent patterns were used to identify the mesophase structure. Samples were subjected to controlled heating at 2^oC/min rate to 90^oC and then cooled to the desired temperature using a CSS450 Linkam stage, mounted on the microscope.

3.4 Results

3.4.1 Phase Behaviour of 85/15 GMO/Water; 0 ≤ Φ ≤ 4%:

An 85:15, GMO/water binary system (viz. not containing PAMAM-G5 ternary component, $\Phi = 0$) forms a lamellar (L_α) phase at room temperature (= 25^oC). The lamellar phase was identified from the characteristic oil-streak textures observed using optical microscopy between cross-polarizers. We also characterised the lamellar phase using SAXS which shows only one peak at q = 0.155 $Å^{-1}$ with a d-spacing of 40 Å. Higher order SAXS peaks from the lamellar structure cannot be observed since they appear at higher q than the range of the instrument at this setting (q_{max} = 0.31 $Å^{-1}$). Upon addition of Φ = 0.5% PAMAM-G5, the L_α phase transforms into a cubic phase. The absence of textures when observed between crossed polarizers is consistent with formation of an optically isotropic cubic phase. SAXS for the ternary mixture shows peaks at q = 0.147, 0.169, 0.225, 0.239 and 0.269 $Å^{-1}$, in peak position ratios of √6: √8: √14: √16… This corresponds to the Ia3d cubic mesophase. At low q, additional peaks were observed at q = 0.0964 $Å^{-1}$ and 0.1148 $Å^{-1}$, viz. with peak positions in a ratio of √2: √3. We note that mesophases with cubic $P4_332$ symmetry show Bragg reflections with characteristic peak ratios of √2, √3, √5 √6, √8, √9, √11, √12, √13, √14, √16, √17, √19…. [21,22]Therefore, the ternary sample GMO/water/PAMAM-G5, at Φ=0.5%, appears to show coexistence between Ia3d and $P4_332$ mesophases.

At higher concentration of PAMAM-G5 (Φ = 1%) we observe that the sample is dark when viewed between crossed polarizers. SAXS confirms the formation of an Ia3d cubic phase with the Bragg reflections shifted to slightly higher q (compared with the Φ = 0.5% sample). This shift to higher q corresponds to a decrease in d-spacing from 42.75 Å to 40.15 Å and in lattice parameter, a from 104.7Å to 99.24 Å. We also observe peaks corresponding to the $P4_332$ mesophase at q < 0.155$Å^{-1}$. The increase in the number of characteristic SAXS peaks corresponding to the $P4_332$ mesophase qualitatively suggests an increase in the fraction

of the $P4_332$ mesophase in the coexisting $P4_332$/Ia3d mixture. Further increase in PAMAM-G5 to Φ = 2% (at constant water fraction, f_w = 15%) results in the development of characteristic textures, observed using polarized optical microscopy, that correspond to the inverse hexagonal (H_{II}) mesophase. SAXS from this sample reveals that the H_{II} mesophase coexists with the $P4_332$ mesophase. SAXS peaks at q = 0.146 $Å^{-1}$ and 0.263 $Å^{-1}$ (in 1: √3 ratio) correspond to the reverse hexagonal, H_{II} phase and seven Bragg peaks corresponding to

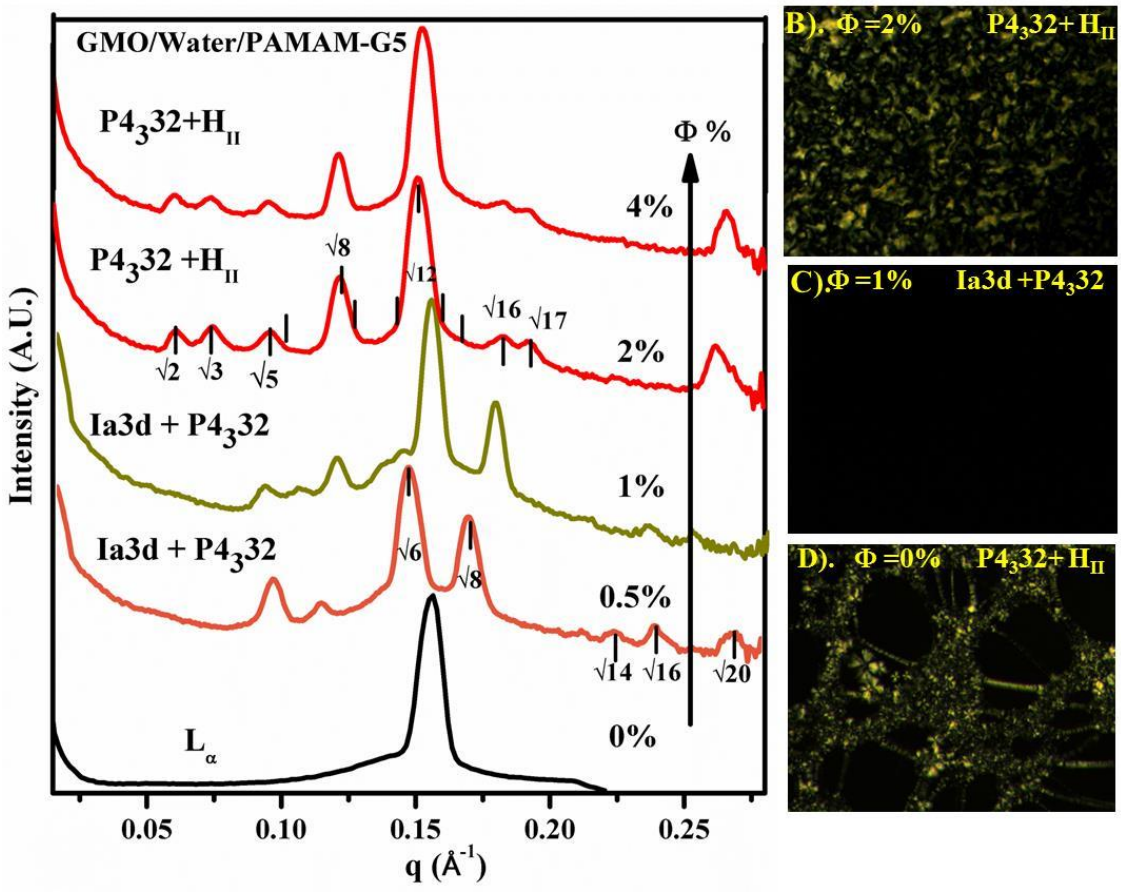

Figure 3.2: (A) SAXS data showing Bragg reflections for GMO/water/PAMAM-G5 ternary system where the water fraction, f_w=15% and for PAMAM-G5 concentration, Φ = 0, 0.5, 1, 2 and 4% (wt. %). SAXS data reveal that the L_α phase is formed at Φ = 0%, that transforms to a coexistence between Ia3d and $P4_332$ at Φ =1% and to coexistence between $P4_332$ and H_{II} at Φ = 2%. Figure 2 B, 2 C & 2 D are the POM images for GMO/water/PAMAM-G5 mesophases at Φ = 0, 1 and 2 wt. %, respectively. Ia3d and $P4_332$ mesophases are isotropic and appear dark between crossed polarizers while the H_{II} and L_α phases are anisotropic and show streak-like textures for lamellar and cone type textures for the hexagonal mesophase.

-the $P4_332$ mesophase can be readily observed (with peak characteristic ratios of √2, √3, √5, √6, √8, √9, √11).[21,22] We plot the SAXS peak positions, q for the peaks from the $P4_332$ phase as a function of $P = (h^2 + k^2 + l^2)^{1/2}$ where h, k, l are the Miller indices (Figure 3). This plot is linear and we obtain a lattice parameter, a = 150 Å, that characterizes the $P4_332$ (Q^{212}) cubic phase.

The $P4_332$ mesophase is retained even at higher PAMAM-G5 concentrations, Φ = 4%. As the dendron concentration is increased, the SAXS peaks corresponding to the $P4_332$ phase are shifted to lower q, indicating an increase in the lattice parameter, while peaks corresponding to the H_{II} phase are shifted to higher q.

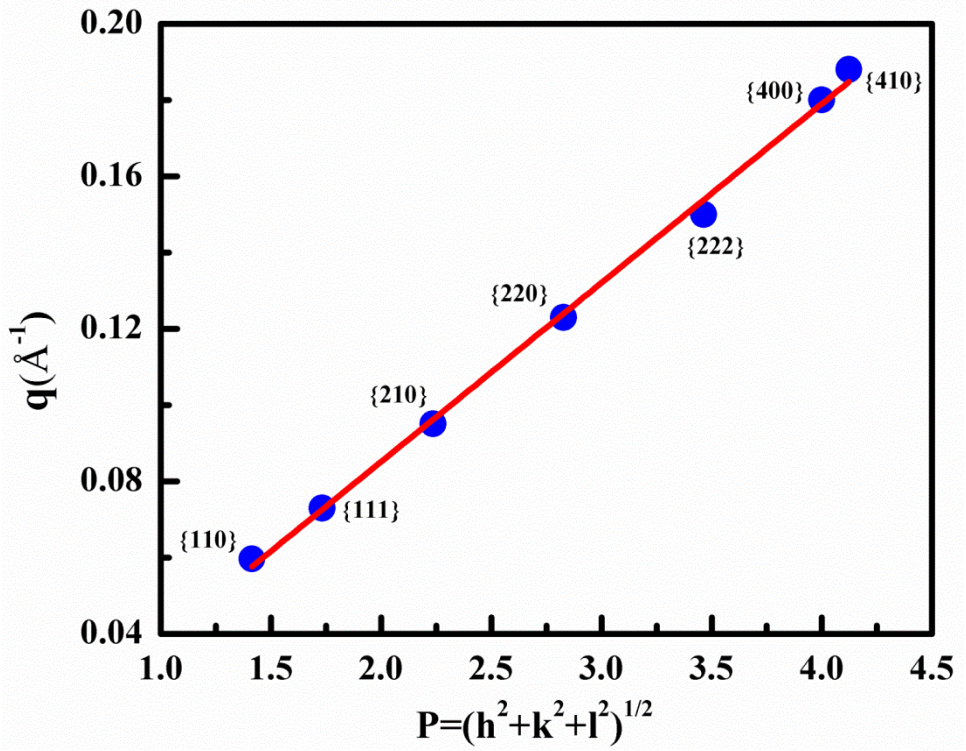

Figure 3.3: Plot of SAXS peak positions, q ($Å^{-1}$) vs P = $\sqrt{(h^2+K^2+l^2)}$ for GMO/water/PAMAM-G5 (Φ = 2%) at 25 °C. We observe seven peaks that correspond to Bragg reflections for {110}, {111}, {210}, {220}, {222}, {400} and {410}. The reciprocal gradient of the slope is used to determines the lattice parameter, a=150 Å.

3.4.2 Phase Behaviour of 80/20 GMO/Water; 0 ≤ Φ ≤ 4%:

GMO-water systems with f_w = 20% also show the formation of the $P4_332$ phase on addition of PAMAM-G5 as a ternary component. The binary GMO/water system organizes into an Ia3d mesophase at room temperature, and this phase is retained in

GMO/water/PAMAM-G5 at Φ = 0.5% (Figure 4). Addition of more PAMAM-G5 (Φ=1%) results in Ia3d/$P4_332$ co-existence, confirmed by Bragg reflections for the $P4_332$ phase observed at low q (Figure 4). As the PAMAM-G5 concentration is further increased (Φ= 2 & 4%) the $P4_332$ mesophase is observed to coexist with an H_{II} mesophase (Figure 4).

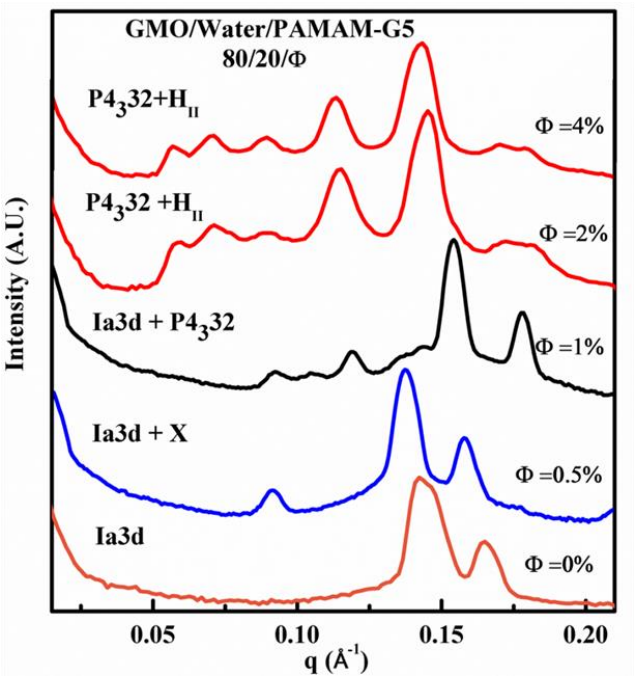

Figure 3.4: SAXS data for ternary GMO/water/PAMAM-G5 system for f_w = 20% and at T=25 °C. Plot shows the effect of PAMAM-G5 concentration (Φ) on constant water fraction (f_w) GMO-water (80/20) system. The PAMAM-G5 concentration varies from Φ = 0,0.5,1 & 4% (by weight).

3.4.3 Phase Behaviour of GMO/Water/PAMAM-G5 as a Function of Temperature:

We have investigated the effect of heating the ternary system, GMO/water/PAMAM-G5 (f_w = 15%, Φ = 0 to 4%) from 25°C to 85°C. The lamellar (L_α) mesophase formed in the GMO/water binary system (f_w = 15%, Φ = 0%) transforms into an Ia3d phase upon heating to 45°C. On heating above 55°C, the Ia3d mesophase transforms into the reverse micellar L_2 mesophase. On addition of PAMAM-G5 (Φ = 0.5%, f_w = 15%) a coexisting Ia3d/$P4_332$ structure forms. On heating between 25 °C< T < 60 °C, this coexisting structure is retained with a small shift in the Ia3d mesophase SAXS peaks to higher q (Figure 5 A & Figure 6 A). At 60°C, three phases Ia3d/$P4_332$/H_{II} co-exist (Figure 5 A & Figure 6 A). On further increase of temperature to 65°C, peaks corresponding to the Ia3d and $P4_332$ mesophases disappear and only the H_{II} mesophase is retained. Conic textures corresponding to the H_{II}

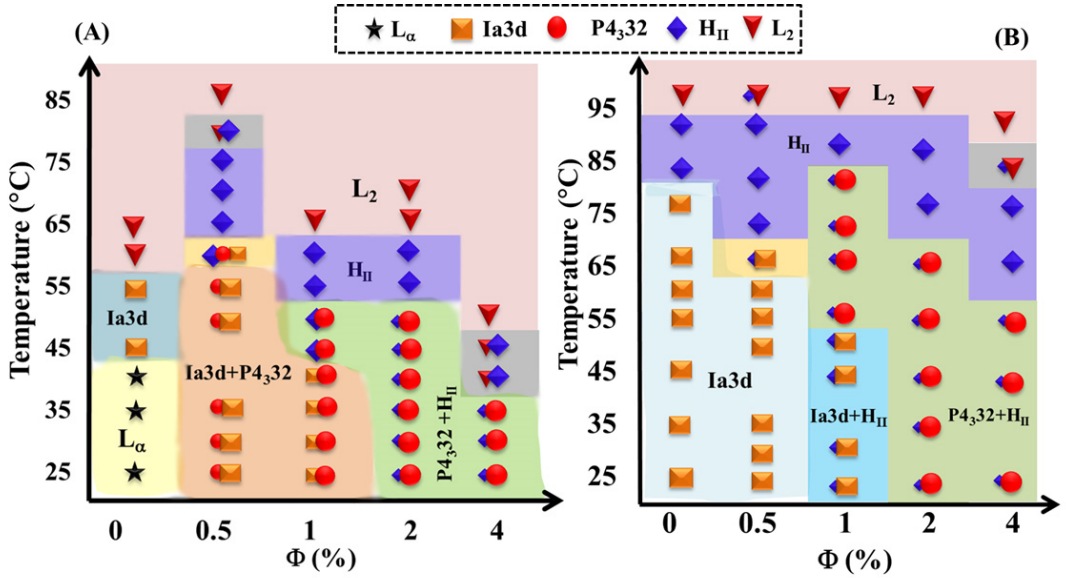

Figure 3.5: (A) Phase diagram for GMO/water/PAMAM-G5 ternary system as a function of PAMAM-G5 concentration (Φ = 0 to 4%) and temperature (from 25 °C to 85 °C). Data is presented for (A) f_w = 15% and (B) f_w = 20%.

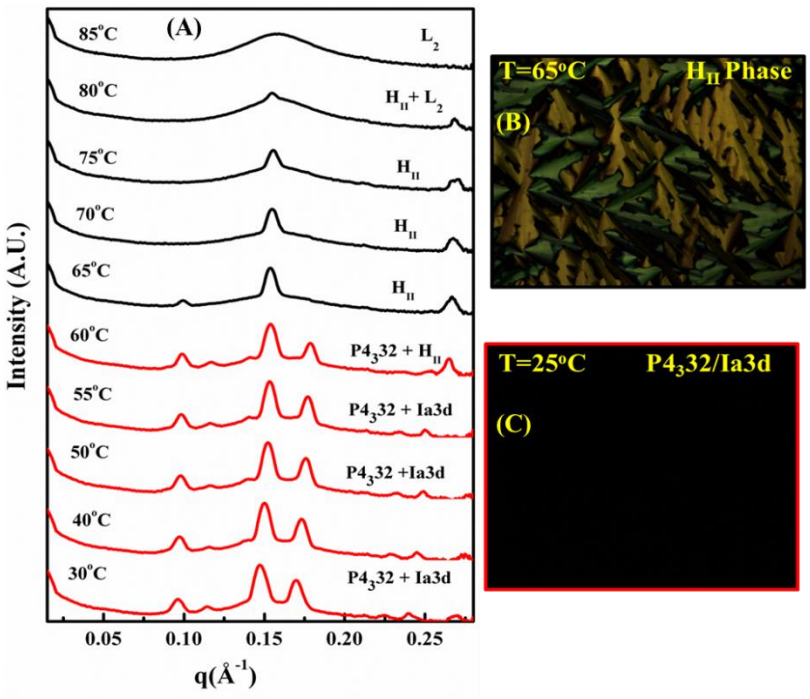

Figure 3.6: (A) SAXS data for ternary GMO/water/PAMAM-G5 (85/15/0.5) at constant Φ = 0.5% & f_w = 15% with temperature varies from 25 °C to 85 °C. The elevation in temperature shows the transition of the mesophases as $P4_332$/Ia3d→$P4_332$/H_{II}→H_{II}→H_{II}/L_2→L_2. (B) POM image shows cone type textures at T = 65 °C, characteristic of the H_{II} mesophase. (C) POM image shows no textures for cubic $P4_332$/Ia3d co-existing mesophases at T = 25 °C.

mesophase are also visible in POM on heating to 65°C (Figure 6 A, B). The H_{II} mesophase transforms to L_2 for T ≥ 80°C (Figure 5 A & Figure 6 A).

For systems with f_w = 15% and Φ = 1%, heating to 45°C results in a transformation from Ia3d/$P4_332$ coexistence to H_{II}/$P4_332$ coexistence (Figure 5 A, Figure 7 A). Further heating to 55°C melts the $P4_332$ mesophase. The H_{II} phase persists until a temperature of 60°C and transforms to the L_2 phase at 70°C. As before, phases were confirmed using both SAXS and POM (Figure 5 A, Figure 7 A & 7 B). At Φ = 2% and 4%, coexisting $P4_332$/H_{II} phases are observed at room temperature. With increase in PAMAM-G5, there is a decrease in the temperature at which the $P4_332$ phase disappears (from 55°C for Φ = 1% and 2% to 40°C for Φ = 4%). For Φ = 2%, the H_{II} mesophase transforms to an L_2 phase at 65°C (Figure 5 A, Figure 8 A). For Φ = 4%, the H_{II} mesophase coexists with the L_2 phase between 35 – 45°C and then transforms to the L_2 phase at higher temperatures (Figure 5 A, Figure 8 B).

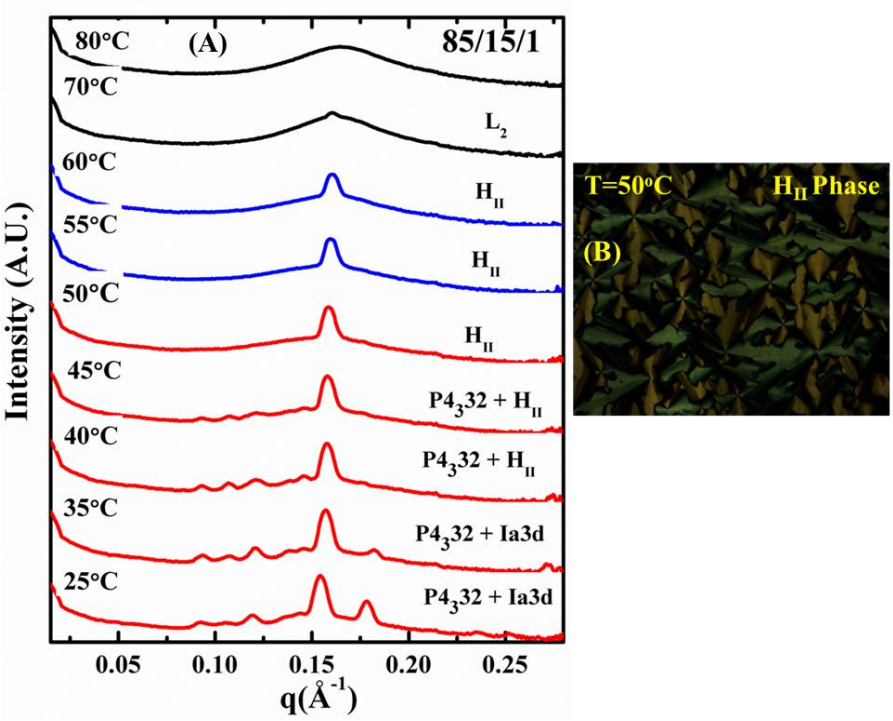

Figure 3.7: (A) SAXS data for ternary GMO/water/PAMAM-G5 (85/15/1) at Φ = 1% & f_w = 15% as temperature is varied from 25 °C to 80 °C. On heating, we observe a transition from $P4_332$/Ia3d → P4332/H_{II} → H_{II} → L_2. (B) POM image shows cone type textures at T = 50 °C characteristic of the H_{II} mesophase.

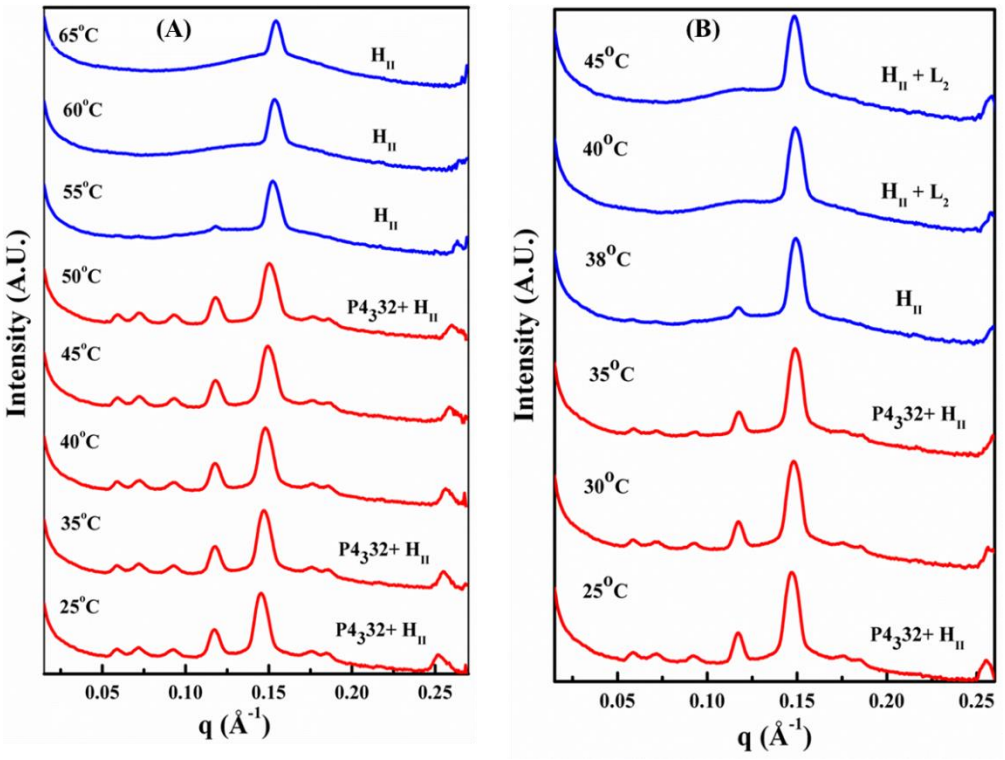

Figure 3.8: (A) SAXS data for ternary GMO/water/PAMAM-G5 (85/15/2) at Φ = 2% & f_w = 15% on heating from 25 °C to 65 °C. (B) SAXS data for ternary GMO/water/PAMAM-G5 (85/15/4) at Φ = 4% & f_w = 15% on heating from 25 °C to 45 °C.

At higher water fraction, f_w = 20%, the Ia3d mesophase formed for Φ = 0 and 0.5% transforms to the H_{II} mesophase at 80°C and 65°C, respectively. On further heating to 90°C, the L_2 phase forms (Figure 5 B, Figure 9 A & 9 B). For Φ = 1%, the Ia3d/H_{II} structure formed at 25°C transforms to $P4_332/H_{II}$ on heating to 55°C. At 85°C, this transforms to the H_{II} mesophase and finally to L_2 at 90°C (Figure 5 B & Figure 9 B). Here too, on increasing Φ, the $P4_332$ phase persists to lower temperature (65°C and 55°C, for Φ from 2% and 4%, respectively). At higher temperatures, there is a transition to the H_{II} phase and finally, the L_2 phase forms above 90°C (Figure 5 B, Figure 10 B).

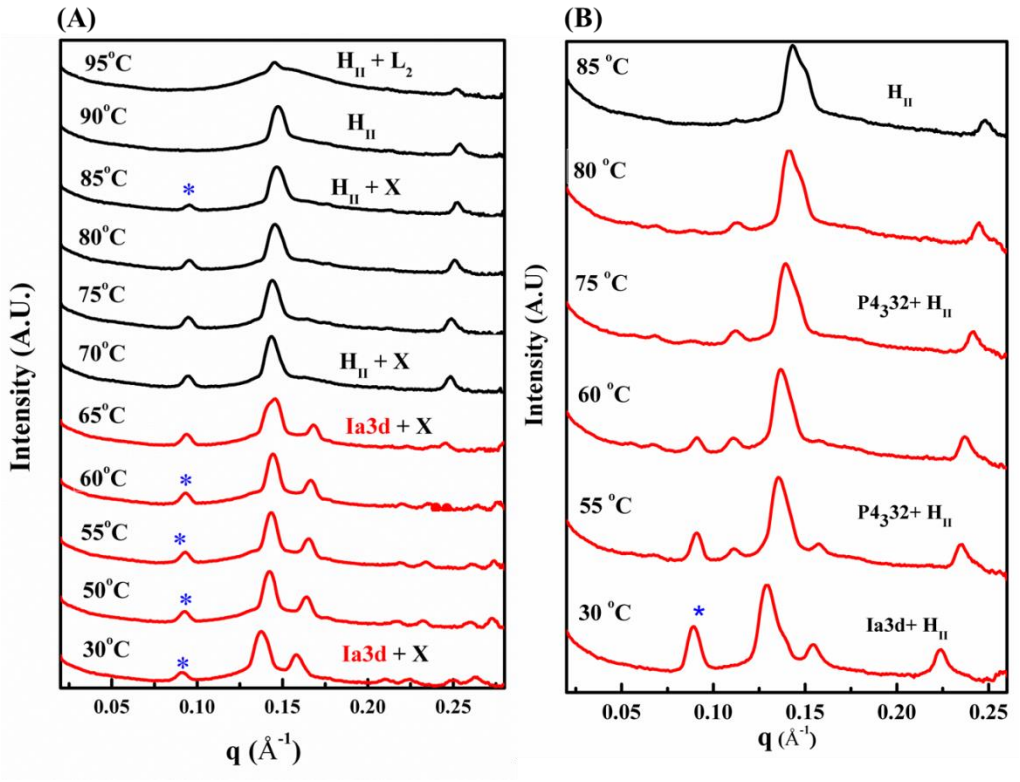

Figure 3.9: (A) SAXS data for ternary GMO/water/PAMAM-G5 (80/20/0.5) at Φ = 0.5% & f_w = 20% on heating from 25 °C to 95 °C. At low q, some peaks corresponding to unknown structures are observed and are marked with (*). (B) SAXS data for ternary GMO/water/PAMAM-G5 (80/20/1) at Φ = 1% & f_w = 20% on heating from 25 °C to 90 °C.

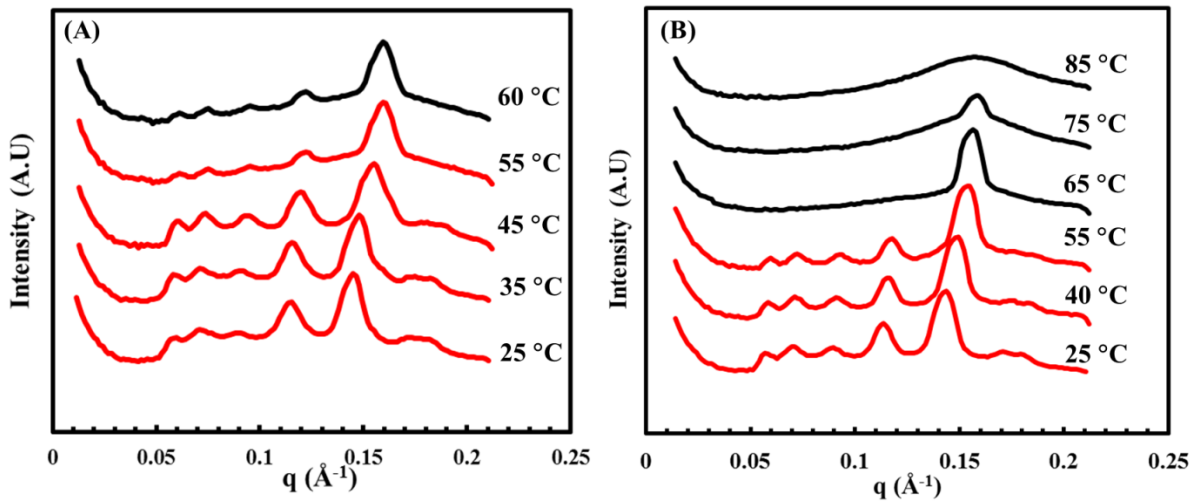

Figure 3.10: (A) SAXS data for ternary GMO/water/PAMAM-G5 (80/20/2) at Φ = 2% & f_w = 20% on heating from 25°C to 95°C. (B) SAXS data for ternary GMO/water/PAMAM-G5 (80/20/4) at Φ = 4% & f_w = 20% on heating from 25°C to 80°C.

3.5 Discussion

The $P4_332$ phase can be thought of as being derived from the Ia3d structure. The Ia3d phase comprises two unconnected three-dimensional networks of rod-like structures linked through a coplanar three-rod junction.[23,24] The $P4_332$ mesophase preserves one of the two 3D networks of rods in the Ia3d cubic mesophase. In the other, every second three rod junction is replaced by a micelle.[15]Thus, the cubic $P4_332$ structure is an intermediate structure between bicontinuous and discontinuous micellar phases.[25]The $P4_332$ mesophase has cubic symmetry, and is dark when observed between crossed polarizers (see, for example: Figure 2 C, for coexisting Ia3d/$P4_332$ mesophases at Φ = 0.5 and 1%). Such intermediate structures with $P4_332$ symmetry are rare and have not been reported in lipid-water binary systems. Such structures have been previously reported only for ternary lipid-water-protein systems[13,14] Mariani et al. have reported the formation of a $P4_332$ phase in ternary systems containing GMO, water and the hydrophilic protein, cytochrome-c.[15]

The GMO-water binary system organizes into L_α and bicontinuous Ia3d and Pn3m cubic phases at room temperature.[26,27]As the temperature is increased to 80^{o}C, there is dehydration of the head group, resulting in an increase in curvature and formation of the H_{II} mesophase. High curvature phases such as the H_{II} phase do not form at room temperature in the binary system. Reverse hexagonal phases can form in ternary systems containing GMO, water and (a) polar moieties with an affinity for water that dehydrate the GMO head group[28-31] or (b) apolar oils that swell the tails and increase the apparent packing factor.[32,33]Even higher curvature Fd3m phases have been reported at room temperature on addition of apolar oils, to compensate for the packing frustration in such systems.[34-40] Recently, we reported a novel route to the Fd3m phase at room temperature, through incorporation of compact, polar macromolecules.[18] These polymers contain amine groups that induce curvature of the GMO bilayers through their strong interactions with the GMO head group. We demonstrated the important role played by the macromolecular architecture in inducing curvature. Branched, compact macromolecules induced the formation of the Fd3m phase through attractive interactions with the GMO head group. In contrast, the attractive interactions between amine groups on the analogous linear polymers and the GMO head groups drove adsorption and spreading of these polymers on the GMO bilayer. Thus, linear amine containing polymers could not induce the formation of high curvature phases.

Specifically, we had shown[18] that PAMAM dendrons synthesized to second (G2), third (G3) and fourth (G4) generations induced Fd3m formation. The dendrons are incorporated into the GMO/water system and induce the formation of curved reverse micellar structures that pack into the F3m phase. The Fd3m phase comprises reverse micelles of two different sizes arranged into an AB_2 type structure. Such AB_2 structures have also been shown to form in bidisperse colloidal systems when the ratio of colloid sizes is in the range of $0.482 \leq B/A \leq 0.624$.[41] There is no colloidal equivalent of the $P4_332$ phase. Our results suggest that the as the size of the PAMAM dendrons increases from G2 to G4, the ratio of the two micellar sizes formed in the GMO/water/PAMAM ternary system is within the range that results in AB_2 structure formation. Increase to G5, however, results in the formation of the $P4_332$ mesophase. G5 has larger molecular dimensions compared with G2 – G4 and has 32 terminal amine groups (compared with 16 for G4). Therefore, it is reasonable to expect that G5 will interact much more strongly with the GMO head group, compared with G2 – G4.

In ternary systems containing G2 – G4, the formation of the Fd3m phase happens through an intermediate H_{II} phase. On heating the Fd3m phase to high temperature, there is a transition to an L_2 phase. In contrast, for the systems containing G5, described in this work, we notice that the $P4_332$ phase coexists with Ia3d, Pn3m or H_{II} phases. On heating, the $P4_332$ phase transforms into the H_{II} phase and then, at higher temperatures, to the L_2 phase.

Thus, while the G5 dendron interacts with the GMO head groups through terminal amine groups, its size precludes formation of the Fd3m phase. Instead, it forms the $P4_332$ phase, intermediate between the Ia3d and the discontinuous micellar phases. We note, again, aspects of the structural similarity between the G5 dendron and cytochrome c. Both are compact objects, decorated with amine groups and with a size approaching 3 nm. It appears that compact moieties in this size range, bearing groups that have attractive interactions with GMO lipid induce formation of the $P4_332$ phase.

3.6 Summary

Inclusion of 5th generation PAMAM dendron (G5) in the GMO/water system results in the formation of the $P4_332$ mesophase, in contrast to the G2 – G4 dendrons that induce formation of the discontinuous reverse micellar Fd3m phase. Formation of the $P4_332$ mesophase is reported for GMO/water systems containing water fractions, f_w = 15% and 20%. For f_w = 15%, we observe $P4_332$/Ia3d coexistence for low PAMAM-G5 concentrations (Φ < 2%) and

$P4_332/H_{II}$ coexistence at Φ = 2 to 4%. Systems with f_w=20% show the formation of the $P4_332$ phase only at higher concentrations (Φ = 2 & 4%), where it coexists with the H_{II} phase. On heating, the $P4_332$ phases transform into the H_{II} phase and eventually into the L_2 phase. Our work has implications for systematic understanding of how a combination of molecular size and branched architecture induces curvature in model lipid systems.

3.7 References:

1. Sugiura, Y.; Ikeda, K.; Nakano, M., High Membrane Curvature Enhances Binding, Conformational Changes, and Fibrillation of Amyloid-β on Lipid Bilayer Surfaces. *Langmuir* **2015,** *31*, 11549-11557.
2. Drin, G.; Antonny, B., Amphipathic Helices and Membrane Curvature. *FEBS Lett.* **2010,** *584*, 1840-1847.
3. Madsen, K. L.; Bhatia, V. K.; Gether, U.; Stamou, D., BAR Domains, Amphipathic Helices and Membrane–Anchored Proteins use the Same Mechanism to Sense Membrane Curvature. *FEBS Lett.***2010,** *584*, 1848-1855.
4. Hyde, S.; Blum, Z.; Landh, T.; Lidin, S.; Ninham, B. W.; Andersson, S.; Larsson, K., *The Language of Shape: the role of curvature in condensed matter: physics, chemistry and biology*. Elsevier: 1996.
5. McMahon, H. T.; Gallop, J. L., Membrane Curvature and Mechanisms of Dynamic Cell Membrane Remodelling. *Nature* **2005,** *438*, 590-596.
6. Zimmerberg, J.; Kozlov, M. M., How Proteins Produce Cellular Membrane Curvature. *Nat. Rev. Mol. Cell Biol.* **2006,** *7*, 9-19.
7. Marsh, D., Elastic Curvature Constants of Lipid Monolayers and Bilayers. *Chem. Phys. Lipids* **2006,** *144*, 146-159.
8. Mouritsen, O. G., Lipids, Curvature, and Nano–Medicine. *Eur. J. Lipid Sci. Technol.* **2011,** *113*, 1174-1187.
9. Luzzati, V.; Vargas, R.; Gulik, A.; Mariani, P.; Seddon, J. M.; Rivas, E., Lipid Polymorphism: A Correction. The Structure of the Cubic Phase of Extinction Symbol Fd--Consists of Two Types of Disjointed Reverse Micelles Embedded in a 3D-Hydrocarbon Matrix. *Biochemistry* **1992,** *31*, 279-285.
10. Kulkarni, C. V., Lipid Crystallization: From Self-Assembly to Hierarchical and Biological Ordering. *Nanoscale* **2013,** *4*, 5779-5791.
11. Luzzati, V., Biological Significance of Lipid Polymorphism: The Cubic Phases. *Curr. Opin. Struct. Biol.* **1997,** *7*, 661-668.
12. Razumas, V.; Talaikyte, Z.; Barauskas, J.; Larsson, K.; Miezis Y.; Nylander, T., Effects of Distearoyl Phosphatidylglycerol and Lysozyme on the Structure of the Monoolein–Water Cubic Phase: X-ray Diffraction and Raman Scattering Studies. *Chem. Phys. Lipids* **1996**, *84*, 123–138.

13. Kraineva, J.; Narayanan, R. A.; Kondrashkina, E.; Thiyagarajan, P.; Winter, R., Kinetics of Lamellar to Cubic and Inter Cubic Phase Transitions of Pure and Cytochrome-c Containing Monoolein Dispersions Monitored by Time-Resolved Small-Angle X-ray Diffraction. *Langmuir* **2005,** *21*, 3559-3571

14. Lendermann, J.; Winter R., Interaction of Cytochrome c with Cubic Monoolein Mesophases at Limited Hydration Conditions: The Effects of Concentration, Temperature and Pressure. *Phys. Chem. Chem. Phys.* **2003**, *5*, 1440–1450.
15. Mariani, P.; Luzzati, V.; Delacroix, H., Cubic phases of lipid-containing systems – structure-analysis and biological implications. *J. Mol. Biol.* **1988**, *204*, 165–188.
16. Tanaka, S.; Maki S.; Ataka, M., Structural Transitions of the Monoolein Bicontinuous Cubic Phase Induced by Inclusion of Protein Lysozyme Solutions. *Phys. Rev. E* **2006**, *73*, 061510.
17. Conn, C. E.; Drummond, C. J., Nanostructured bicontinuous cubic lipid self-assembly materials as matrices for protein encapsulation. *Soft Matter* **2013**.
18. Kumar, M.; Patil, N. G.; Choudhury, C. K.; Roy, S.; Ambade, A. V.; Kumaraswamy, G., Compact Polar Moieties Induce Lipid–Water Systems to Form Discontinuous Reverse Micellar Phase. *Soft Matter* **2015,** *11*, 5417-5424.
19. Kumar, M.; Kumaraswamy, G., Phase Behaviour of the Ternary System: Monoolein–Water–Branched Polyethylenimine. *Soft Matter* **2015**, *11*, 5705-5711.
20. Deshpande, S.; Venugopal, E.; Ramagiri, S.; Bellare, J. R.; Kumaraswamy, G.; Singh, N., Enhancing Cubosome Functionality by Coating with a Single Layer of Poly-ε-lysine. *ACS Appl. Mater. Interfaces* **2014,** *6*, 17126-17133.
21. Angelova, A.; Ionov, R.; Koch, M. H. J.; Rapp, G., Interaction of the Peptide Antibiotic Alamethicin with Bilayer and Non-Bilayer Forming Lipids: Influence of Increasing Alamethicin Concentration on the Lipids Supramolecular Structures. *Arch. Biochemistry Biophys.* **2000,** *378*, 93-106.
22. Mazzoni, S.; Barbosa, L. R. S.; Funari, S. S.; Itri, R.; Mariani, P., Cytochrome-c Affects the Monoolein Polymorphism: Consequences for Stability and Loading Efficiency of Drug Delivery Systems. *Langmuir* **2016,** *32*, 873-881.
23. Luzzati, V.; Spegt, P. A., Polymorphism of lipids. *Nature* **1967,** *215*, 701-704.
24. Luzzati, V., X-ray Diffraction Studies of Lipid-Water Systems. *Biol. Membr.* **1968,** *1*, 71-123.

25. Luzzati, V.; Vargas, R.; Mariani, P.; Gulik, A.; Delacroix, H., Cubic Phases of Lipid-Containing Systems: Elements of a Theory and Biological Connotations. *J. Mol. Biol.* **1993,** *229*, 540-551.
26. Briggs, J.; Chung, H.; Caffrey, M., The Temperature-Composition Phase Diagram and Mesophase Structure Characterization of the Monoolein/Water System. *J. De Phys. II* **1996,** *6*, 723-751.
27. Qiu, H.; Caffrey, M., The phase Diagram of the Monoolein/Water System: Metastability and Equilibrium Aspects. *Biomaterials* **2000,** *21*, 223-234.
28. Mezzenga, R.; Grigorov, M.; Zhang, Z.; Servais, C.; Sagalowicz, L.; Romoscanu, A. I.; Khanna, V.; Meyer, C., Polysaccharide-Induced Order-to-Order Transitions in Lyotropic Liquid Crystals. *Langmuir* **2005,** *21*, 6165-6169.
29. Rizwan, S. B.; Hanley, T.; Boyd, B. J.; Rades, T.; Hook, S., Liquid Crystalline Systems of Phytantriol and Glyceryl Monooleate Containing a Hydrophilic Protein: Characterisation, Swelling and Release Kinetics. *J. Pharm. Sci.* **2009,** *98*, 4191-4204.
30. Amar-Yuli, I.; Garti, N., Transitions Induced by Solubilized Fat into Reverse Hexagonal Mesophases. *Colloids Surf. B Biointerfaces* **2005,** *43*, 72-82.
31. Amar-Yuli, I.; Libster, D.; Aserin, A.; Garti, N., Solubilization of Food Bioactives within Lyotropic Liquid Crystalline Mesophases. *Curr. Opin. Colloid Interface Sci.* **2009,** *14*, 21-32.
32. Shearman, G. C.; Tyler, A. I. I.; Brooks, N. J.; Templer, R. H.; Ces, O.; Law, R. V.; Seddon, J. M., Ordered Micellar and Inverse Micellar Lyotropic Phases. *Liq. Cryst.* **2010,** *37*, 679-694.
33. Rappolt, M.; Cacho-Nerin, F.; Morello, C.; Yaghmur, A., How the Chain Configuration Governs the Packing of Inverted Micelles in the Cubic Fd3m Phase. *Soft Matter* **2013,** *9*, 6291.
34. Sagalowicz, L.; Guillot, S.; Acquistapace, S.; Schmitt, B.; Maurer, M.; Yaghmur, A.; De Campo, L.; Rouvet, M.; Leser, M.; Glatter, O., Influence of Vitamin E Acetate and Other Lipids on the Phase Behavior of Mesophases Based on Unsaturated Monoglycerides. *Langmuir* **2013,** *29*, 8222-8232.
35. Yaghmur, A.; de Campo, L.; Sagalowicz, L.; Leser, M. E.; Glatter, O., Emulsified Microemulsions and Oil-Containing Liquid Crystalline Phases. *Langmuir* **2005,** *21*, 569-577.

36. Yaghmur, A.; De Campo, L.; Salentinig, S.; Sagalowicz, L.; Leser, M. E.; Glatter, O., Oil-Loaded Monolinolein-Based Particles with Confined Inverse Discontinuous Cubic Structure (Fd3m). *Langmuir* **2005,** *22*, 517-521.
37. Yaghmur, A.; De Campo, L.; Sagalowicz, L.; Leser, M. E.; Glatter, O., Emulsified Microemulsions and Oil-Containing Liquid Crystalline Phases. *Langmuir* **2004,** *21*, 569-577.
38. Yaghmur, A.; Rappolt, M.; Ale, I.; Chandrashekhar, V. K., Chapter Five - The Micellar Cubic Fd3m Phase: Recent Advances in the Structural Characterization and Potential Applications. In *Advances in Planar Lipid Bilayers and Liposomes*, Academic Press: **2013**, *18*, 111-145.
39. Pouzot, M.; Mezzenga, R.; Leser, M.; Sagalowicz, L.; Guillot, S.; Glatter, O., Structural and Rheological Investigation of Fd3m Inverse Micellar Cubic Phases. *Langmuir* **2007,** *23*, 9618-9628.
40. Shearman, G. C.; Ces, O.; Templer, R. H.; Seddon, J. M., Inverse Lyotropic Phases of Lipids and Membrane Curvature. *J. Phys. Condens. Matter* **2006,** *18*, S1105.
41. Murray, M. J.; Sanders, J. V., Close-Packed Structures of Spheres of two Different Sizes II. The Packing Densities of Likely Arrangements. *Philos. Mag. A* **1980,** *42*, 721-740.

Chapter 4

Phase behaviour of the ternary system: Monoolein/Water/branched Polyethylenimine

4.1 Introduction

Organized lipid/water systems are important since they are encountered in several biological processes[1] and, since they have wide ranging technological applications.[2-7] Specifically, glycerol monooleate (or GMO) has emerged as a molecule with great promise as a nanostructured amphiphilic delivery vehicle.[8-11] GMO is a hydrophobic lipid (HLB value = 3.8) that is commercially used as a food emulsifier. The GMO/water system exhibits rich phase behaviour at room temperature, forming lamellar and bicontinuous cubic phases with gyroid and double diamond architectures. Due to the large miscibility gap for the lipid, the double diamond bicontinuous phase can coexist with excess water.[12] This allows formulation of the extremely rigid and hard-to-process cubic phases into low viscosity aqueous dispersions of lipid particles with internal mesophase structure.[13-14] Recently, novel processing strategies have emerged to prepare nanostructured oil-in-water and water-in-oil emulsions that have significant application potential.[15]

Useful functional materials can be realized by introduction of colloidal nanoparticles or polymers within mesophases.[16] Incorporation of polymers in a mesophase is governed by a complex interplay of polymer-mesophase interactions and by the conformational entropy change of the polymer on confinement in the mesophase.[17-20] Incorporation of ternary components can also result in a change in mesophase organization.[21-31] Typically, the effect of addition of a ternary component is rationalized through its effect on the packing parameter, $\gamma = V/a_g l_c$, [32] (where V and l_c are the volume and length of the hydrophobic tail, and a_g is the area of the polar head group). The packing parameter presents a convenient geometric framework to interpret mesophase behaviour. For $\gamma = 1$, the lamellar phase forms. For $\gamma \approx 1/2$, the increase in effective head group size is accommodated by increasing the curvature of the self-assembled lipid structure and, a hexagonal phase forms. For $\gamma \approx 1/3$, higher curvature micellar phases are observed. Similarly, an increase in γ results in formation of mesophases with reverse curvature (viz. reverse water in oil phases). Incorporation of ternary components influences γ and therefore changes the curvature. Thus, for example, incorporation of phosphatidylinositol promotes membrane curvature in model dioleoylphosphatidylcholine membranes.[33] In GMO/water systems, Caffrey has demonstrated that addition of alkyl glycosides results in a decrease in γ towards 1, such that bicontinuous cubic phases transform into

lamellar phases.[34] On the other hand, addition of sugars is reported to result in a decrease the lattice parameter in GMO/water, favouring the formation of high curvature inverse phases.[21,35-36] While formation of the reverse hexagonal phase has been reported on addition of several ternary hydrophilic moieties,[37] the ordered reverse micellar Fd3m phase typically forms only on addition of apolar oils. These apolar oils are localized in the spaces around the reverse micelles and solubilize the lipid tails. Thus, hydrophobic lipids like monolinolein (MLO) and, monoolein (GMO) readily form the Fd3m phase on addition of oils such as tetradecane(TC)[38-39] or limolene,[40] hexadecane[41] (HD) or Vitamin-E.[42] In these examples, formation of the Fd3m phase results, since the apolar oils relieve the packing frustration of lipid tails.[43-45]

In Chapter 2 and in a recent publication,[46] we demonstrated that addition of a small quantity of hydrophilic polymer could result in transformation of the GMO/water system into an Fd3m phase, without any added oil. We demonstrated that polar macromolecular entities (i) with a compact architecture and (ii) bearing groups that interacted strongly with the GMO headgroup, were capable of inducing sufficient curvature in the lipid assembly to form an Fd3m phase. Thus, polyamidoamine (PAMAM) dendrons with terminal amine groups that interact with the GMO, and with a compact dendritic structure induced the Fd3m phase in GMO/water while, remarkably, the linear analogue of the PAMAM did not. Thus, we established a new route to tuning the curvature of GMO/water assemblies that is critically dependent on the chain architecture of the ternary polar polymeric inclusion. Synthesis of perfectly branched PAMAM dendrons is challenging. However, we have established that other readily available polar ternary inclusions, such as branched polyethylenimine and silsesquioxane cages that have compact molecular shapes and that interact strongly with GMO also induce the formation of the Fd3m phase.

In this Chapter, we explore the GMO/water/branched PEI phase diagram in detail. Polyethyleneimine (PEI) interacts strongly with phospholipid bilayers[47] and has been reported to be a highly effective non-viral vector for gene delivery to cells. PEI is a branched polymer that bears primary, secondary and tertiary amine groups. As the PEI amine groups are protonated at different pH,[48] we can use variable pH NMR studies to probe the structure of branched PEI. The structure of the PEI used in this work was characterized previously.[49] In this Chapter, we examine systems whose pH is maintained at 10, where the PEI amines have a very low degree of protonation.

Operating at a pH = 10 also ensures that the GMO does not undergo hydrolytic degradation. We present a comprehensive study of the equilibrium phase behaviour that explores the effect of addition of small weight fractions of PEI (up to 4% by weight) to GMO/water. We examine various GMO/water ratios (weight fractions of water ranging from 10-40%) at temperatures from ambient (25^{o}C) to 80^{o}C. We also explore the effect of PEI molecular weight by investigating polymers with molecular weights of 0.8, 2 and 25 kDa. We establish the composition window in which the GMO/water/PEI system forms the Fd3m phase and demonstrate that there is an optimal PEI molecular weight at which the Fd3m is most stable.

4.2 Experimental Section

4.2.1 Materials:

Glycerol monooleate (trade name: Rylo MG 20 Pharma, Schematic in Figure 4.1) was generously supplied by Danisco India. In this work, we refer to the commercial Rylo Sample as GMO. We have performed acid-base titration on Rylo and measure an acid value of 2.3. We have previously reported detailed characterisation of GMO.[11] All experiments were carried out with the same batch of GMO that was stored at -80^{o}C to avoid degradation. Polyethylenimine (PEI) of different molecular weight (Supplier specified as M_w = 0.8 kDa, PDI = 1.3; 2 kDa, PDI = 1.1 and 25 kDa, PDI = 2.5) and with a branched architecture, were obtained as aqueous dispersions from Sigma Aldrich and used as received (Schematic in Figure 4.1). High purity glycerol monooleate (HP-GMO, purity > 99.9%) was purchased from Sigma Aldrich and used as received.

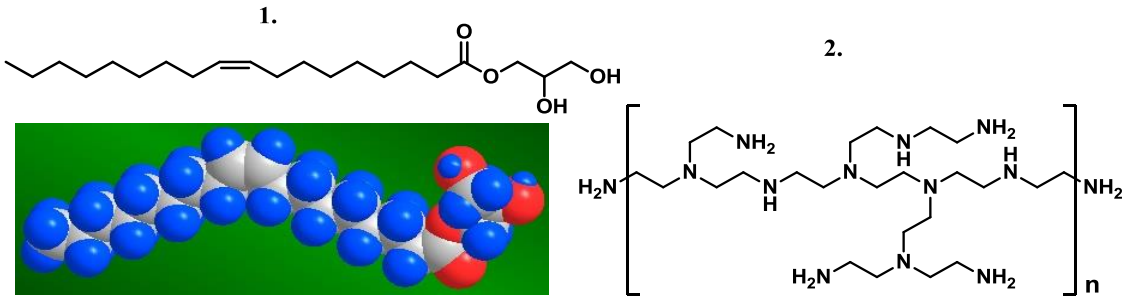

Figure 4.1: (1a) Structure of GMO; (1b) 3D structure of GMO; (2) A schematic representation of branched PEI containing primary, secondary and tertiary amines.

4.3 Characterisation

We measured pH using a Mettler Toledo instrument (SevenMulti), calibrated with standard pH solutions. Samples were characterized using Small-angle X-ray scattering (SAXS) and, polarised optical microscopy (POM).

4.3.1 Small Angle X-rays Scattering (SAXS):

SAXS was performed using a Bruker Nanostar equipped with Cu rotating anode, tungsten filament and three pinhole collimation. We operated the SAXS at a voltage of 45 kV and 18 mA current. Data was collected using a 2D gas filled HiStar detector, over a q-range of 0.01-0.2 $Å^{-1}$ (sample to detector distance of 105 cm). The detector was calibrated using a standard silver behenate sample. Data was collected until the detector registered at least a million counts. The scattered 2-D data is isotropic and is circularly averaged using Bruker offline software to reduce to 1-D. Samples were filled in a capillary tube (diameter 2 mm; wall thickness ~ 10 μm) with a metal holder. Samples loaded in the capillaries were heated to 90^{o}C to eliminate the effect of shearing while loading in the capillary and then cooled to room temperature for measurements. Temperature dependent experiments were performed using a Peltier heating stage. The temperature was controlled using a temperature controller to an accuracy of ±0.1^{o}C.

4.3.2 Polarised Optical Microscopy (POM):

Optical microscopy was performed on an Olympus BX-50, mounted with a Nikon camera. We used a CSS450 Linkam stage for controlled heating of the samples. Samples were sandwiched between the heated bottom plate of the CSS450 and a glass cover slip. Samples were heated at 5^{o}C/minute to 80^{o}C and subsequently cooled to room temperature.

4.4 Preparation of GMO/water/PEI mesophase

GMO/water/PEI ternary samples were prepared at constant pH (= 10, obtained by decreasing the pH using 70% w/v nitric acid solution, obtained from Merck India). All samples were prepared using distilled deionised water of resistivity 18.2 MΩ.cm. The nomenclature followed in this Chapter is as follows: f_w represents the weight fraction of water relative to GMO while, Φ represents the weight fraction of added PEI in the GMO/water/PEI system. Thus, for example, a system with f_w = 20% and Φ = 2% comprises

(by weight) 78.4% GMO, 19.6% water (78.4 + 19.6 = 98; 19.6/ (78.4 + 19.6) = 0.2) and 2% PEI. In a typical sample preparation, we first thaw the GMO in an oven at ~80^{o}C. We use a 50 wt% aqueous PEI stock solution (pH = 12.8) and directly add this to GMO. Water is added to adjust the ratio of GMO to water and to adjust the pH to 10. For example, 1 g of a sample containing 90:10 GMO: water with 2% PEI was prepared by adding 4 mg of the PEI stock solution (50 wt%) to 78 mg of water, and then adding this to 882 mg of GMO warmed to 80^{o}C. GMO, water and PEI were mixed in a closed vial and the temperature was repeatedly cycled to 80^{o}C. Finally, the sample was equilibrated in the vial by storing for 10 to 15 days at room temperature. Other GMO/water/PEI compositions were prepared in a similar manner.

4.5 Results

We begin with a description of ternary systems containing PEI with a molecular weight of 2 kDa in GMO/water. We describe the equilibrium phases formed by this ternary system at room temperature for 10% $\leq$ $f_w \leq$ 40% and for $\Phi \leq$ 4%. Subsequently, we examine the temperature dependence of the phase behaviour and present the phase diagram in composition-temperature space. Finally, we investigate the effect of varying the molecular weight of the PEI.

4.5.1 GMO/water/PEI-2kDa Organization at Room Temperature: Variation of PEI Concentration (Φ) and Water Content (f_w):

An 85/15 GMO/water binary system (viz. f_w = 15%, Φ = 0) forms a lamellar (L_α) phase at room temperature (= 25^{o}C) (Figure 4.2). The lamellar phase is identified by characteristic streak-shaped textures between crossed polarizers (Figure 4.2 c). SAXS on lamellar phases gives peaks whose positions are in the ratio of 1:2:3:.. We observe a SAXS peak at q = 0.160 Å^{-1}, corresponding to a d-spacing of 39 Å (Figure 4.2 a). Higher order peaks cannot be observed as the SAXS instrument configuration limits the q range to less than 0.2 Å^{-1}.

On addition of a small fraction of PEI (Φ = 0.3%), the L_α phase transforms into a bicontinuous cubic Ia3d phase. This phase is characterized by SAXS peaks, whose peak positions are in the ratio of $\sqrt{6}$: $\sqrt{8}$: $\sqrt{14}$ (Figure 4.2 a). For higher PEI concentrations (Φ = 1%) the system organizes into an inverse hexagonal phase (H_{II}), with characteristic textures observed between crossed polarizers (Figure 4.2 b). SAXS

peak positions from the H_{II} phase are in the ratio of 1: √3: √4: √7… Again, as for the L_α phase, only the first SAXS peak is observed in the experimental q-range, and this corresponds to a d-spacing of 46 Å. On further increasing Φ to 2%, the H_{II} phase transforms into a discontinuous phase with Fd3m symmetry, identified using the SAXS peak positions. We identify 7 peaks for the Fd3m phase, and index these in accordance to literature reports.[2,50] A plot of the peak positions against $(h^2+k^2+l^2)^{1/2}$, where h, k, l are the Miller indices that characterize the peak, yields a straight line passing through the origin (Figure 4.3). This confirms that the GMO/water/2 kDa PEI system forms an Fd3m phase for f_w = 15% and Φ = 2%. From the SAXS data, we calculate the lattice parameter associated with the Fd3m phase as 157 Å. The Fd3m phase comprises reverse micelles of two different sizes organized with cubic order to form an AB_2 crystal structure. Due to the cubic symmetry of the Fd3m phase, it appears dark between crossed polarizers. We observe that the formation of the Fd3m phase is correlated with the development of turbidity. Previously, discontinuous reverse micellar Fd3m phases have been reported to form in lipid systems only on addition of apolar ternary components.[38-42] Therefore, the formation of an Fd3m phase on addition of water soluble, polar PEI must follow a different path.

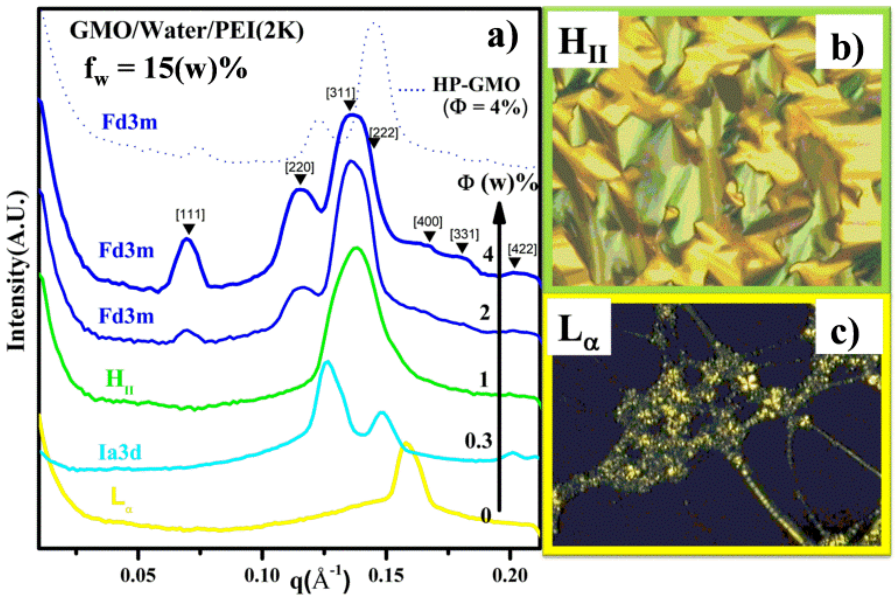

Figure 4.2: (a) SAXS for GMO/water/2 kDa PEI systems (f_w = 15%) as a function of PEI fraction (Φ). Data for ternary systems containing HP-GMO is also shown. Optical micrograph between crossed polarizers for the ternary system at (b) Φ = 0% (L_α phase) and (c) Φ = 1% (H_{II} phase).

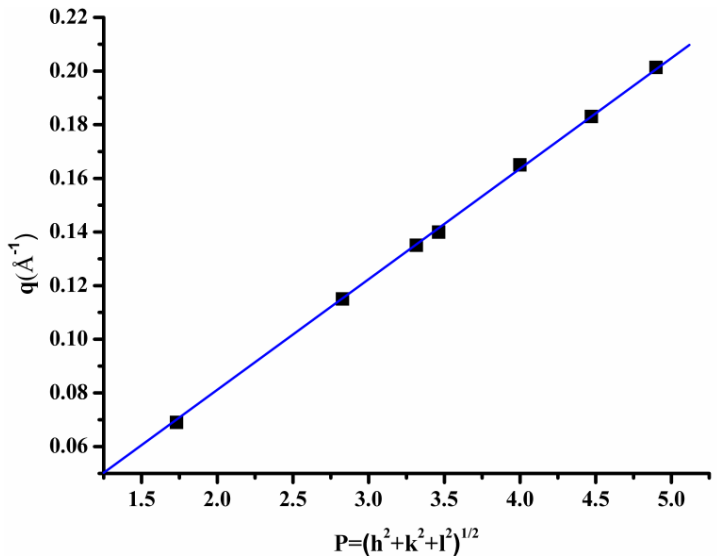

Figure 4.3: A plot of the peak reciprocal spacing, q ($Å^{-1}$) as a function of $P= (h^2+k^2+l^2)^{1/2}$ is a straight line through the origin.

Addition of hydrophilic molecules, such as glucose, has been reported[21] to shift the Lα/cubic/H_{II} phase boundaries in lipid-water systems, in a manner similar[32] to this work. This has been rationalized by considering the packing parameter, γ, defined earlier. Addition of hydrophilic molecules reduces hydration of the head group, thus shrinking the head group area. This results in an increase in γ, and a tendency to transform from the lamellar phase to cubic and then to hexagonal. Formation of a reverse micellar phase on addition of hydrophilic moieties would necessitate an increase in γ from 1 (for the L_α phase) to ≈ 3, corresponding to a nearly 3-fold reduction in A. We believe that such a large reduction in the effective head group area, by dehydration of the head group by PEI is unlikely. Therefore, for the GMO/water/PEI systems, the mechanistic origin of the phase transition cannot be attributed to geometric packing considerations.

Recently, we have demonstrated[46] that while compact dendritic ternary additives induce the formation of the Fd3m phase in GMO/water, their linear analogues do not. This is consistent with our hypothesis that geometric packing considerations alone cannot explain these transitions. Rather, we believe that the formation of the Fd3m phase arises from a strong attractive interaction between the GMO head group and the compact, branched PEI molecules. This is consistent with

the data presented here on GMO/water/PEI systems. It is remarkable that only very small added fractions of the PEI are sufficient to induce phase transitions in the GMO/water system: the H_{II} phase forms on addition of only Φ = 1% PEI, while the Fd3m phase forms on addition of as little as Φ = 2% PEI. In comparison, we note that in GMO/water/oil ternary systems, ≈ 20% of apolar oil needs to be added to form the Fd3m phase.

The Fd3m phase persists on increasing the PEI content to Φ = 4% (Figure 4.2). We note that the d spacing that characterizes the Fd3m phase does not change significantly on increasing Φ from 2% (156 Å) to 4% (157 Å). Formation of the Fd3m phase in the GMO/water/PEI ternary system cannot be attributed to impurities in the commercial GMO used in this investigation. We have prepared a few ternary compositions containing high purity GMO (HP-GMO), water and 2 kDa PEI, and observe qualitatively similar phase behaviour. For example, the ternary system prepared using HP-GMO at f_w = 15%, Φ = 4% also shows the formation of the Fd3m phase (Figure 4.2 a, dotted line). However, we observe that there is a decrease in the d-spacing for the Fd3m phase prepared using HP-GMO (to 78.5 Å, relative to 91 Å for commercial GMO).

We observe that at all f_w between 10-40%, the GMO/water system transitions to the H_{II} phase, and subsequently to the Fd3m phase with increase in PEI content, Φ (Figure 4.4). For f_w = 10%, increasing Φ results in transformation of the L_α phase into a bicontinuous Ia3d phase (at low Φ = 0.3%), H_{II} phase (for $\Phi \leq 2\%$) and formation of a discontinuous reverse micellar Fd3m phase for Φ = 4%. Thus, while the sequence of phase transitions with increasing Φ (L_α to Ia3d to H_{II} to Fd3m) is similar for f_w = 10 and 15%, the window for H_{II} phase formation ($\Phi \leq 2\%$) is larger for f_w = 10%.

With increase in water content, $20\% \leq f_w \leq 30\%$, the binary GMO/water system forms the Ia3d phase. The Ia3d phase is retained for addition of small fractions of PEI (Φ = 0.5%). For higher Φ = 1%, the Ia3d phase is transformed into the reverse hexagonal phase, H_{II}. On increasing Φ to 2%, the GMO/water/2 kDa PEI system forms the Fd3m phase. Similarly, for higher water content $30\% < f_w \leq 40\%$, the double diamond Pn3m phase forms (characterized by SAXS peaks, whose positions

are in the ratio of √2: √3: √4). For ternary systems at these f_w too, we observe the formation of a reverse hexagonal H_{II} phase for $\Phi = 1\%$ and of the Fd3m phase for $2\% \leq \Phi \leq 4\%$. Thus, while GMO/water systems form L_α, Ia3d and Pn3m phases with increasing f_w between 10-40%, at all these f_w, they organize to form an H_{II} phase at intermediate Φ and transform into an Fd3m phase at higher Φ.

4.5.2. GMO/Water/PEI-2 kDa: Effect of Temperature:

On heating, the GMO/water binary system transforms into an isotropic reverse micellar phase (L_2) for $10\% \leq f_w \leq 40\%$. For low $f_w = 10\%$, GMO/water directly transforms from the L_α to the L_2 phase above ≈ 40°C (Figure 4.4). For $10\% < f_w \leq 20\%$, the L_α phase transforms into the cubic Ia3d (above 25°C) and finally to the L_2 phase (between 45-60°C). At higher $f_w < 35\%$, there is a transition from the Ia3d to the Pn3m phase on heating to 30-50°C, and then into the H_{II} phase and finally into the L_2 phase (> 65°C). Finally, for $f_w > 35\%$, the cubic Pn3m phase transforms into the H_{II} phase (at ≈ 60°C) and finally to the L_2 phase (between 70-75°C). The temperature dependence of the lipid phase behaviour can been rationalized using packing parameter arguments. With increase in temperature, there is a larger entropic free energy penalty for water molecules associated with the head group. Therefore, an increase in temperature results in a concomitant increase in P that corresponds to a transition from L_α through cubic, hexagonal and, inverse micellar phases. For $f_w = 10\%$, addition of PEI ($0.5\% \leq \Phi \leq 4\%$) induces the formation of the H_{II} phase at 25°C, that transforms into the L_2 phase between 60-80°C. For f_w = 15-40% and, for $\Phi = 1\%$, the H_{II} phase forms at room temperature and transforms into the L_2 phase between 50-75°C (Figure 4.4). For f_w = 15-40% and, $2\% \leq \Phi \leq 4\%$, the Fd3m phase forms at 25°C and transforms on heating into the L_2 phase (between 40-65°C, Figure 4.4).

The Fd3m/L_2 transition happens at higher temperature (≈ 65°C) for $\Phi = 2\%$ and decreases to ≈ 40°C with increase in Φ. Thus, in general, we observe that in ternary compositions containing PEI, transition temperatures to higher curvature states are suppressed relative to the binary GMO/water system. The higher the PEI concentration (Φ) in the ternary system, the lower is the transition temperature to the L_2 phase. Again, we note that the high curvature reverse micellar Fd3m phase is not accessible for the binary GMO/water system. Addition of PEI ($\Phi \geq 2\%$) to GMO/water affords the formation of reverse micellar phases at sufficiently low temperatures, where the micelles can crystallize

into an AB_2 cubic structure (the Fd3m phase). On heating, the cubic ordering of the micelles cannot be sustained and the Fd3m phase transitions to an isotropic reverse micellar phase.

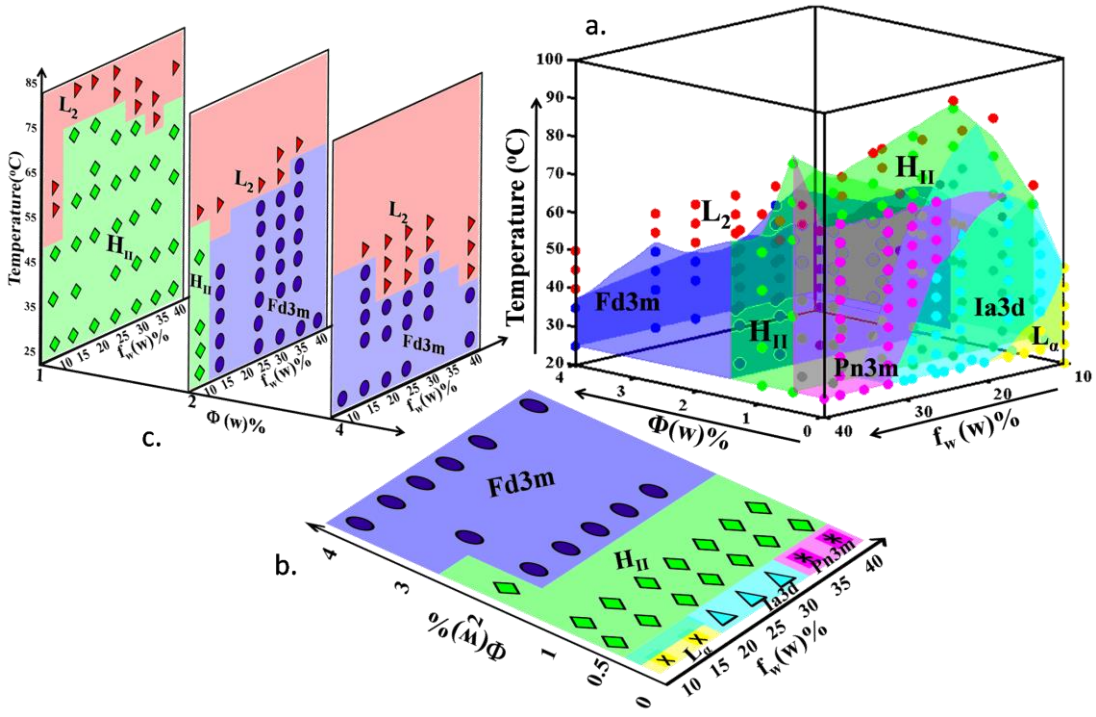

Figure 4.4: (a) Ternary GMO/H_2O/2 kDa PEI phase diagram as a function of f_w, Φ and temperature. Slices of the phase diagram showing the phase behaviour at (b) T = 25°C; (c) Φ= 1, 2 and 4%.

4.6 Influence of PEI molecular weight

Finally, we investigate the influence of PEI molecular weight on the phase behaviour of GMO/water/PEI. We present data for ternary systems containing PEI with molecular weights, M_w = 0.8 kDa and 25 kDa and, contrast with data on systems containing 2 kDa PEI. Ternary systems containing 0.8 kDa PEI show similar behaviour as those containing 2 kDa PEI, at matched Φ (Figure 4.5). For $f_w \leq 15\%$, GMO/water transitions from an L_α phase at Φ = 0% to an H_{II} phase at Φ = 0.5%.

We do not observe an intermediate cubic phase for the ternary system containing 0.8 kDa PEI. Similar to the case of 2 kDa PEI, the f_w = 10% system stays in the H_{II} phase up to Φ = 4%. At f_w = 15% the H_{II} phase transforms into the Fd3m for Φ

between 2-4%. For $20\% \leq f_w \leq 30\%$, the Ia3d phase transforms into the H_{II} phase up for $\Phi = 0.5\%$, and into the Fd3m phase at Φ between 2-4%. Thus, the H_{II}/Fd3m phase transition happens only for higher PEI loadings for the lower molecular weight polymer.

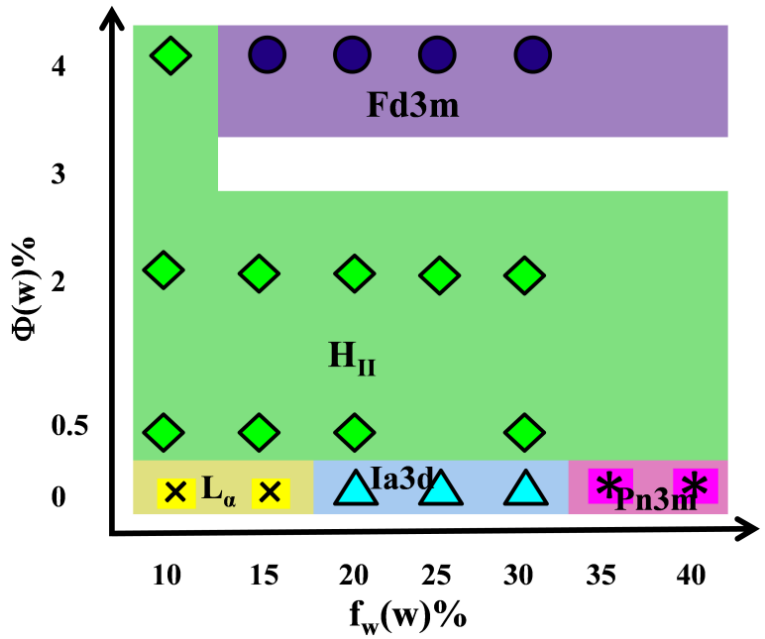

Figure 4.5: Phase behaviour of the ternary system GMO/water/0.8 kDa PEI at T = 25°C

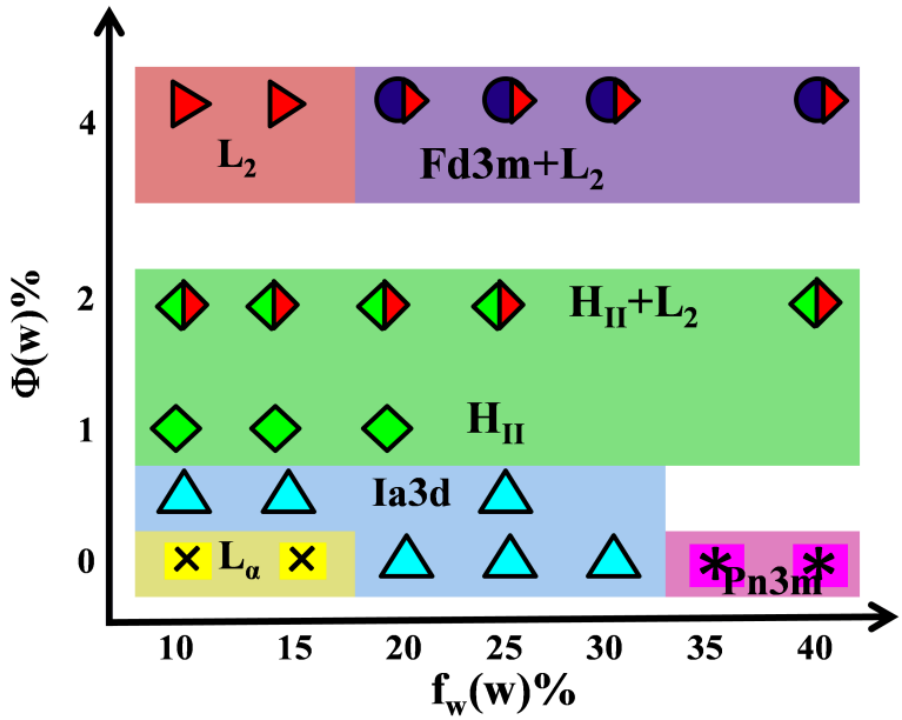

Figure 4.6: Phase behaviour of the ternary system GMO/water/25 kDa PEI at T = 25°C

For systems containing the high molecular weight polymer (25 kDa PEI), the formation of the reverse micellar Fd3m phase is significantly inhibited (Figure 4.6). SAXS peaks corresponding to the Fd3m phase are observed only for samples with $f_w \geq$ 20% and Φ = 4%. However, here the Fd3m phase coexists with the isotropic L_2 phase. L_2/H_{II} phase coexistence is observed at room temperature for $10\% \leq f_w \leq 40\%$ at Φ = 2%, unlike systems containing 2 kDa PEI, where the L_2 phase is never observed at 25^{o}C. For ternary systems containing 25 kDa PEI, increasing Φ leads to a transition from L_α to cubic Ia3d (Φ = 0.5%) to H_{II} (Φ = 1%) to H_{II}/L_2 (Φ = 2%) and finally L_2 (Φ = 4%) for low water content ($f_w \leq 15\%$) compositions. For higher water content ($f_w \geq$ 20%), the cubic phases formed at Φ = 0% transition into an H_{II} phase at Φ = 1%; H_{II}/L_2 coexistence at Φ = 2% and Fd3m/L_2 coexistence at Φ = 4% (Figure 4.6).

4.7 Discussion

Our data suggests that addition of 2 kDa PEI is most efficacious in inducing the formation of the Fd3m phase. Our previous investigations suggest that formation of the Fd3m phase happens due to strong attractive interactions between the lipid headgroup and PEI amines.[46]The compact shape of the branched PEI is essential for inducing Fd3m phase formation. Analogous linear molecules bearing amine groups do not induce Fd3m formation in GMO/water systems.[46] Following our previous work,[46] we believe that topologically compact molecules, such as the branched PEI, are unable to extend on the GMO surface to maximize head-group amine interactions. Therefore, GMO engulfs the PEI molecules to create high curvature assemblies.

The Fd3m phase comprises micelles of two different sizes packed into an AB_2 structure. While other single component lipids have been shown[51] to organize to form such bidisperse micellar assemblies, neat GMO/water systems are not known to form an Fd3m phase. In the present study, it is possible that localization of the PEI molecules within micellar GMO structures is responsible for the formation of the Fd3m phase. The Fd3m phase forms when the two micelles in the AB_2 structure have a size ratio of $0.482 \leq B/A \leq 0.624$.[52]Our data suggests that the 2 kDa PEI has the right molecular size to facilitate formation of the Fd3m phase. The high molecular weight 25 kDa PEI has a molecular size that is significantly larger than the 2 kDa polymers. Accordingly, we observe a stronger tendency to form the less ordered isotropic L_2

phase. We also note that the 25 kDa PEI has a higher polydispersity index relative to the 0.8 and 2 kDa PEI. Therefore, the formation of the H_{II} and Fd3m phases that coexist with the L_2 phase for ternary systems comprising 25 kDa PEI might be a consequence of the PEI polydispersity. Sorting of added polymer chains by their molecular weight ("sieving") by surfactant mesophases has been reported in the literature.[18] It is possible that the low molecular mass components of the polydisperse 25 kDa PEI are responsible for formation of the H_{II} and Fd3m phases in GMO/water, that coexist with the disordered L_2 phase.

The equilibrium structure formed when PEI is incorporated in GMO/water is governed by several factors. Firstly, PEI interacts with GMO and, dehydrates the head group size resulting in a change in the effective head group size. The conformational entropy of the PEI is reduced when it is incorporated within the organized lipid structure. This change in conformational entropy is a function of polymer architecture: chain molecular weight and branched structure. Our results indicate that this combination of factors results in an enhanced stability window for the Fd3m phase for a PEI molecular weight of 2 kDa.

4.8 Summary

We present a detailed investigation of the phase behaviour of ternary glycerol monooleate/water/PEI systems. GMO/water systems containing small fractions (Φ = 2-4%) of low molecular weight PEI (Mw = 0.8 kDa, 2 kDa) form an ordered reverse micellar cubic phase with Fd3m symmetry. For higher molecular, relatively polydisperse PEI (Mw = 25 kDa), the Fd3m phase forms at Φ = 4% PEI, in coexistence with the isotropic L_2 phase. For all compositions, we observe an Fd3m/L_2 phase transition on heating to sufficiently high temperatures. The formation of the discontinuous reverse micellar Fd3m phase at room temperature has implications for systems for controlled delivery of water soluble actives. Diffusion of encapsulated actives through a discontinuous phase (such as the Fd3m) is anticipated to be dramatically slower as compared to through bicontinuous cubic phases, suggesting the use of Fd3m cubosomes for slow release formulations. Further, our investigation reveals that the temperature window for stability of the Fd3m phase is a strong function of the PEI molecular weight. This work provides guidelines for the design of

polymer chain architecture (viz. branching, molecular weight and exposed functional groups) of ternary inclusions for optimal design of temperature stable, slow release formulations.

4.9 References

1. Siegel, D. P., The Modified Stalk Mechanism of Lamellar/Inverted Phase Transitions and Its Implications for Membrane Fusion. *Biophys. J.* **1999**, *76*, 291-313.
2. Fong, C.; Le, T.; Drummond, C. J., Lyotropic Liquid Crystal Engineering–Ordered Nanostructured Small Molecule Amphiphile Self-Assembly Materials by Design. *Chem. Soc. Rev.* **2012**, *41*, 1297-1322
3. Angelova, A.; Angelov, B.; Garamus, V. M.; Couvreur, P.; Lesieur, S., Small-Angle X-Ray Scattering Investigations of Biomolecular Confinement, Loading, and Release from Liquid-Crystalline Nanochannel Assemblies. *J. Phys. Chem. Lett.* **2012**, *3*, 445-457.
4. Mezzenga, R.; Schurtenberger, P.; Burbidge, A.; Michel, M., Understanding Foods as Soft Materials. *Nat. Mater.* **2005**, *4*, 729-740
5. Caffrey, M., Membrane Protein Crystallization. *J. Struct. Biol.* **2003**, *142*, 108-132.
6. Ostermeier, C.; Michel, H., Crystallization of Membrane Proteins. *Curr. Opin. Struct. Biol.* **1997**, *7*, 697-701.
7. Mann, S.; Ozin, G. A., Synthesis of Inorganic Materials with Complex Form. *Nature* **1996**, *382*, 313-318
8. Kulkarni, C. V.; Wachter, W.; Iglesias-Salto, G.; Engelskirchen, S.; Ahualli, S., Monoolein: A Magic Lipid? *Phys. Chem. Chem. Phys.* **2011**, *13*, 3004-3021.
9. Ganem-Quintanar, A.; Quintanar-Guerrero, D.; Buri, P., Monoolein: A Review of the Pharmaceutical Applications. *Drug Dev. Ind. Pharm.* **2000**, *26*, 809-820.
10. Drummond, C. J.; Fong, C., Surfactant Self-Assembly Objects as Novel Drug Delivery Vehicles. *Curr. Opin. Colloid Interface Sci.* **1999**, *4*, 449-456.
11. Deshpande, S.; Venugopal, E.; Ramagiri, S.; Bellare, J. R.; Kumaraswamy, G.; Singh, N., Enhancing Cubosome Functionality by Coating With a Single Layer of Poly-ε-Lysine. *ACS App. Mater. Interfaces* **2014**, *6*, 17126-17133.
12. Landh, T., Phase-Behavior in the System Pine Oil Monoglycerides-Poloxamer-407-Water at 20 °C. *J. Phys. Chem.* **1994**, *98*, 8453-8467.
13. Barauskas, J.; Johnsson, M.; Tiberg, F., Self-Assembled Lipid Superstructures: Beyond Vesicles and Liposomes. *Nano Lett.* **2005**, *5*, 1615-1619.
14. Spicer, P. T., Progress in Liquid Crystalline Dispersions: Cubosomes. *Curr. Opin. Colloid Interface Sci.* **2005**, *10*, 274-279

15. Kulkarni, C. V.; Mezzenga, R.; Glatter, O., Water-In-Oil Nanostructured Emulsions: Towards the Structural Hierarchy of Liquid Crystalline Materials. *Soft Matter* **2010**, *6*, 5615-5624.
16. Kumaraswamy, G.; Sharma, K. P., Polymer and Colloidal Inclusions in Lyotropic Lamellar and Hexagonal Surfactant Mesophases. *Advances in Planar Lipid Bilayers and Liposomes* **2013**, *18*, 181.
17. Wadekar, M. N.; Pasricha, R.; Gaikwad, A. B.; Kumaraswamy, G., Polymerization in Surfactant Liquid Crystalline Phases. *Chem. Mater.* **2005**, *17*, 2460-2465.
18. Pacios, I. E.; Renamayor, C. S.; Horta, A.; Thuresson, K.; Lindman, B., Nanometric Sieving of Polymer Coils by a Lamellar Liquid Crystal: Surfactant AOT and Poly dimethylacrylamide. *Macromolecules* **2005**, *38*, 1949-1957
19. Guymon, C. A.; Hoggan, E. N.; Clark, N. A.; Rieker, T. P.; Walba, D. M.; Bowman, C. N., Effects Of Monomer Structure on Their Organization and Polymerization in A Smectic Liquid Crystal. *Science* **1997**, *275*, 57-59.
20. Warriner, H. E.; Idziak, S. H.; Slack, N. L.; Davidson, P.; Safinya, C. R., Lamellar Biogels: Fluid-Membrane-Based Hydrogels Containing Polymer Lipids. *Science* **1996**, *271*, 969-973.
21. Mezzenga, R.; Grigorov, M.; Zhang, Z.; Servais, C.; Sagalowicz, L.; Romoscanu, A. I.; Khanna, V.; Meyer, C., Polysaccharide-Induced Order-To-Order Transitions in Lyotropic Liquid Crystals. *Langmuir* **2005**, *21*, 6165-6169.
22. Yaghmur, A.; Laggner, P.; Zhang, S.; Rappolt, M., Tuning Curvature and Stability of Monoolein Bilayers by Designer Lipid-Like Peptide Surfactants. *PLoS One* **2007**, *2*, 479.
23. Bilalov, A.; Elsing, J.; Haas, E.; Schmidt, C.; Olsson, U., Embedding DNA In Surfactant Mesophases: The Phase Diagram of the Ternary System Dodecyltrimethylammonium–DNA/Monoolein/Water in Comparison to the DNA-Free Analogue. *J. Colloid Interface Sci.* **2013**, *394*, 360-367
24. Rädler, J. O.; Koltover, I.; Salditt, T.; Safinya, C. R., Structure of DNA-Cationic Liposome Complexes: DNA Intercalation in Multilamellar Membranes in Distinct Inter helical Packing Regimes. *Science* **1997**, *275*, 810-814.
25. Ericsson, B.; Larsson, K.; Fontell, K., A Cubic Protein-Monoolein-Water Phase. *BBA-Biomembr.* **1983**, *729*, 23-27.
26. Larsson, K., Cubic Lipid-Water Phases: Structures and Bio-membrane Aspects. *J. Phys. Chem.* **1989**, *93*, 7304-7314.

27. Tanaka, S.; Maki, S.; Ataka, M., Structural Transitions of The Monoolein Bicontinuous Cubic Phase Induced by Inclusion of Protein Lysozyme Solutions. *Phys. Rev. E* **2006**, *73*, 061510.
28. Guillot, S.; Salentinig, S.; Chemelli, A.; Sagalowicz, L.; Leser, M. E.; Glatter, O., Influence of the Stabilizer Concentration on the Internal Liquid Crystalline Order Aand the Size of Oil-Loaded Monolinolein-Based Dispersions. *Langmuir* **2010**, *26*, 6222-6229
29. Angelov, B.; Angelova, A.; Papahadjopoulos-Sternberg, B.; Lesieur, S.; Sadoc, J. F.; Ollivon, M.; Couvreur, P., Detailed Structure of Diamond-Type Lipid Cubic Nanoparticles. *J. Am. Chem. Soc.* **2006**, *128*, 5813-5817.
30. Leal, C.; Ewert, K. K.; Bouxsein, N. F.; Shirazi, R. S.; Li, Y.; Safinya, C. R., Stacking of Short DNA Induces the Gyroid Cubic-To-Inverted Hexagonal Phase Transition in Lipid–DNA Complexes. *Soft Matter* **2013**, *9*, 795-804.
31. Angelova, A.; Angelov, B.; Mutafchieva, R.; Lesieur, S.; Couvreur, P., Self-Assembled Multicompartment Liquid Crystalline Lipid Carriers for Protein, Peptide, and Nucleic Acid Drug Delivery. *Acc. Chem. Res.* **2010,** 44, 147-156.
32. Israelachvili, J. N., *Intermolecular and Surface Forces. 2nd Edition*, Academic Press, New York, **2011**.
33. Mulet, X.; Templer, R. H.; Woscholski, R.; Ces, O., Evidence That Phosphatidylinositol Promotes Curved Membrane Interfaces. *Langmuir* **2008**, *24*, 8443-8447.
34. Misquitta, Y.; Caffrey, M., Detergents Destabilize the Cubic Phase of Monoolein: Implications for Membrane Protein Crystallization. *Biophys. J.* **2003**, *85*, 3084-3096
35. Cherezov, V.; Clogston, J.; Papiz, M. Z.; Caffrey, M., Room To Move: Crystallizing Membrane Proteins in Swollen Lipidic Mesophases. *J. Mol. Biol.* **2006**, *357*, 1605-1618.
36. Wang, Z.; Zheng, L.; Inoue, T., Effect of Sucrose on the Structure of A Cubic Phase Formed from A Monoolein/Water Mixture. *Langmuir* **2007**, *23*, 3637-3645
37. Amar-Yuli, I.; Wachtel, E.; Shoshan, E. B.; Danino, D.; Aserin, A.; Garti, N., Hexosome and Hexagonal Phases Mediated by Hydration and Polymeric Stabilizer. *Langmuir* **2007**, *23*, 3637-3645.
38. Yaghmur, A.; De Campo, L.; Salentinig, S.; Sagalowicz, L.; Leser, M. E.; Glatter, O., Oil-Loaded Monolinolein-Based Particles with Confined Inverse Discontinuous Cubic Structure (Fd3m). *Langmuir* **2006**, *22*, 517-521.

39. Yaghmur, A.; De Campo, L.; Sagalowicz, L.; Leser, M. E.; Glatter, O., Emulsified Microemulsions and Oil-Containing Liquid Crystalline Phases. *Langmuir* **2005**, *21*, 569-577.
40. Pouzot, M.; Mezzenga, R.; Leser, M. E.; Sagalowicz, L.; Guillot, S.; Glatter, O., Structural and Rheological Investigation of Fd3m Inverse Micellar Cubic Phases. *Langmuir* **2007**, *23*, 9618-9628.
41. Phan, S.; Fong, W. K.; Kirby, N.; Hanley, T.; Boyd, B. J., Evaluating the Link between Self-Assembled Mesophase Structure and Drug Release. *Int. J. Pharm.* **2011**, *421*, 176-182.
42. Sagalowicz, L.; Guillot, S.; Acquistapace, S.; Schmitt, B.; Maurer, M.; Yaghmur, A.; De Campo, L.; Rouvet, M.; Leser, M.; Glatter, O., Influence Of Vitamin E Acetate and Other Lipids on the Phase Behavior of Mesophases Based On Unsaturated Monoglycerides. *Langmuir* **2013**, *29*, 8222- 8232.
43. Shearman, G.; Tyler, A.; Brooks, N.; Templer, R.; Ces, O.; Law, R.; Seddon, J., Ordered Micellar and Inverse Micellar Lyotropic Phases. *Liq. Cryst.* **2010**, *37*, 679-694.
44. Seddon, J.; Robins, J.; Gulik-Krzywicki, T.; Delacroix, H., Inverse Micellar Phases of Phospholipids and Glycolipids. *Phys. Chem. Chem. Phys.* **2000**, *2*, 4485-4493
45. Duesing, P.; Templer, R.; Seddon, J., Quantifying Packing Frustration Energy in Inverse Lyotropic Mesophases. *Langmuir* **1997**, *13*, 351-359.
46. Kumar, M.; Patil, N. G.; Choudhury, C. K.; Roy, S.; Ambade, A. V.; Kumaraswamy, G., Compact Polar Moieties Induce Lipid–Water Systems to Form Discontinuous Reverse Micellar Phase. *Soft Matter* **2015**, *11*, 5417-5424.
47. Choudhury, C. K.; Kumar, A.; Roy, S., Characterization of Conformation and Interaction of Gene Delivery Vector Polyethylenimine with Phospholipid Bilayer at Different Protonation State. *Biomacromolecules* **2013**, *14*, 3759-3768.
48. Choudhury, C. K.; Roy, S., Structural and Dynamical Properties of Polyethylenimine in explicit Water at Different Protonation States: A Molecular Dynamics Study. *Soft Matter* **2013**, *9*, 2269-2281.
49. Sharma, K. P.; Choudhury, C. K.; Srivastava, S.; Davis, H.; Rajamohanan, P.; Roy, S.; Kumaraswamy, G., Assembly of Polyethyleneimine in the Hexagonal Mesophase of Nonionic Surfactant: Effect Of pH And Temperature. *J. Phys. Chem. B* 2011, **115**, 9059-9069
50. Luzzati, V.; Vargas, R.; Gulik, A.; Mariani, P.; Seddon, J. M.; Rivas, E., Lipid polymorphism: a correction. The Structure of the Cubic Phase of Extinction Symbol

Fd3m Consists of Two Types of Disjointed Reverse Micelles Embedded in A 3-D Hydrocarbon Matrix. *J. Biochem.* **1992**, *31*, 279-285.

51. Seddon, J. M.; Zeb, N.; Templer, R. H.; McElhaney, R. N.; Mannock, D. A., An Fd3m Lyotropic Cubic Phase in A Binary Glycolipid/Water System. *Langmuir* **1996**, *12*, 5250-5253.
52. Murray, M.; Sanders, J., Close-Packed Structures of Spheres of Two Different Sizes II. the Packing Densities of Likely Arrangements. *Philosophical Magazine A* **1980**, *42*, 721-740

Chapter 5

Effect of Mesophase Domain Structure on Drug Release from Glycerol Monooleate Mesophases

5.1 Introduction

Liquid crystalline mesophases, based on self-assembly of amphiphilic lipids have emerged as promising systems for the delivery of pharmaceutical compounds.[1-3] Such systems have several advantages: (i) Lipid mesophases represent equilibrium phases. Therefore, the structures are robust to environmental changes encountered during storage and transportation of the formulations. (ii) The amphiphilic nature of the lipid assemblies make it possible to load these matrices with either hydrophilic or hydrophobic drugs, or with a combination of these – sometimes without change in mesophase structure.[4-7] This is especially advantageous when multiple therapeutics are required to be delivered simultaneously, for example, in the case of fixed dose combinations used to treat tuberculosis.[8] (iii) Several lipid mesophases, including several cubic phases, are characterized by a locally lamellar structure, reminiscent of cellular bilayers. These allow them to maintain proteins in their bioactive native conformation, and make them particularly well suited for delivery of macromolecules.[9-11] (iv) Encapsulation of drugs in lipid mesophases allow the possibility of controlling their release rate. (v) Finally, the disadvantage of working with high viscosity lipid mesophase gels can be overcome by formulating them into low viscosity water dispersible nanoparticles, that retain the ordered self-assembled lipid structure.[12-17] This makes it possible to prepare low viscosity injectable formulations containing drug-encapsulated lipid nanoparticles.

A lipid that has attracted considerable attention as a potential drug delivery matrix is glycerol monooleate (GMO). GMO is a naturally derived amphiphilic lipid that is biocompatible and biodegradable.[18]The GMO/water binary system organizes into several different ordered phases at room temperature, depending on the water content in the system.[19,20] Of specific interest for drug delivery applications[22-23] are bicontinuous cubic phases: at low water content, GMO/water organizes into an ordered phase with Ia3d symmetry at room temperature and ambient pressure; with increase in water content, the system forms a cubic phase with Pn3m symmetry. At even higher water content, the Pn3m phase coexists with an excess water phase. In this phase, it is possible to disperse the mesophase to form an aqueous colloidal dispersion, where colloidal lipid particles retain Pn3m ordering and are stabilized by the adsorption of polyethylene oxide-polypropylene oxide block copolymers .[16] These ordered lipid colloids are called cubosomes. Recent studies have investigated release of hydrophilic drugs encapsulated in cubosomes.[7,24] Due to the bicontinuous architecture of the Pn3m phase, the aqueous channels in cubosomes are connected with the aqueous matrix. Therefore, cubosomes that contain water soluble drugs

exhibit a burst release.[7,24] This is not desirable in situations where a sustained slow release of drug is required. Therefore, different strategies have been reported in the literature to prevent burst release of encapsulated drugs. These include the modification of the encapsulated drug to reduce its water solubility,[25] layer-by-layer coating of cubosomes using polyelectrolytes[24] and coating the cubosomes using cationic polymers such as poly-ε-lysine.[7] Recently, we have demonstrated a new route to access the discontinuous cubic micellar phase with Fd3m symmetry in GMO/water systems at room temperature.[26,27]In this phase, spherical inverse micelles are packed into an AB_2 cubic phase structure, and there are no channels connecting the aqueous micellar cores. Thus, release of hydrophilic drugs from such matrices is significantly slower than for the bicontinuous phases.[28]

Experiments that characterize release characteristics often employ a simple 1-D geometry, with the drug-loaded matrix in contact with a buffer. The buffer is periodically assayed to evaluate drug release. Several models have been developed to represent the release of drugs from sustained release formulations, including polymeric matrices and lipid mesophases. Among the most widely used models is the Higuchi model[29] that was developed to model diffusive release of drugs encapsulated in a homogeneous matrix. Here, a 1-D diffusion model is solved and an approximate solution is obtained under quasi-steady state conditions for short release times. In the Higuchi equation, the total amount released is proportional to the square root of the time of release, and these are related through an apparent diffusion coefficient that characterizes the rapidity of release. The Higuchi model has been extended to non-homogeneous matrices, including porous matrices. However, for release experiments from lipid mesophase matrices, the original form of the Higuchi equation (for homogeneous matrices) is typically employed.[29,30]Apart from the Higuchi relation, power law forms have also been employed to fit release data.[31]Another semi-empirical model that has been employed to model release data is the Hixon-Crowell cube root relation, that is applicable to release due to dissolution of drug particles.[30,32] Here, we focus on the Higuchi model due to its wide use, especially in modeling release from lyotropic mesophases. In ordered lyotropic mesophases, the samples are never monodomain – rather, they are polydomain with macroscopic samples comprising an isotropic distribution of domain orientations. It is intuitive that release of drug from lyotropic mesophases would be influenced by the polydomain structure of the sample. However, this is not considered in the Higuchi model. Here, we report release experiments from GMO mesophases containing a water soluble drug, Naproxen sodium. We contrast release from mesophases with Pn3m and

Fd3m architecture, and observe that release from the Fd3m phase is considerably slower than from the bicontinuous phase.[29] We also show that mesophase samples prepared by cooling at different rates exhibit different release rates. We attribute this to the domain structure in the mesophase sample and present a model for release from polydomain samples.

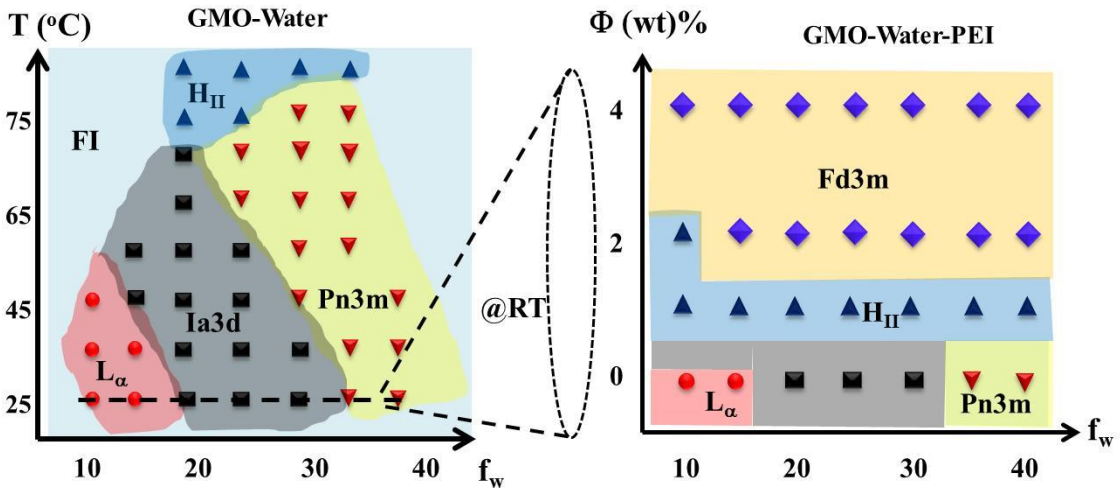

Figure 5.1: (a) Phase diagram of GMO/water system as a function of the water fraction (f_w) and temperature. (b) GMO/water/PEI ternary phase diagram as a function of water fraction (f_w) and PEI content (Φ) at 25 °C. On incorporation of PEI, the system accesses the reverse hexagonal H_{II} phase and the discontinuous cubic micellar Fd3m mesophase at ambient temperature.

5.2 Experimental Section

5.2.1 Materials:

A commercial sample of glycerol monooleate was supplied to us by Danisco, India (trade name: Rylo MG 20 Pharma). In this work, we refer to this sample as GMO. GMO is >98% pure and we have previously reported its characterization.[7,26,27] polyethylenimine (b-PEI) with molecular weight (Mw) ≈ 2 kDa was purchased from Sigma-Aldrich as a 50% (w/w) aqueous solution and was used as received. Hydrophilic drug naproxen sodium (NaP) was purchased from Sigma-Aldrich and used as received. Phosphate buffer solution at pH 7.2 was prepared using Millipore Milli-Q water (resistivity = 18.2 MΩ.cm). The chemical structures of all the molecules used in this work are shown in the figure 5.2.

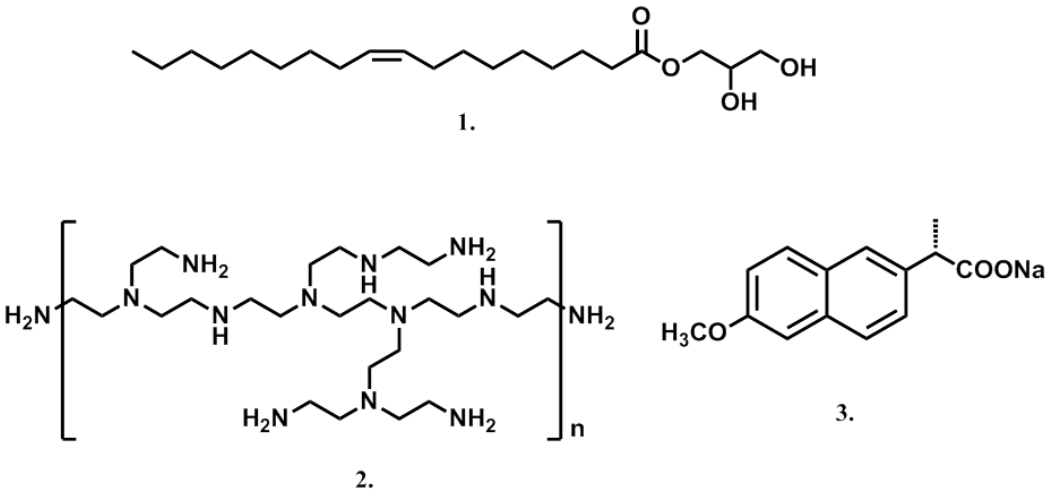

Figure 5.2: Chemical structures of molecules (1) Glycerol-monooleate (GMO); (2) Poly-ethyleneimine (PEI), Mw~2k; (3) Naproxen sodium.

5.2.2 Sample Preparation:

GMO is a white solid at room temperature. We prepare binary systems by mixing molten GMO (at ≈ 80^{o}C) with phosphate buffer (pH = 7.2). All samples reported here are prepared using phosphate buffer – however, we interchangeably refer to them as GMO/"water" systems, or "water" channels. Ternary systems are prepared by mixing molten GMO with PEI dissolved in phosphate buffer. We study the release of water soluble drug, NaP, encapsulated in GMO mesophases. In this work, our main objective is to compare the release from Pn3m and Fd3m mesophases. Here, we do not investigate the loading capacity of NaP in these mesophases. Rather, we use a small concentration of NaP (0.05% by weight of the GMO/water mesophase), simply as a marker to monitor release from the aqueous phase. At these low concentrations, NaP does not perturb the GMO phase diagram. NaP is dissolved into the phosphate buffer and then mixed with GMO during sample preparation. Sample homogeneity is ensured by performing repeated cycles of vortexing and heating to 80 $^{\circ}$C. Finally, the sample is stored at room temperature for a minimum of 3 days for equilibration.

Samples were prepared at different ratios of GMO to phosphate buffer (80/20, 70/30, 65/35). We represent the fraction of phosphate buffer solvent as $f_{w.}$ At high f_w, GMO/water forms a two phase system with a gel-like mesophase in equilibrium with an excess water phase. Therefore, here we have restricted our investigations to systems with $f_w < 40\%$. As an example, to prepare 500 mg of a NaP containing binary GMO/water system with $f_w = 30\%$,

we mix 0.25 mg of NaP with 149.925 mg of phosphate buffer and then add this to 349.825 mg (= 149.925 x 7/3) of GMO at 80°C in a borosil glass vial. Similarly, we prepare 500 mg of a ternary system containing Φ = 2% PEI by mixing 10 mg PEI (taken as 50% w/v aqueous solution) with 0.25 mg NaP and 146.925 mg phosphate buffer. This is then added to 342.825 mg (= 146.925 x 7/3) of GMO held at 80°C and the sample is prepared by repeated vortexing and mixing.

5.2.3 Release Study:

After equilibration for several days, the sample vial contains a uniform mesophase in the shape of a disk with diameter 1.3 cm (equal to the inner diameter of the borosil vial), and thickness 0.5 cm. GMO mesophases are insoluble in water and can co-exist with excess buffer. Therefore, release measurements were performed by directly adding 2 ml of pH 7.2 phosphate buffer on the surface of the disk-like sample. We gently poured buffer over the top surface of the phase so that the flat top interface is not disturbed. The time when excess buffer is brought into contact with mesophase is defined as the initial time, t = 0. Sample vials were maintained under constant gentle shaking to ensure that there are no spatial gradients of NaP in the buffer during the release experiment. We periodically replace buffer from the vial with fresh phosphate buffer, following a previously reported[33] protocol to simulate perfect sink conditions during release studies. All release experiments were carried out in triplicate, at room temperature (=25°C).

Release was monitored by measuring the intensity of the NaP absorption peak (λ = 230 nm) using a UV-visible spectrophotometer. Phosphate buffer was used as reference to subtract the background. We use a calibration curve obtained using NaP solutions of known concentrations in buffer (Figure 5.3) to quantitate NaP release.

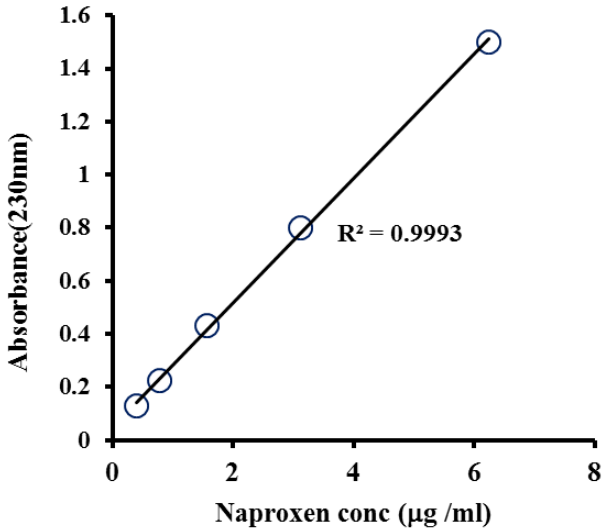

Figure 5.3: Calibration of the naproxen sodium drug.

5.3 Characterisation tools

5.3.1 Small angle X-rays scattering (SAXS):

We use small angle X-ray scattering (SAXS) to characterize the mesophase microstructure. SAXS was performed using NANO-Viewer, Rigaku. The instrument is equipped with a micro-focus source and rotating Cu anode operated at 40 kV and 30 mA. We use Cu Kα radiation with wavelength, $\lambda = 1.54$ Å. A Confocal Max Flux (CMF) mirror and three slit collimation system was used to generate a monochromatic, collimated beam. The sample to detector distance is set at 738 mm and the detector was calibrated using a silver behenate standard. Data was collected on a HyPix-3000 2D semiconductor detector with pixel size of 100 μm^2. The detector count rate exceeds 10^6 cps/pixel resulting in relatively low noise in the data. A Linkam HFSX-350-CAP stage (Linkam, UK) was used to mount the sample in the X-ray beam. The sample was placed between two Kapton sheets with a 1 mm gap, set with an O-ring spacer. Data was collected for a q range between 0.01 $Å^{-1}$ – 0.28 $Å^{-1}$, and the 2D data was integrated using offline Rigaku SAXS analysis software. Mesophase characteristic peaks were indexed using 'Scatter' software. The Ia3d phase is characterized by peaks with positions in the ratio of √6:√8:√11... For the Fd3m phase, peaks are in the ratio of √3:√8:√11:√14….. , and for the Pn3m phase, peaks are in the ratio of √2:√3:√4:√6:√8…

5.4 Results and Discussion

The GMO mesophases investigated in this work are prepared using phosphate buffer. The phase behaviour of the samples prepared using buffer (at f_w = 15, 20%) is similar to those prepared using water. Therefore, as mentioned in the Experimental Section, we use water and buffer interchangeably in this paper when referring to mesophase samples. However, we reiterate that all samples reported in this work were prepared using phosphate buffer.

Naproxen sodium is a water soluble small molecule. Therefore, it is localized in the water channels of the GMO/water liquid crystalline cubic phases (LCCP). Further, we anticipate that release of NaP is not dependent on the water channel size[27] (since the size of the water channels, ≈ 3-4 nm, is significantly larger than the molecular size of NaP). Finally, we note that at the low loadings of NaP used here, drug encapsulation does not change the GMO/water phase behaviour (Figure 5.4).

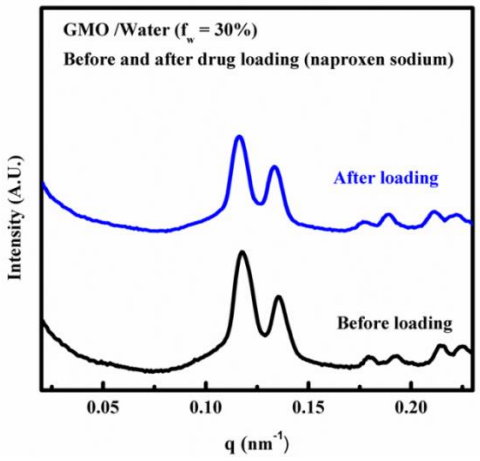

Figure 5.4: Small angle X-ray scattering (SAXS) data for Ia3d phase formed with and without naproxen sodium (0.05% by weight) in GMO/water (70/30) system.

We begin by investigating the influence of water fraction on the release of NaP from GMO/water mesophases. GMO organizes into an Ia3d phase for 35% > $f_w \geq$ 20 and into a Pn3m phase for higher water fractions, $f_w \geq$ 35% (Figure 5.5 a). With increase in water content, the lattice parameter increases. When f_w is increased from 20% to 30%, there is a change in the Ia3d lattice parameter from 113.2 Å to 133.7 Å (Figure 5.5 a). In the Pn3m phase, the lattice parameter increases from 87.8 Å for f_w = 35% and saturates for higher water fractions ($f_w \geq$ 40%), when the Pn3m mesophase is in equilibrium with an excess water phase

(Figure 5.5 a). Release studies performed on Pn3m samples with $f_w \geq 40\%$ show an apparent burst release due to the NaP in the excess water phase. This is not representative of release of drug encapsulated *within* the mesophase. Therefore, we restrict our investigations to release from mesophases with $f_w < 40\%$.

We observe that the NaP release is quantitatively identical, within experimental error, for release from all the samples investigated (Figure 5.5 b), despite the change in lattice parameter as f_w increases from 20 to 30%, and despite the change in mesophase symmetry as f_w is increased to 35%. Release studies are performed by incubating disk shaped mesophase samples with an excess of buffer. When these samples come into contact with buffer, they equilibrate and transform into a saturated Pn3m phase, characterized by a lattice parameter of 95 Å. Therefore, in all samples, release happens from a solvent-saturated Pn3m phase. Since the release profiles of NaP from samples with f_w = 20, 30 and 35% are approximately identical, this suggests that release is characteristic of samples in the saturated Pn3m phase. Thus, samples transform into the saturated Pn3m phase on coming into contact with the buffer and NaP release happens from this phase. For all samples, ≈ 15% of the encapsulated NaP is released after 25 hours, ≈ 25% after 50 hours, and ≈ 55% is released after 350 hours. NaP continues to release slowly beyond 350 hours (Figure 5.5 b).

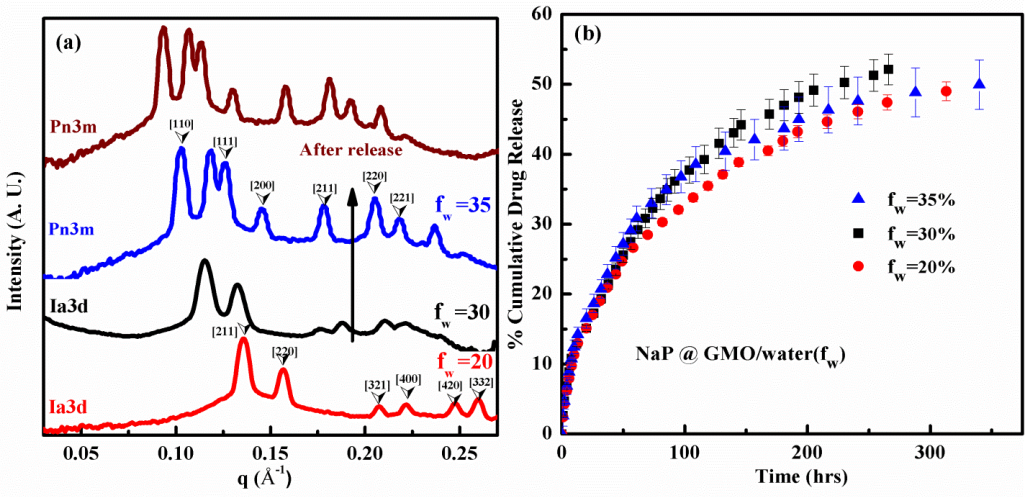

Figure 5.5: (a) SAXS on GMO/water samples. As prepared samples with f_w = 20, 30% shows peaks corresponding to the Ia3d phase. We observe the Pn3m mesophase for f_w = 35%. On incubating with buffer for release measurements, the as-prepared samples transforms into a Pn3m phase. (b) Percentage cumulative drug release as a function of time for GMO/water mesophases prepared with f_w = 20, 30 and 35%

5.4.1 Release of naproxen sodium from GMO/water/PEI mesophase:

Incorporation of Φ = 2% branched polyethyleneimine (PEI) in the GMO/water system induces formation of the discontinuous reverse micellar Fd3m phase (Figure 5.1 b). Here, we contrast release of NaP from a GMO/water mesophase with f_w = 30% with that from a GMO/water mesophase with f_w = 30% and containing PEI, Φ = 2% (Figure 5.6 a). The as prepared GMO/water/Φ = 2% PEI sample equilibrates to an Fd3m phase characterized by a lattice parameter = 146.9 Å. After incubating with buffer for 300 hours for release experiments, we observe no phase change. However, the lattice parameter for the Fd3m changes to 143.8 Å (Figure 5.6 b). We note that the release is approximately equal to that from another sample prepared in the Fd3m phase, with Φ = 2% and f_w = 20%. Thus, we anticipate that release happens from "saturated" Fd3m samples equilibrated to a lattice parameter of 143.8 Å.

There is a significant difference in NaP release from the bicontinuous Pn3m and discontinuous Fd3m phases. The Fd3m mesophase shows much slower release with only 3% NaP released in 25 hours (compare with 15% for the Pn3m) (Figure 5.6 a). After incubation with buffer for 350 hours, the Fd3m mesophase releases only 13% of the NaP, compared with 55% for the Pn3m phase. As NaP is water soluble, we anticipate that it remains in the aqueous channels in the Pn3m mesophase and within the aqueous reverse micellar core in the Fd3m mesophase. As the Pn3m structure is characterized by bicontinuous water channels, it is reasonable that NaP contained in these channels readily diffuses out to the buffer. In contrast, the Fd3m phase comprises inverse micellar structures with discontinuous aqueous cores. Therefore, NaP in these cores cannot readily diffuse out to the buffer as in the Pn3m phase and thus, release of NaP is retarded.

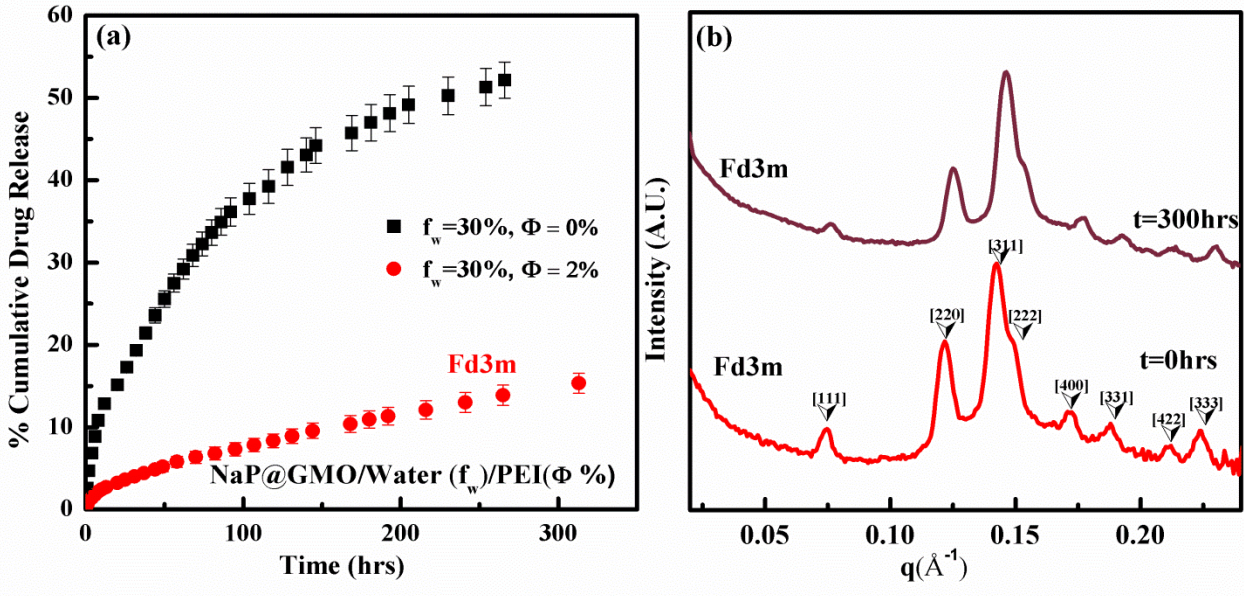

Figure 5.6: (a) Release of NaP from GMO/water/Φ = 0% and GMO/water/Φ = 2% PEI mesophase samples at room temperature. (b) SAXS from GMO/water/Φ = 2% PEI mesophase as prepared and after NaP release into buffer for 300 hours.

5.4.2 Fickian 1D-diffusion model for NaP release:

A 1-D Fickian diffusion model has been used in the literature to describe release data from mesophases.[28,34] Higuchi provided an approximate solution that is valid at short times for release through 1-D diffusion from a homogeneous matrix. We model our release data using Higuchi's equation as:

$$\text{Amount released} = 2C_o \pi r^2 \sqrt{\frac{Dt}{\pi}} \quad (1)$$

Where C_o is the initial concentration of NaP in the mesophase, l is the thickness of the mesophase matrix, r is the radius of cylindrical mesophase disk and, D is the apparent diffusivity. This solution is valid for $t \ll \frac{4\pi l^2}{(D\pi^2)}$. We assume that release happens from a saturated mesophase, consistent with our data (Figure 5.5 b) As the buffer is continuously agitated, we assume that there are no concentration gradients in the buffer. Since we periodically replace the buffer, we assume perfect sink conditions. Release data for NaP from Pn3m and Fd3m mesophases, along with the fits to the data based on the Higuchi model are shown in Figure 5.7.

We observe that our fits yield a significantly lower value of diffusivity in case of discontinuous Fd3m mesophase (D = 2.1 x 10^{-13} m^2/s) relative to the bicontinuous Pn3m

mesophase (D = 3.2 x 10^{-12} m^2/s). These values are in good agreement with the literature.[28]

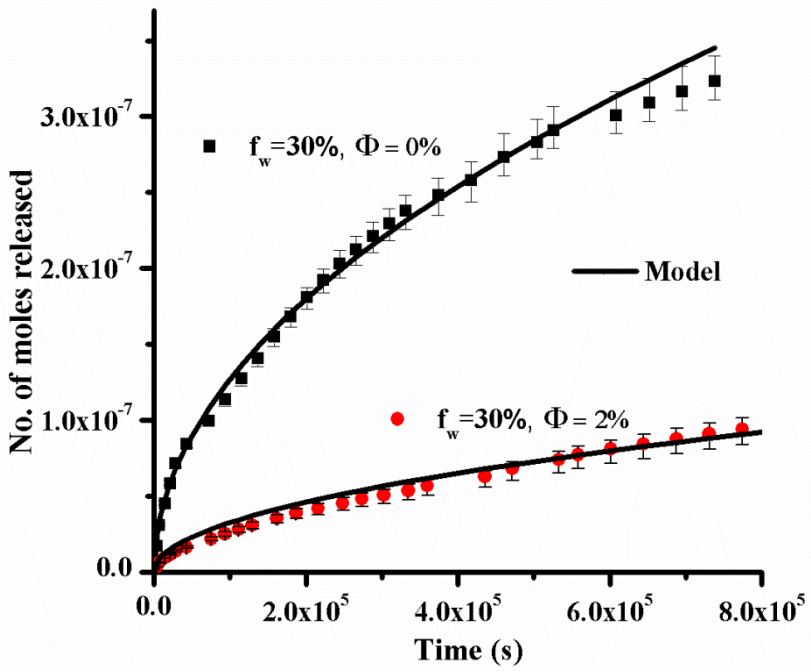

Figure 5.7: Results for NaP released into the buffer are shown with a fit based on the Higuchi model as a solid line. We show data for release from GMO/water samples with Pn3m structure (in black) and from GMO/water/2% PEI samples with Fd3m structure (in red) (f_w = 30% for both samples).

Higuchi's 1-D diffusion model assumes diffusion through a homogeneous mesophase. However, we have shown recently that when GMO/water/PEI is cooled from the disordered isotropic phase at 80°C to room temperature, there is the formation of an intermediate hexagonal phase, organized as a multi-domain structure.[26,27] Using optical microscopy, we observe that the hexagonal phase nucleates at room temperature and domains grow until impingement. On storing at room temperature, the sample equilibrates and the hexagonal phase transforms to the Fd3m phase over several hours. The Fd3m phase has cubic symmetry – therefore, the mesophase sample appears dark between crossed polarizers. However, it is reasonable to assume that the multi domain structure is preserved. In GMO/water samples, the cubic Pn3m phase appears dark between crossed polarizers. However, it is reasonable to assume that the Pn3m mesophase sample too is characterized by a polydisperse multidomain structure, even though we cannot visualize it.The 1-D diffusion model neglects the domain structure of the mesophase and assumes a homogeneous mesophase. Therefore, Higuchi's

equation does not provide any insights on the effect of the domain structure on diffusion. We now present data to show dependence of release rate on domain size.

5.4.3 Effect of sample cooling rate on NaP:

Mesophase samples are prepared by cooling GMO mixtures from 80 °C to room temperature and allowing them to equilibrate. Mesophase domains nucleate and grow as the samples are cooled. We anticipate that rapid cooling should result in more profuse, denser nucleation and the formation of smaller domains. Thus, rapid cooling should result in faster release of encapsulated NaP. We used a Linkam CSS450 stage to control the heating/cooling rate. We heated the sample to the isotropic phase transition temperature (80°C) in the Linkam stage and then cooled it with two different cooling rates (8°C/min & 38°C/min). We use polarized optical microscopy to investigate the domain size distribution for the hexagonal phase formed in ternary GMO/water/PEI samples, before the transition to the Fd3m phase.

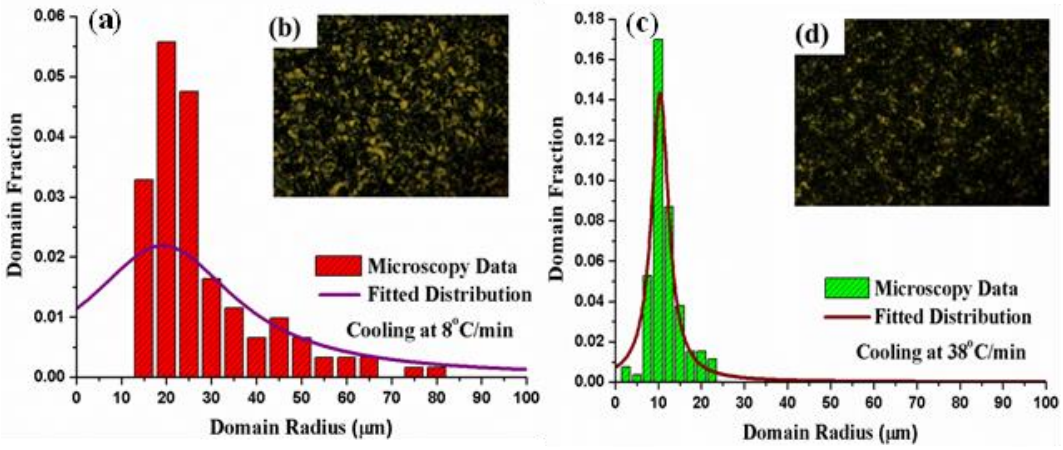

Figure 5.8: (a) Domain size distribution for the H_{II} mesophase with cooling rate 8°C/min. (b) Polarized optical microscopy (POM) image of H_{II} phase formed with 2% PEI before its transition into an equilibrium Fd3m mesophase (c) Domain size distribution for the H_{II} mesophase formed by a faster cooling rate = 38°C/min, (d) The polarized optical image (POM) image shows smaller domains of the H_{II} mesophase formed with the higher cooling rate (38°C/min).

We observe that there is a clear effect of cooling rate on the domain size distribution in the hexagonal phase. As expected, slower cooling rate (8°C/min) results in the formation of larger textures and faster cooling rate results in smaller domains of the H_{II} mesophase

(Figure 5.8 b, and 5.8 d). The domain size distribution obtained from optical microscopy is shown in Figures 5.8 a, c; the number average domain size varies from ≈ 20 μm for a cooling rate 8°C/min to ≈ 10 μm for cooling at 38°C/min.

To examine the effect of domain size on release, we prepared binary (70/30 GMO/water) and ternary (GMO/water/PEI, 70/30/Φ =2%) samples in vials for drug release studies, at the same cooling rates as the microscopy experiments. Our data clearly reveal that the release of NaP from mesophases prepared at different cooling rates is different (Figure 5.9). Mesophases (both bicontinuous and discontinuous) prepared at a cooling rate of 38°C/min release NaP faster when compared with corresponding samples cooled at 8°C/min. While it is possible to capture this effect by fitting the data with an apparent diffusivity in the Higuchi model, this model does not establish a connection between the change in domain size and the value of the diffusivity. Therefore, we now present a model for drug release that incorporates the effect of the mesophase domain size.

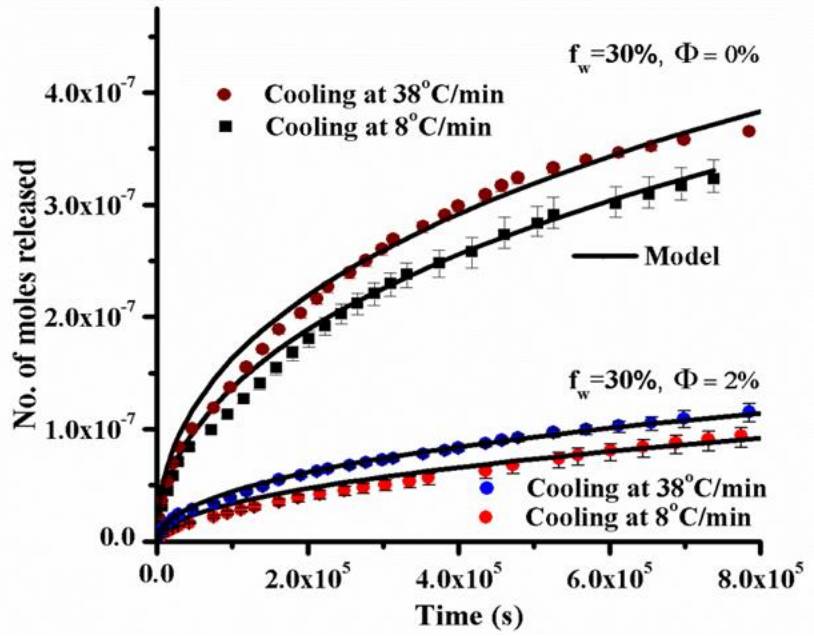

Figure 5.9: Release of NaP from mesophases prepared at different cooling rates 38°C/min and 8°C/min, respectively fitted with the polydisperse spherical domain model.

5.4.4 Polydisperse spherical domains model:

We present a simplified model wherein the sample is comprised of spherical mesophase domains (Figure 5.10) that are uniformly loaded with NaP. NaP diffuses out of the spherical domains and is released into the buffer sink, through domain boundaries. We assume that release is limited by diffusion out of the spherical domains, and not by diffusion through domain boundaries. We use the following 1-D equation for radial diffusion through a single spherical domain:

$$\frac{\partial C}{\partial t} = D\left[\frac{\partial^2 C}{\partial r^2} + \frac{2}{r}\frac{\partial C}{\partial r}\right] \qquad (2)$$

where C is the concentration of drug, r is the radial coordinate within the sphere and D is the diffusivity through the spherical domain. We use the solution to this equation to obtain the total amount of NaP released from the sample as:

$$Amount = \int_0^\infty f(R)dR \left\{\frac{4}{3}\pi R^3 C_o\left[1 - \frac{6}{\pi^2}\sum_{n=1}^{\infty}\frac{e^{-\frac{Dn^2\pi^2}{R^2}t}}{n^2}\right]\right\} \qquad (3)$$

where R is the radius of a spherical domain and $f(R)$ is the domain size distribution. An approximate solution for the series in equation (3) is not available since $t \ll \frac{R^2}{\pi^2 D}$ does not hold for the typical diffusion times and mesophase domain sizes in our experiments. Therefore, we fit out data by solving (3) numerically and truncate the series to n = 1000. Increasing n beyond 1000 does not appreciably change the value of the numerical solution. For simplicity, we use a Lorentzian form for $f(R)$. Therefore, there are three fitting parameters in this model: the diffusivity (D) that determines radial diffusion in the spherical domains, a mean domain radius (b) and the width of the domain size distribution (w).

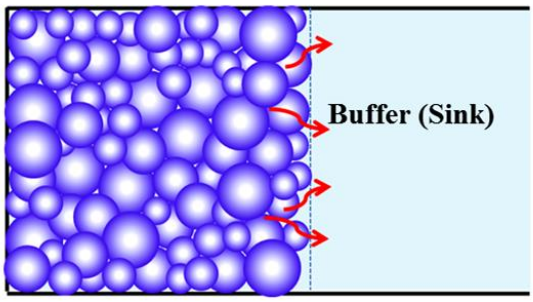

Figure 5.10: Schematic showing the domain size distribution in the bulk mesophase. NaP released from these domains is transported to the buffer sink through interdomain regions.

We show the best fit to the release data from both Pn3m and Fd3m samples, at the two cooling rates in Figure 5.9. The model parameters for the fit are listed in Table 5.1. The domain size distributions that correspond to this fit are plotted as solid lines in Figures 5.8 a, c. There are several features for this model fit that are noteworthy:

i. Firstly, this model accounts in a natural way, for the effect of domain size on drug release.

ii. The distribution of domain sizes from the fit to the data (for release from the Fd3m phase) correspond reasonably well to the size distribution for H_{II} domains from independent optical microscopy characterization (compare experimental data for domain sizes from optical microscopy with the solid line for the distribution from the fit to the release data, Figures 5.8 a, c). For both cooling rates, we observe that the average domain size from the microscopy data matches the peak size from the fit and the spread of domain sizes is also similar. The domain size distribution from optical microscopy of slowly cooled samples (8 $^{\circ}$C/min) is not symmetric, while the fit to the release data assumes a Lorentzian distribution. Despite this, the average domain size from the microscopy data and the fit match well. Release happens from the Fd3m domains and not from the H_{II} phase. However, since the H_{II} phase forms as an intermediate phase to the Fd3m phase, it is reasonable that the domain structure for the H_{II} phase is preserved in the Fd3m phase. The match between the domain size distributions obtained from fitting the release data, and direct optical microscopy measurements is very satisfying. Thus, while this model uses three parameters for fitting the release data, it appears the domain size distribution matches reasonably well with direct experimental measurements, where available.

iii. The diffusivities obtained from the fit to the release data reveal that the diffusion constant that characterizes the Pn3m phase is an order of magnitude larger than that for the Fd3m phase. This is consistent with the ratio of diffusivities for these phases from the Higuchi equation. However, there is no significant change in the diffusion constant for a given mesophase with cooling rate. Therefore, the diffusivity that we obtain appears to be a characteristic of the local structure of the mesophase, unlike the case of the apparent diffusivity from the Higuchi model (that varies substantially with

cooling rate). The actual value of the diffusivities obtained from the polydisperse sphere model are significantly lower than the apparent diffusivities from the 1-D Higuchi. We obtain an apparent diffusivity for NaP diffusion at room temperature = 8.5 x 10^{-16} m^2/s for the Pn3m phase and = 4.3 x 10^{-17} m^2/s for the discontinuous Fd3m phase. We emphasize that, given the simplifications in our model, the diffusivity that we calculate is also an apparent diffusivity. However, it appears to characterize the influence of mesophase structure on release in a more physically consistent way as compared to the Higuchi model, which assumes a homogeneous sample and disregards domain structure.

GMO/Water/PEI (8 °C/min, 38 °C/min)	D (m^2/s)	b (μm)	w (μm)
70/30/0	8.5 x 10^{-16}	17.4	25
70/30/2	4.3 x 10^{-17}	19.2	20
70/30/0	1.1 x 10^{-15}	7.09	2.5
70/30/2	4.8 x 10^{-17}	10.4	2.4

Table 5.1: Fitting parameters for different concentrations of PEI at different cooling rates.

5.5 Summary

We demonstrate that diffusion of hydrophilic model drug, NaP, from discontinuous Fd3m mesophase is about an order of magnitude slower than from the bicontinuous Pn3m structure. We examine drug diffusion from a cylindrical mesophase sample and obtain the diffusivity from a model fit to the drug release data. The data is fitted well by the Higuchi model for 1D diffusivity through homogeneous samples. However, this model is incapable of capturing the effect of the multidomain structure of the mesophase samples. We demonstrate that drug-loaded mesophase samples cooled at different rates exhibit differences in domain size and also show different release rates. Samples cooled rapidly have smaller domains and exhibit faster drug release. An alternate model that represents the mesophase sample as comprising of polydisperse spherical domains is able to fit the release data well. The domain size distribution obtained from the fit to the release data show a reasonable match with direct measurements of domain size (for an intermediate anisotropic H_{II} phase) using optical microscopy. The diffusivity obtained for the polydisperse spherical domain model is not strongly influenced by the cooling rate used to prepare the mesophase, suggesting that it is characteristic of the local lipid organization in the mesophase. The

values of diffusivity obtained from the polydisperse spherical domain model are significantly lower than those from the Higuchi model. However, the ratio of diffusivities for the Fd3m and Pn3m phases are comparable.

5.6 References

1. Agrawal, A. K.; Kumar, K.; Swarnakar, N. K.; Kushwah, V.; Jain, S., "Liquid Crystalline Nanoparticles": Rationally Designed Vehicle to Improve Stability and Therapeutic Efficacy of Insulin Following Oral Administration. *Mol. Pharm.* **2017**.
2. Le, T. C.; Mulet, X.; Burden, F. R.; Winkler, D. A., Predicting the Complex Phase Behavior of Self-Assembling Drug Delivery Nanoparticles. *Mol. Pharm.* **2013,** *10*, 1368-1377.
3. Pham, A. C.; Hong, L.; Montagnat, O.; Nowell, C. J.; Nguyen, T. H.; Boyd, B. J., In Vivo Formation of Cubic Phase in situ After Oral Administration of Cubic Phase Precursor Formulation Provides Long Duration Gastric Retention and Absorption for Poorly Water-Soluble Drugs. *Mol. Pharm.* **2015,** *13*, 280-286.
4. Mulet, X.; Boyd, B. J.; Drummond, C. J. Advances in Drug Delivery and Medical Imaging Using Colloidal Lyotropic Liquid Crystalline Dispersions. *J. Colloid Interface Sci.* **2013**, *393*,1−20.
5. Pan, X.; Han, K.; Peng, X.; Yang, Z.; Qin, L.; Zhu, C.; Huang, X.; Shi, X.; Dian, L.; Lu, M.; Wu, C. Nanostructured Cubosomes as Advanced Drug Delivery System. *Curr. Pharm. Des.* **2013,** *19*, 6290− 6297.
6. Guo, C.; Wang, J.; Cao, F.; Lee, R. J.; Zhai, G. Lyotropic Liquid Crystal Systems in Drug Delivery. *Drug Discov. Today* **2010**, *15*, 1032−1040.
7. Deshpande, S.; Venugopal, E.; Ramagiri, S.; Bellare, J. R.; Kumaraswamy, G.; Singh, N., Enhancing cubosome functionality by coating with a single layer of poly-ε-lysine. *ACS Appl. Mater. Interfaces* **2014,** *6*, 17126-17133.
8. Agrawal, S.; Singh, I.; Kaur, K. J.; Bhade, S. R.; Kaul, C. L.; Panchagnula, R., Comparative Bioavailability of Rifampicin, Isoniazid and Pyrazinamide from a Four Drug Fixed Dose Combination with Separate Formulations at the Same Dose Levels. *Int. J. Pharm.* **2004,** *276*, 41-49.
9. Lendermann, J.; Winter, R., Interaction of Cytochrome c with Cubic Monoolein Mesophases at Limited Hydration Conditions: The Effects of Concentration, Temperature and Pressure. *Phys. Chem. Chem. Phys.* **2003,** *5*, 1440-1450.
10. Kraineva, J.; Smirnovas, V.; Winter, R., Effects of Lipid Confinement on Insulin Stability and Amyloid Formation. *Langmuir* **2007,** *23*, 7118-7126.

11. Cherezov, V., Lipidic Cubic Phase Technologies for Membrane Protein Structural Studies. *Curr. Opin. Struct. Biol.* **2011,** *21,* 559-566.
12. Barauskas, J.; Johnsson, M.; Joabsson, F.; Tiberg, F. Cubic Phase Nanoparticles (Cubosome): Principles for Controlling Size, Structure, and Stability. *Langmuir* **2005**, *21*, 2569−2577.
13. Wörle, G.; Siekmann, B.; Koch, M. H. J.; Bunjes, H. Transformation of Vesicular into Cubic Nanoparticles by Autoclaving of Aqueous Monoolein/poloxamer Dispersions. *Eur. J. Pharm. Sci.* **2006**, *27*, 44−53
14. Barauskas, J.; Johnsson, M.; Joabsson, F.; Tiberg, F., Cubic Phase Nanoparticles (cubosome): Principles for Controlling Size, Structure, and Stability. *Langmuir* **2005,** *21*, 2569-2577.
15. Barauskas, J.; Johnsson, M.; Tiberg, F., Self-assembled Lipid Superstructures: Beyond Vesicles and Liposomes. *Nano let.* **2005,** *5*, 1615-1619.
16. Spicer, P. T.; Hayden, K. L.; Lynch, M. L.; Ofori-Boateng, A.; Burns, J. L., Novel Process for Producing Cubic Liquid Crystalline Nanoparticles (cubosomes). *Langmuir* **2001,** *17*, 5748-5756.
17. Yaghmur, A.; Glatter, O., Characterization and Potential Applications of Nanostructured Aqueous Dispersions. *Adv. Colloid Interface Sci.* **2009,** *147,* 333-342.
18. Kulkarni, C. V.; Wachter, W.; Iglesias-Salto, G.; Engelskirchen, S.; Ahualli, S., Monoolein: A Magic Lipid? *Phys. Chem. Chem. Phys.* **2011,** 13, 3004-3021.
19. Briggs, J.; Chung, H.; Caffrey, M., The Temperature-Composition Phase Diagram and Mesophase Structure Characterization of the Monoolein/Water System. *J.Dde Phys. II* **1996,** *6*, 723-751.
20. Qiu, H.; Caffrey, M., The Phase Diagram of the Monoolein/Water System: Metastability and Equilibrium Aspects. *Biomaterials* **2000,** *21*, 223-234.
21. Drummond, C. J.; Fong, C., Surfactant Self-Assembly Objects as Novel Drug Delivery Vehicles. *Curr. Opin. Colloid Interface Sci.***1999,** *4*, 449-456.
22. Boyd, B. J.; Whittaker, D. V.; Khoo, S. M.; Davey, G., Lyotropic Liquid Crystalline Phases Formed from Glycerate Surfactants as Sustained Release Drug Delivery Systems. *Int. J. Pharm.* **2006,** *309,* 218-226.
23. Shah, J. C.; Sadhale, Y.; Chilukuri, D. M., Cubic Phase Gels as Drug Delivery Systems. *Adv. Drug Deliv. Rev.* **2001,** *47,* 229-250.

24. Driever, C. D.; Mulet, X.; Waddington, L. J.; Postma, A.; Thissen, H.; Caruso, F.; Drummond, C. J. Layer-by-Layer Polymer Coating on Discrete Particles of Cubic Lyotropic Liquid Crystalline Dispersions (Cubosomes). *Langmuir* **2013**, *29*, 12891−12900.

25. Nguyen, T. H.; Hanley, T.; Porter, C. J. H.; Boyd, B. J., Nanostructured Liquid Crystalline Particles Provide Long Duration Sustained-Release Effect for a Poorly Water Soluble Drug after Oral Administration. *J. Control. Release* **2011,** *153*, 180-186.
26. Kumar, M.; Patil, N. G.; Choudhury, C. K.; Roy, S.; Ambade, A. V.; Kumaraswamy, G., Compact Polar Moieties Induce Lipid–Water Systems to Form Discontinuous Reverse Micellar Phase. *Soft Matter* **2015,** *11*, 5417-5424
27. Kumar, M.; Kumaraswamy, G., Phase Behaviour of the Ternary System: Monoolein–Water–Branched Polyethylenimine. *Soft Matter* **2015,** *11*, 5705-5711.
28. Phan, S.; Fong, W. K.; Kirby, N.; Hanley, T.; Boyd, B. J., Evaluating the Link Between Self-Assembled Mesophase Structure and Drug Release. *Int. J. Pharm.* **2011,** *421*, 176-182.
29. Higuchi, I. W., Diffusional Models Useful in Biopharmaceutics Drug Release Rate Processes. *J. Phrma. Sci.* **1967**, *56*, 315.
30. Singhvi, G.; Singh, M., Review: In-Vitro Drug Release Characterization Models. *Int. J. Pharm. Stud. Res.* **2011,** *2*, 77-84.
31. Siepmann, J.; Peppas, N. A., Modeling of Drug Release from Delivery Systems Based on Hydroxypropyl Methylcellulose (HPMC). *Adv. Drug Deliv. Rev.* **2012,** *64*, 163-174.
32. Dash, S.; Murthy, P. N.; Nath, L.; Chowdhury, P., Kinetic Modeling on Drug Release from Controlled Drug Delivery Systems. *Acta Pol. Pharm.* **2010,** *67*, 217-23.
33. Negrini, R.; Mezzenga, R., pH-Responsive Lyotropic Liquid Crystals for Controlled Drug Delivery. *Langmuir* **2011,** *27*, 5296-5303.
34. Martiel, I.; Baumann, N.; Vallooran, J. J.; Bergfreund, J.; Sagalowicz, L.; Mezzenga, R., Oil and Drug Control the Release rate From Lyotropic Liquid Crystals. *J. Control. Release* **2015,** *204*, 78-84.

Chapter 6

Aqueous Dispersions of Lipid Nanoparticles Wet Hydrophobic and Superhydrophobic Surfaces

6.1 Introduction

Wetting of substrates has important technological implications for applications ranging from inkjet printing,[1] spray painting,[2] accretion of ice on aircraft wings and power cables,[3-6] antibiotic resistance of biofilms[7] and delivery of agrochemicals to plants.[8,9] Retention of pesticide sprays on plants, for example, is governed by wetting of leaf surfaces by spray droplets. Typically, leaf surfaces are hydrophobic due to a protective natural coat of microcrystalline epicuticular wax.[10] Therefore, aqueous sprays used to deliver pesticide bounce off leaves, resulting in run-off that wastes pesticide and adversely impacts the environment by polluting soil and ground water. In India, organochlorine and organophosphorous pesticide residues associated with endocrine disruption and immune suppression, have been found in ground and surface waters[11,12] as well as in food.[13,14] Therefore, there is an urgent need to improve the efficiency of pesticide delivery to crops.

Often, pesticides are sprayed in conjunction with adjuvants that assist in retention of sprays on the leaf surface and that enhance penetration to increase foliar uptake.[15,16] Common commercially used adjuvants include nonionic surfactants that are used as spreaders or wetting agents. These decrease the surface tension of the aqueous spray, thereby decreasing the tendency of drops to retract after impinging and spreading on the leaf surface. However, these surfactants often dissolve epicuticular wax coating on the leaves and irreversibly damage surface microstructures and are thus phytotoxic.[17] Reduction of the surface tension also results in the formation of smaller drops and in excessive misting during spraying. An alternate method that has been proposed in the literature[18] to improve spray retention on leaf surfaces is to dissolve water soluble high molecular weight polymers at low concentrations in the spray solution. This has been demonstrated to be effective in retarding the retraction of drops impinged on hydrophobic substrates.

The challenge of improving pesticide delivery continues to be an active area of research and several advances have been reported recently. Song et. al. have demonstrated that a two-tailed vesicle forming surfactant, AOT, is capable of rapid migration to the drop-air interface to form ordered multilamellar assemblies that reduce surface tension.[9] This surface structuration happens over very short time scales, during fast drop impact experiments, and allows the spreading drop to penetrate air pockets on superhydrophobic surfaces, inducing a transition to a wetting state. They demonstrate that addition of AOT above a critical concentration is capable of preventing retraction of drops impacted on horizontal as well as inclined superhydrophobic surfaces. A different approach has been

reported by Damak et. al. who simultaneously impinge two sprays, each containing an oppositely charged polyelectrolyte solution, directly on a superhydrophobic surface.[8] The oppositely charged polyelectrolytes form coacervates that deposit as precipitates on the surface. These precipitates pin aqueous drops on the surface, preventing retraction.

Here, we report that aqueous nanoparticle dispersions of a commercially available, bio-derived, food-grade lipid, glycerol monooleate, induce adhesion of drops on hydrophobic and inclined superhydrophobic substrates. The lipid nanoparticles are characterized by an ordered internal cubic phase structure formed by self-assembly of the lipid molecules. Such cubic phase nanoparticles, termed cubosomes, are stabilized in aqueous dispersion using an amphiphilic block copolymer.[19,20] We demonstrate that during drop impact experiments, cubosomes rapidly modify the surface wettability of hydrophobic substrates by diffusing to the substrate and reorganizing to form a uniform thin film. The modified surfaces are hydrophilic and aqueous drops adhere to these strongly, such that drop retraction is eliminated. Aqueous cubosome dispersions do not roll off inclined natural superhydrophobic surfaces such as lotus leaves, and form continuous wetting films when sprayed on inclined lotus leaves. We demonstrate that the improvement of drop delivery to hydrophobic surfaces through cubosome dispersions is not effected through a reduction in surface tension – cubosomes diffuse slowly to the drop-air interface, in contrast to vesicle forming surfactants such as AOT or regular surfactants. We briefly describe the structure and properties of glycerol monooleate before we present our results.

Glycerol monooleate, also known as monoolein, is a hydrophobic lipid that is water insoluble.[21] In the presence of water, it self-assembles to exhibit rich phase behavior, forming lamellar, hexagonal and bicontinuous cubic phases with gyroid or double diamond symmetry.[22] Of particular interest to this work is that the hydrophobicity of glycerol monooleate opens a miscibility gap in the phase diagram so that the double diamond Pn3m phase coexists with excess water.[22] Therefore, application of mechanical shear can be employed to convert the gel-like Pn3m bulk phase to lipid nanoparticles that retain internal cubic phase molecular ordering. Amphiphilic block copolymers such as Pluronic F127 form ternary phases locally at the surface of these lipid nanoparticles, and sterically stabilize them to form a stable aqueous dispersion of cubosomes. Cubosomes can simultaneously encapsulate hydrophobic and hydrophilic molecules and are promising candidates for delivery of drugs, [23-28] flavor and perfume compounds,[29,30] agrochemicals[31-33] and other actives.[34-38]Here, we focus on an aspect that has not received attention previously, and investigate the wetting of hydrophobic surfaces using drop impact experiments. We now

present results that demonstrate the remarkable surface wettability transformation induced by cubosomes dispersions during drop impact.

6.2 Experimental Section

6.2.1 Materials:

Glycerol monooleate (GMO, commercial name: Rylo MG20 Pharma, >98% purity) was received as generous gift sample from Danisco, India. Detailed characterization of GMO has been reported previously.[19] Tween 20 was obtained from Sigma Aldrich and used as received. Pluronic F127, block co-polymer of polyethylene and polypropylene glycol was received from BASF. Distilled deionized water with a resistivity of 18 MΩcm was used for cubosome preparation.

6.2.2 Cubosome Preparation:

Cubosomes were prepared using previously reported literature protocols.[19] Glycerol monooleate (GMO) is a white solid at room temperature, and was stored at -80°C to prevent chemical degradation. Before sample preparation, we melt the GMO by heating it at 80°C. The GMO/F127 blend was prepared by mixing GMO and Pluronic (F127) in 100:5 ratio. The blend was mixed by stirring and heating it at 80°C for 30 minutes. Finally we add the blend to water. For example, to prepare 10 g sample solution, 0.315 g of GMO/F127 blend (in 100:5 ratio) were mixed with 9.695 g of DI water. The GMO/F127/water blend was mixed using an Ultra Turrax T25 from IKA operated at 10000 rpm for 10-15 minutes. The white milky solution indicates the formation of lipid nanoparticles, known as *cubosomes*.

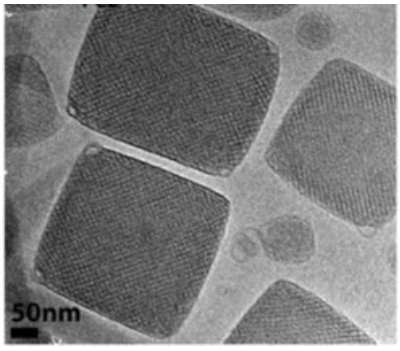

Figure 6.1: Representative cryo-TEM of cubosomes. We acknowledge help from Shobha Ramagiri and Jayesh Bellare, Indian Institute of Technology Bombay, Mumbai, for this cryo-TEM image.

6.2.3 Preparation of Hydrophobic Surface:

Firstly, we cleaned the glass slide using an acidic piranha etch. The etched slides were stored in water. Before hydrophobic modification, we dried the etched glass slide using a stream of N_2. We took toluene in a petri dish and dipped the dry glass slide into it and placed it on a magnetic/heating stirrer. Then, we added 10-15µl of octyl silane drops to the toluene while stirring. Silanization of the glass surface was carried out at 60^{o}C. Finally we rinsed the modified glass slide with copious amounts of toluene to remove excess/unreacted octyl silane. Hydrophobization was confirmed by measuring the contact angle of water on the modified glass surface (θ=104±2°).

6.2.4 High Speed Imaging Set up:

For drop impact experiments, we record videos using a high speed video camera that grabs 3000 frames/s with an exposure of 40 µs. The camera was inclined at 15^{o} to improve the drop visualisation (Figure 6.2). We generate a liquid drop with the help of a Harvard syringe pump connected to a needle through silicon tube of inner diameter 2 mm. The inner diameter of needle nozzle is 0.35(±0.01) mm, the nozzle of same inner diameter was used for all the experiments (yields a droplet volume ~ 10 µl). We heat the needle tip slightly before injecting the liquid through it, which allows us to generate a symmetrical liquid droplet. Initially, the drop of diameter 2.25 ±0.1 mm (averaged over many drops before it impacts). The drop is impacted on the target surface from 30cm height with an impact velocity of 2.42 m/s. After recording the videos of drop impingement on the substrate, we analyse the drop dynamics using Image J software.

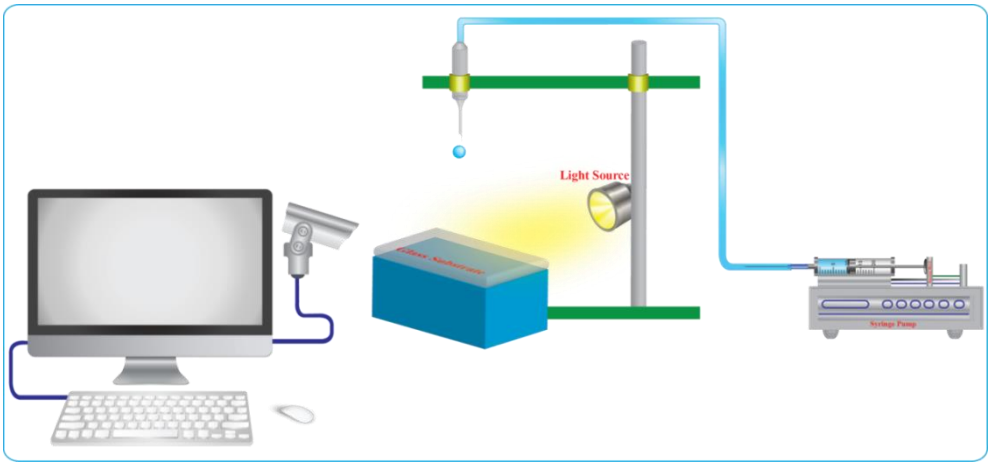

Figure 6.2: Experimental set up for high speed imaging of drop impact.

6.3 Characterisation

6.3.1 Dynamic Light Scattering (DLS):

Dynamic Light Scattering was performed on samples equilibrated at room temperature for 2 days, using BIC 90 Plus Particle size analyser from Brookhaven Instruments Corporation, USA. This instrument is equipped with a He-Ne laser (λ= 632.8 nm) and intensity correlations were measured at a fixed angle = 90^o. The mean size of the lipid nanoparticles was measured to be 200 ±10 nm.

6.3.2 Ellipsometry Measurements:

We used a silicon wafer of dimensions 1*1cm^2. The wafer was piranha etched to clean the surface and then it was modified with octyl silane to render it hydrophobic. On the modified surface, we impinged 1% lipid nanoparticle drop of size ~2.2 mm. The substrate with impinged drop was rinsed with DI water and then dried before carrying out ellipsometry measurements.

Multi angle spectroscopic ellipsometry measurements were performed on a hydrophobized silicon substrate before and after the impact of an aqueous lipid nanoparticle drop on the hydrophobic silicon surface. We used a commercial spectroscopic ellipsometer, M2000 from Woollam Inc., Lincoln, Nebraska, USA. We measure the amplitude ψ, for incident angles between 60° to 80°, and for different wavelengths between 200-1000 nm. We analysed the film thickness formed by the adsorbed lipid particles from the measured ψ curve by using WASE software, supplied by the manufacturer. Data was fitted using a three layer Cauchy model considering the thin film as transparent.

6.3.3 Contact Angle (AOC) and Dynamic Surface Tension (ST) Measurements:

For contact angle measurements, “contact angle goniometer” system equipped with CCD camera was used. Image analysis was done using SCA20 software (Dataphysics Instruments, GmbH, Germany). Sessile drop method was used for these measurements where droplet of 5 µL of different liquids was gently placed on the hydrophobic glass surface and on the lotus leaf. Angle of contact was monitored 5 times in a second continually for 10 min time window. We performed dynamic surface tension measurements using the same goniometer set-up. A precise liquid release system was used to generate a pendant drop of 10 µL.

Measurements were made over 10 minutes at a rate of 10 /s.

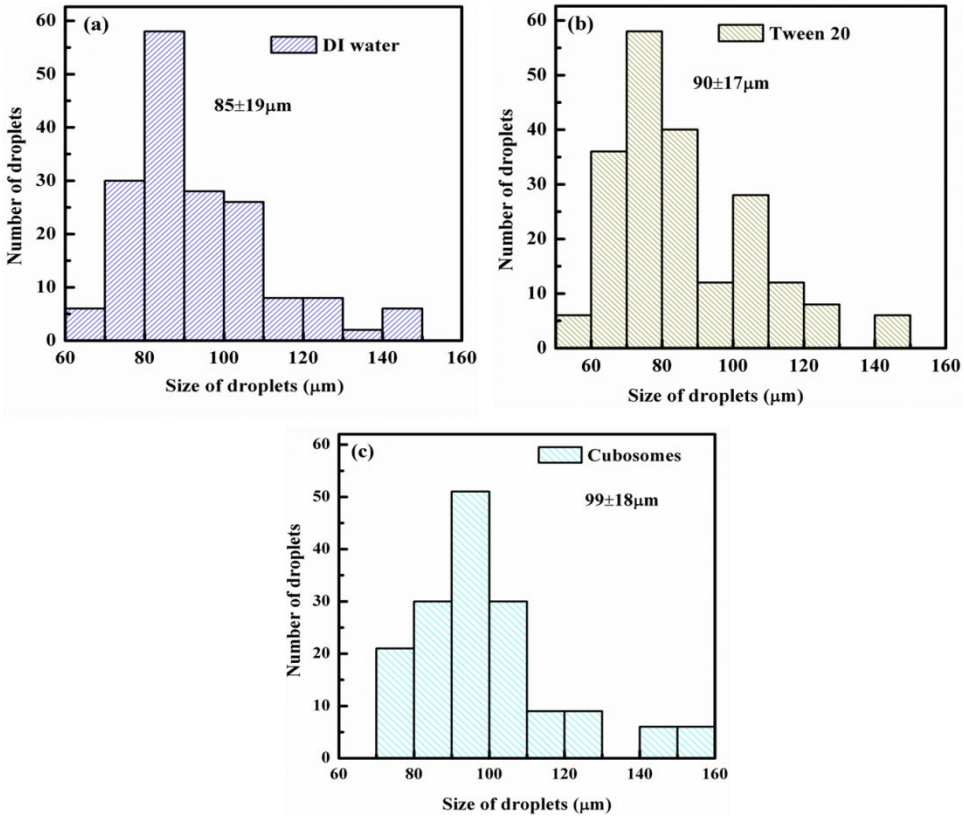

Figure 6.3: Droplet size distribution for liquids sprayed using the commercial sprayer used in our experiments. Liquid was sprayed and droplets issuing from the nozzle were imaged in air, before they impacted a substrate. We present data for droplet size distributions for (a) water, (b) 1% Tween 20, (c) 1% Cubosomes.

6.3.4 Characterization of Spray:

We used a commercial spray bottle. Droplets of issuing from the nozzle of the spray bottle were characterized using high speed video camera. This sprayer produces fine droplets, as shown in Figure 6.3. The volume capacity of the bottle is 50ml. Before each experiment, we rinsed the spray bottle with acetone to remove any organic impurity present in the bottle. We dried the bottle inside the oven to evaporate the solvent completely. All the spray experiments were carried out using the same spay nozzle.

6.4 Results and Discussion

Aqueous dispersions containing ≈ 200 nm glycerol monooleate "cubosomes" (nanoparticles characterized by bicontinuous channels with Pn3m cubic symmetry) were prepared using reported protocols.[19] We investigate the impingement of a drop of aqueous lipid nanoparticle dispersion on a hydrophobic surface and compare with the behavior of drops of water and of aqueous surfactant (1% Tween 20). High speed video imaging reveals that the spreading of lipid nanoparticle dispersion, surfactant and water drops after impact is similar – however, *retraction* of lipid nanoparticle dispersions is qualitatively different (Figure 6.4). We now describe the drop impact experiments in detail.

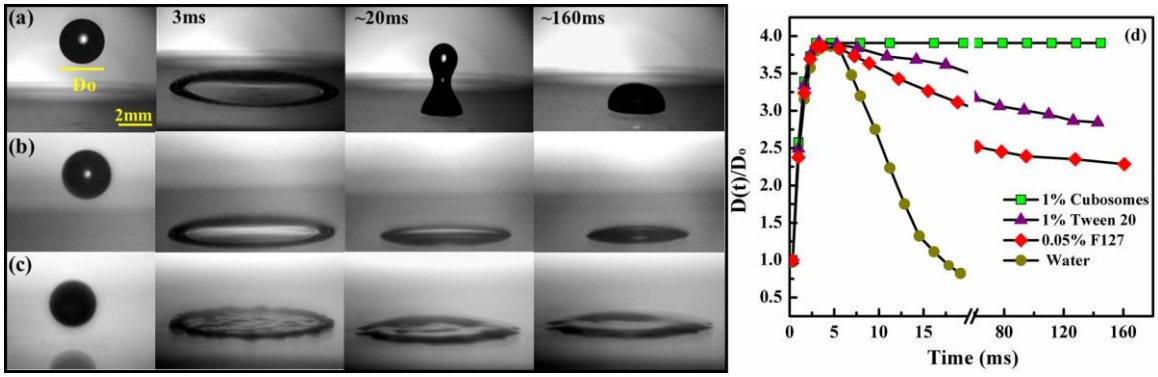

Figure 6.4: Sequence of photographs shows the spreading of a drop of (a) water, (b) 1% Tween 20 and (c) 1% lipid nanoparticle dispersion, on impacting a hydrophobized glass surface. The photographs show the behaviour of the drop before impact (first panel) and at approximately 3, 20 and 160 ms after impact. The drop diameter before impact, D_o ≈ 2.25±0.1 mm and the impact velocity, V=2.42m/s in all experiments. (d) Time dependent drop size D(t), normalized by D_o, for drop impact experiments.

When water is impinged on a hydrophobized glass surface at high impact velocity (V=2.42 m/s) the drop spreads, driven by inertial forces generated on impact (Figure 6.4, top row). At ≈ 3 ms after impact, the drop spreads radially to a maximum diameter, D_m/D_o ≈ 3.8 (where D_o is the diameter of the impinged drop ≈ 2.25 mm). The spreading of drops of 1% Tween 20 and 1% aqueous cubosome dispersion is similar to that of water (Figures 6.4 b, c). We note that the time dependent spreading diameter (normalized by the initial drop size), $D(t)/D_o$, is largely indistinguishable for all three systems in the first few ms after impact, when the drops spread on the surface (Figure 6.4 d). This is not surprising since spreading is governed largely by the inertia of drop impact, and is similar for all three systems. The Reynolds number, Re, provides a non-dimensional measure of the relative importance of

inertial forces to viscous. Similarly, the Weber number, We, provides a measure of the importance of inertial forces relative to surface tension. For drop impact, $Re = \rho D_o V/\mu \approx 3000$ and $We = \rho D_o V^2/\sigma$ ranges from 180 – 450, where ρ and μ are the density and viscosity of the drop, respectively; V is the velocity of the drop at impact and σ is the air-liquid surface tension. Both Re and We >> 1; thus, inertial forces dominate drop spreading after impact.

After the water drop has spread to its maximum size, D_m, it retracts since water does not wet the hydrophobic substrate. We observe that the drop retracts continuously, with a velocity ≈ 0.7 m/s, and after ≈ 20 ms forms a liquid column with diameter smaller than that of the initial drop (Figure 6.4 a, d). Retraction of water drops impinged on hydrophobic surfaces is governed by a balance between inertial and capillary forces,[39,40] parameterized by the Capillary number, $Ca = V\mu/\sigma$. Since water has a large surface tension (σ = 72 mN/m), Ca ≈ 10^{-2} and we observe rapid drop retraction. Addition of surfactants significantly reduces the surface tension and retards drop retraction. Therefore, surfactants such as Tween 20 are commonly used as commercial "spreading agents" (called adjuvants, in aqueous agrochemicals spray formulations). Addition of 1% (by weight) of Tween 20 to water reduces the surface tension to ≈ 35 mN/m. The retraction of a drop of Tween 20 solution on a hydrophobic surface is significantly slower when compared with water – the drop diameter decreases continually with a retraction velocity ≈ 0.06 m/s, to a diameter of about $3D_o$ at ≈100 ms after impact.

Lipid dispersions show qualitatively different retraction after spreading. For 1% lipid dispersions, we observe no decrease in drop diameter even at 160 ms after impact (Figure 6.4 c, d). As the drop spreads, there is a rim at the propagating circular front due to the inertial pressure head that drives flow on the hydrophobic surface. After ≈ 3 ms, when the cubosome drop has spread to its maximum size, D_m, this rim decays to leave a film with approximately uniform height. However, the drop size does not decrease from D_m.

What is the origin of this remarkable retardation of drop retraction by the lipid nanoparticle dispersion? There are three mechanisms that are believed to govern retraction of aqueous drops on hydrophobic surfaces. (i) Water soluble polymeric additives, such as polyethyleneoxide, have been reported to retard retraction of water drops on hydrophobic surfaces.[18,41]This has been attributed to elongational stresses generated during drop retraction[18] Recently, it has been suggested that chain stretching rather than elongational stresses retards drop retraction.[42]Our cubosome dispersion is stabilized using a

polyethyleneoxide/polypropyleneoxide triblock copolymer, Pluronic F127. This block copolymer is bound to the cubosome surface and is not in solution. In a control experiment, we observe that drops containing F127 in solution (at a concentration of 0.05%, corresponding to that used to stabilize the 1% lipid dispersion) retract after spreading on hydrophobized glass. The retardation of drop retraction by 0.05% F127 is much less effective than even the 1% Tween 20 (Figure 6.4 d). Thus, the absence of retraction for lipid dispersions cannot be attributed to the high molecular weight water-soluble polymers used in preparation of the dispersion. (ii) Small molecule surfactants reduce the surface tension and increase the Capillary number, thus retarding the surface tension driven retraction process. The lipid dispersions used in our experiments have low equilibrium surface tension (≈ 29 mN/m) relative to water (72 mN/m).

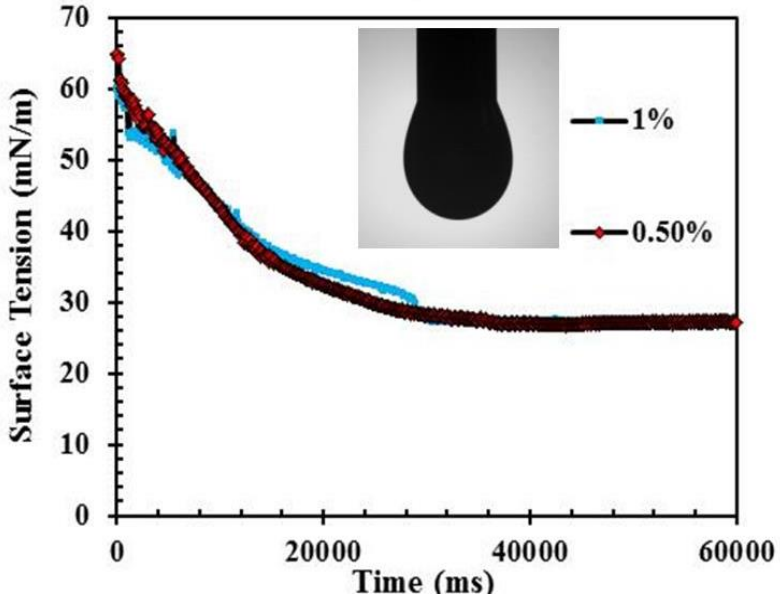

Figure 6.5: The dynamic surface tension of an aqueous drop of lipid nanoparticles is measured using pendant drop method. We used drops of lipid nano particle dispersions at different concentrations viz. Φ=0.5% and 1% and measured the dynamic surface tension for 60 seconds. We observe that the drop attains an equilibrium surface tension ~29mN/m in ~30seconds.

However, dynamic surface tension experiments using the pendant drop method reveal that the surface tension of an aqueous drop of lipid dispersion decreases over time scales of ~O(30 s), viz. much longer than spreading times in the drop impact experiment (Figure 6.5). Thus, decrease in surface tension at the air-water interface is *not* the cause for lower drop retraction.

Clearly cubosomes do not form aggregate structures at the air-water interface, similar to those recently reported for vesicle forming AOT surfactant solutions. In the millisecond time scales that characterize drop impact, the dynamic surface tension data suggest that lipid dispersion drops should retract like water drops. This is consistent with drop impact experiments at lower lipid concentrations (Figure 6.6).

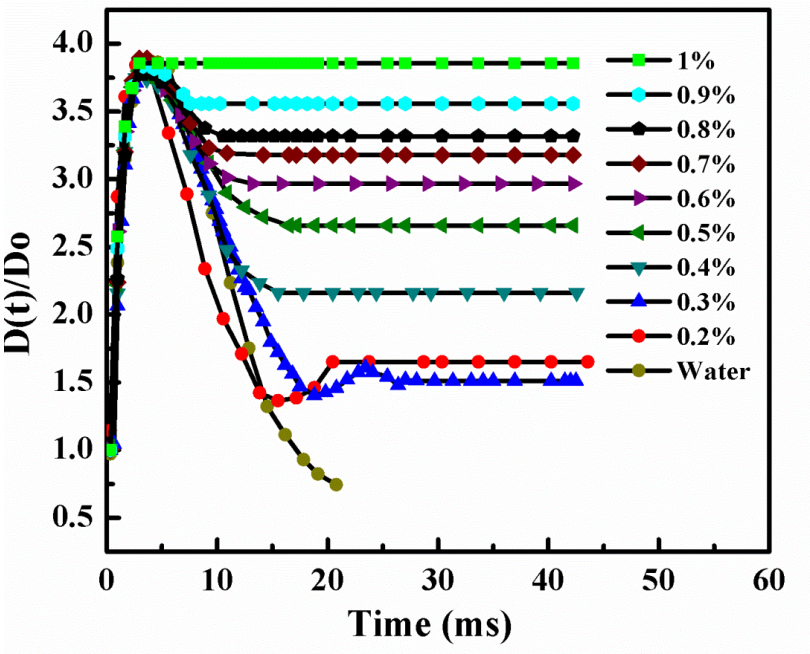

Figure 6.6: Spreading and retraction of drops aqueous dispersions of lipid nanoparticles at different concentrations viz. Φ from 0.2 to 1% (w/w). Data for spreading and retraction of a water drop is also shown, for ease of comparison.

Indeed, for aqueous lipid dispersions at low concentration (< 1%) drop retraction initially follows that of water. However, the drop size subsequently deviates from that of the water drop and further retraction is completely arrested. We note that this behavior is qualitatively different from the continuous slow retraction exhibited by drops of aqueous surfactant. (iii) Finally, another mechanism that could curb drop retraction is modification of the substrate surface wettability. We now investigate if lipid dispersions are capable of modifying the hydrophobic substrate to eliminate drop retraction within a few milliseconds during spreading.

We use multiangle spectroscopic ellipsometry to investigate if lipid nanoparticles in the dispersion modify the hydrophobic surface by adsorbing on it. Here, we impinge a drop of lipid dispersion on a reflective silicon substrate, hydrophobized using octyl silane in a

manner similar to the glass surfaces. Immediately after the drop spreads, the substrate was rinsed using deionized water and was subsequently dried. The amplitude ratio, ψ and phase difference, Δ obtained from our experiments were analysed using WASE software, supplied with the ellipsometer. Ellipsometry was initially performed on the hydrophobic silicon substrate and was fitted with a two layer model (silicon substrate/hydrophobized oxide layer). The substrate after drop impingement could not be fitted with a two layer model. Therefore, we used a three layer model: silicon substrate/hydrophobized oxide layer/lipid film. The lipid layer was modeled using a Cauchy model ($n = A + B\lambda^{-2} + C\lambda^{-4}$), assuming that the lipid film does not absorb light in the wavelength range used. We used mean square error minimization to obtain the best fit to our data using the following parameters: A= 1.45, B=0.01, C = 0 and refractive index, n = 1.480. Our data can be fit with a lipid layer thickness of approximately 2 nm, in all our experiments.

Ellipsometry revealed the formation of an adsorbed layer with a thickness of about 2 nm on the hydrophobic surface (Figure 6.7 a). This results in a dramatic change in surface wettability: the contact angle of a water droplet decreases to $\approx 20^{o}$ (compare with $\approx 102^{o}$ for the as prepared hydrophobic surface, Figures 6.7 b, c). We note that the thickness of the adsorbed layer is significantly smaller than the size of the cubosome particles in aqueous dispersion (mean size ≈ 200 nm). Thus, it appears that the cubosomes rapidly diffuse to the surface, reorganize and adsorb to form a thin hydrophilic coating during the process of drop impact. Literature reports indicate that it takes several minutes for cubosome dispersions at comparable concentrations to adsorb onto hydrophobic surfaces to form several nanometer-thick films.[43,44] However, our data indicates that cubosomes reorganize and adsorb in millisecond time scales, during drop spreading on hydrophobic surfaces, and dramatically change the wettability of hydrophobic surfaces.

To understand the process by which cubosomes adsorb and modify the hydrophobic surface during drop spreading, we analyze data from drop impact experiments at different lipid concentrations, ϕ (Figure 6.6). We observe that the retraction of aqueous drops of lipid nanoparticles are arrested at what we refer to as a stagnation point (Figure 6.8). The stagnation drop diameter increases and the time to reach the stagnation point decreases with increasing lipid concentration. For lipid dispersions $\geq$ 1%, we observe no drop retraction from the maximum diameter attained on impact under these experimental conditions. We now analyze the stagnation point at which the radius of the retracting drop is arrested. We obtain the stagnation drop size, D_s, as the plateau value of $D(t)/D_o$ for the retracting drop and

define a stagnation time, τ_s, as the time after drop impact where the size of the retracting drop deviates from that of a water drop (Figure 6.8). We observe that D_s^2 scales linearly with ϕ (Figure 6.9 a). This is intuitive and suggests that the size of the region that is surface modified is directly proportional to the lipid concentration in the dispersion.

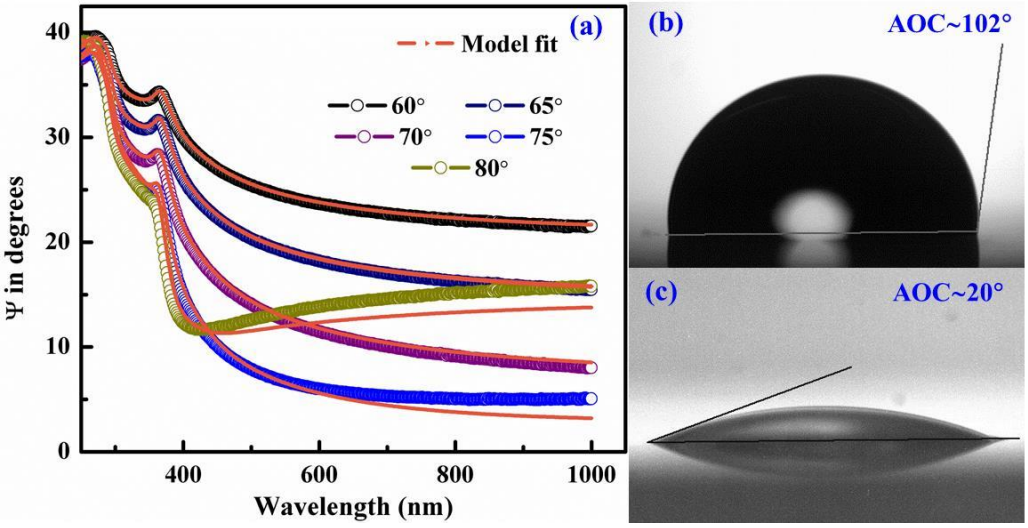

Figure 6.7: (a) Ellipsometry was performed at angles ranging from 60 to 80^o and using light of wavelength ranging from 200 to 1000 nm. The substrate was a hydrophobic silicon wafer on which a drop of aqueous 1% dispersion of lipid nanoparticle was impinged, as described in the manuscript. The data was fitted using a Cauchy model to estimate a thickness of about 2 nm for the adsorbed film. Contact angle (AOC) of a water drop (5 μl) on a hydrophobized silicon surface (b) as prepared and (c) after formation of the adsorbed lipid film during the drop impact experiment.

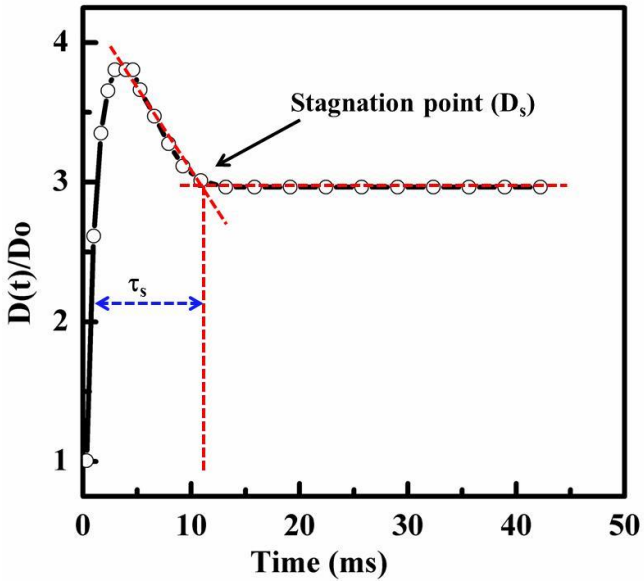

Figure 6.8: The plot shows the retraction of lipid nanoparticle drop impinged on a hydrophobic surface. The point where retraction stops is termed as stagnation point, D_s, whereas the time corresponds to D_s, known as stagnation time, τ_s.

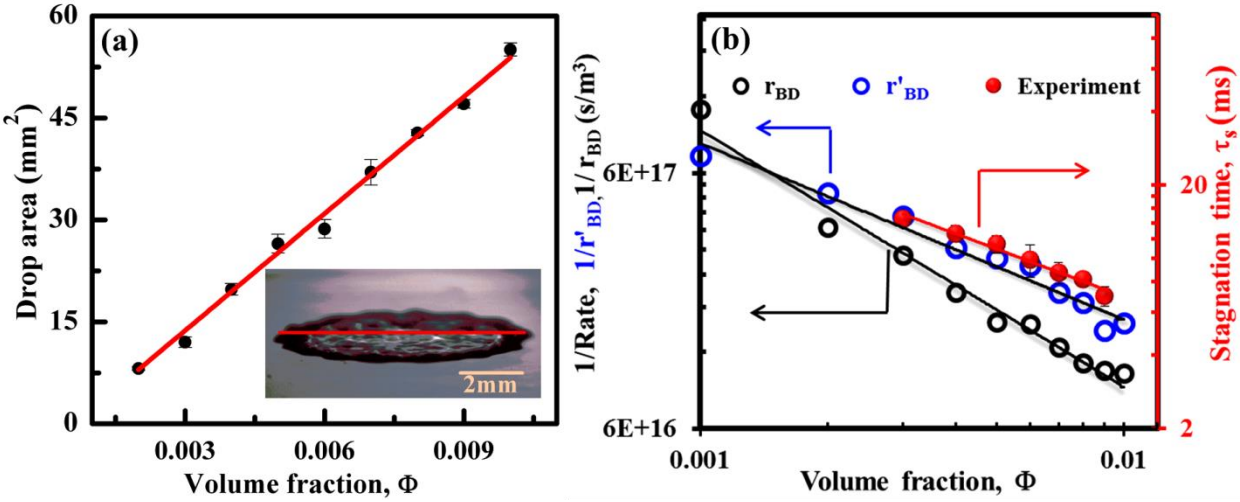

Figure 6.9: (a) Drop area at the stagnation varies linearly with the cubosomes concentration (b) Comparision between reciprocal of adsorption rate $(r_{BD})^{-1}$ and the experimental stagnation time.

Interestingly, τ_s scales as $\phi^{-0.65}$. If the formation of an adsorbed layer was controlled entirely by diffusion of cubosomes to the hydrophobic surface, one would anticipate that $\tau_s \sim$

ϕ^{-1}. This is consistent with Brownian dynamics simulations carried out by Narendiran from IIT Madras (Kumar et al. manuscript in preparation). The "adsorption" flux obtained from Brownian dynamics simulations is approximately linear in time (Figure 6.10) and we obtain the adsorption rate, r_{BD}, as the slope of the volume flux across the bottom face of the simulation box versus simulation time. We observe that the rate at cubosome diffusion to the substrate, $r_{BD} \sim \phi$. The time scale for diffusion to the substrate scales as r_{BD}^{-1} viz. as $\sim \phi^{-1}$.

Narendiran carried out Brownian dynamics simulations that make several simplifying assumptions: cubosomes are modeled as hard spheres and hydrodynamic interactions are ignored. However, we believe that these are not responsible for the discrepancy between the ϕ–dependence of τ_s and r_{BD}^{-1}. Rather, we believe that this discrepancy arises from the time taken for reorganization of cubosomes diffusing to the substrate to form a thin adsorbed film. Therefore, we introduce a time scale for cubosome reorganization that is independent of ϕ and is proportional to the mass of the lipid nanoparticle.

To account for the time taken for cubosome reorganization, we introduce a time scale that is proportional to the nanoparticle volume (Figure 6.11). Therefore, a nanoparticle that diffuses across the bottom face of the simulation box at time, t', forms a film at time t" = t'+ kV, where V is the nanoparticle volume and k is a fitting constant. We now obtain the adsorption rate, r'_{BD} as the slope of the volume of adsorbed film formed as a function of time, t". We adjust k such that the dependence of r'^{-1}_{BD} on cubosome concentration matches that of the experimental saturation time, τ_s. We note that we obtain close match to the experimental Φ-dependence for $k = 8 \times 10^{18}$ m^3/s.

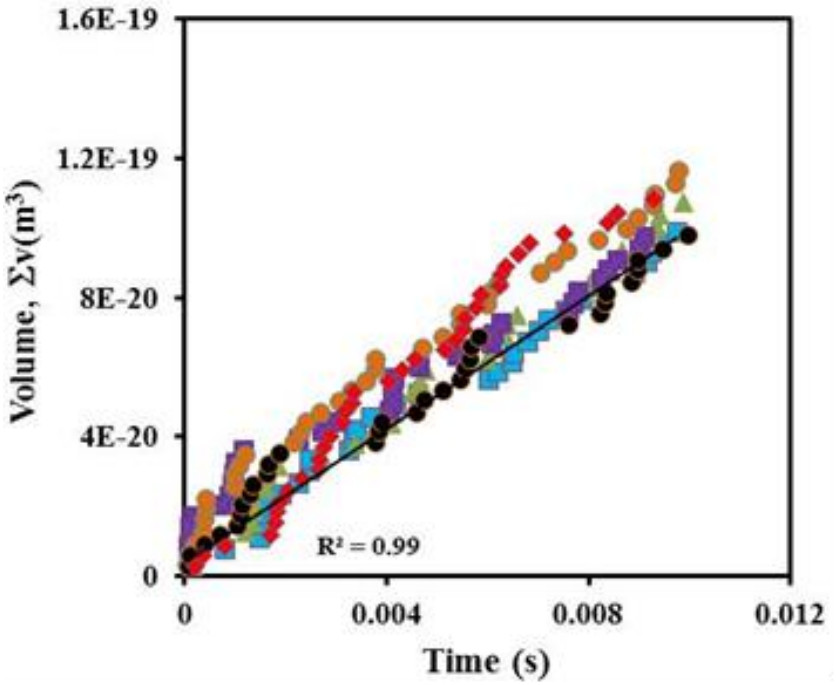

Figure 6.10: The cumulative adsorbed volume of cubosomes obtained from multiple simulation runs for cubosome concentration, Φ=0.9%. The adsorbed volume of cubosomes varies linearly with time. The adsorption rate, r_{BD}, is obtained as the slope of this data. Similar data was obtained for simulations at different cubosome concentrations.

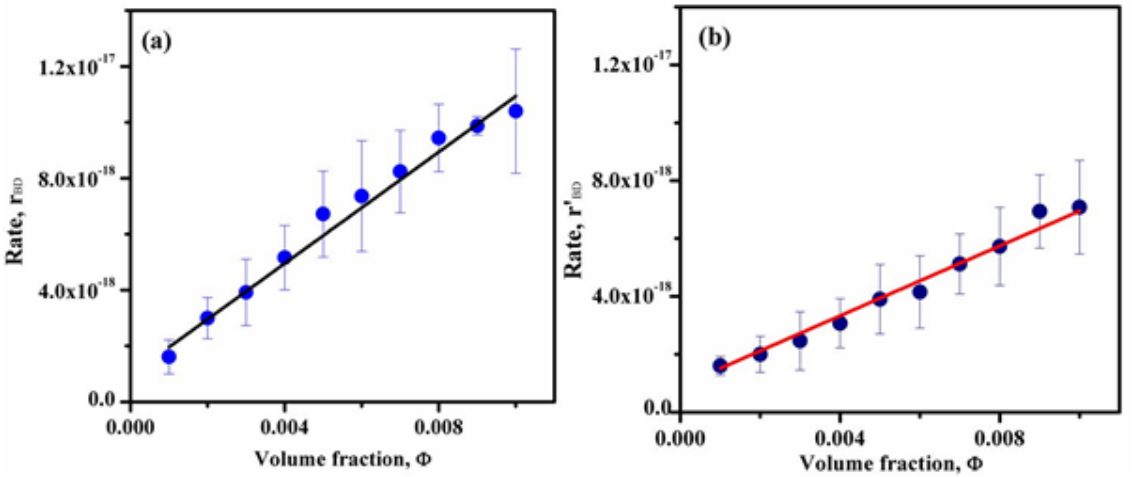

Figure 6.11: (a) The rate of nanoparticle diffusion across the bottom face, r_{BD} is plotted for different nanoparticle concentration, Φ. We observe that r_{BD} is linear in Φ. (b) We obtain the rate for nanoparticle adsorption to form a film, as described in the Simulation Methods, r'_{BD}. We adjust the fitting parameter, k, so that the Φ –dependence of r'^{-1}_{BD} matches that of τ_s, obtained from experiments.

6.5 Wetting on Superhydrophobic Lotus Leaf Surface

6.5.1 Contact Angle on Horizontal Lotus Leaf:

We now examine the interaction between cubosome dispersions and superhydrophobic surfaces. Superhydrophobic surfaces exhibit water contact angles close to 160^{o}, that cannot be obtained by surface hydrophobization alone. Superhydrophobicity results from a combination of hydrophobicity with surface roughness. Surface roughness leads to different wetting states when drops are impinged on superhydrophobic surfaces, depending on drop impact velocity.[45,46] We now describe the behaviour of drops deposited on a natural water repellent superhydrophobic surface, lotus leaves (*Nelumbo nucifera)* characterized by an equilibrium water contact angle (CA) $\approx 155^{o}$. Lotus leaves exhibit superhydrophobicity due to the composite micro-nano roughness of epicuticular wax crystals.[47,48] We first describe the behavior of drops placed slowly on horizontal and inclined lotus leaves, and then describe fast drop impact and spraying.

We measure the contact angle of liquid drops (volume = 5 μl) gently placed on a horizontal lotus leaf surface (Figure 6.12). Water drops show a contact angle, CA ≈ 155° on the lotus leaf and the CA value does not change with time. A drop of 1% Tween 20 drop shows an initial CA ≈ 143°, lower than for the water drop, and this CA decreases to about 137° over 10 minutes. The behaviour of the cubosome drop is very different when compared with water and 1% Tween 20. For a 1% cubosome dispersion, the CA decreases dramatically with time. The drop of cubosome dispersion starts with a CA ≈ 130° and decreases to near 0^{o} within 10 minutes.

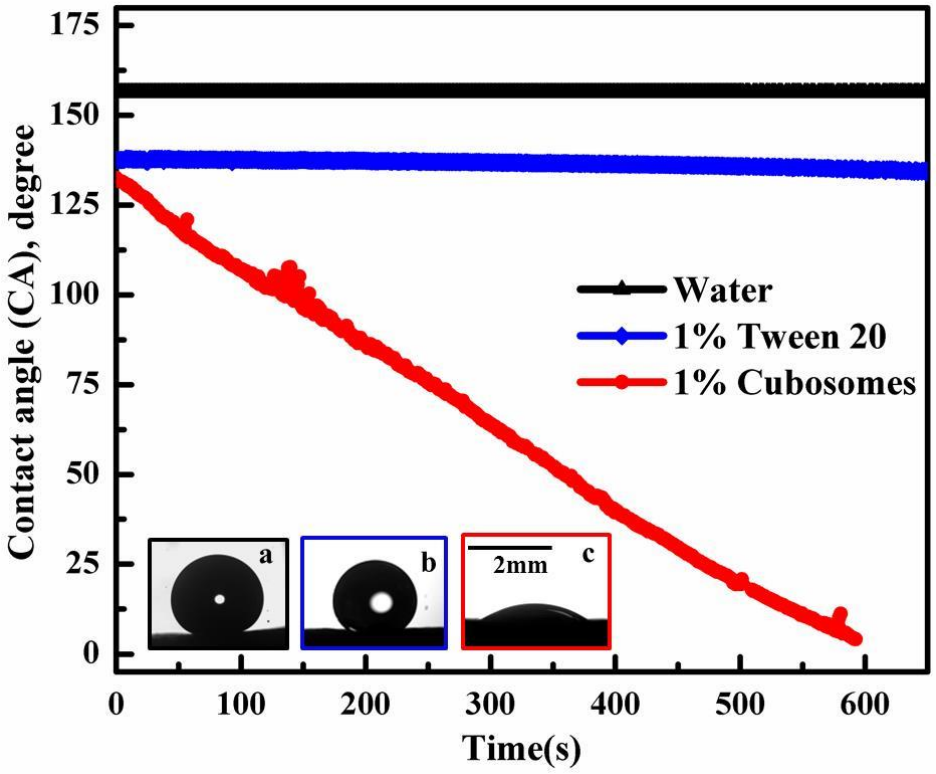

Figure 6.12: Shape adopted on a horizontal lotus leaf of a 5μl drop of (a) water (b) 1% Tween 20 and (c) 1% aqueous cubosome dispersion. Images are taken 5 minutes after drop deposition on the leaf surface. (d) The contact angle for the water drop remains constant at ≈155^{o} over 10 minutes, while that for cubosomes decreases continuously with time until the drop flattens on the lotus leaf surface.

6.5.2 Drop Rolling on Inclined Lotus Leaf:

We now examine the behaviour of a drop of diameter ≈ 2.2 mm, placed gently on an inclined lotus leaf surface, using a needle positioned about 2 mm above the leaf surface. The leaf is laid flat and adhered to a glass slide inclined at 15^{o} from the horizontal. Each experiment was repeated at least thrice, using a fresh lotus leaf. When a drop of water is placed on the inclined lotus leaf, it rapidly rolls off (Figure 6.13). The drop appears approximately spherical as it rolls off the leaf, with advancing and receding contact angles (ACA and RCA) that are nearly identical at 146±3^{o} and 144.3±3^{o}, respectively (Table 6.1). There is essentially no contact angle hysteresis (CAH), with implications for the drops rolling off the superhydrophobic surface.[49,50] We observe that the displacement, S of the drop center of mass along the surface of the increases-

Liquid drop, volume=10μl	Receding contact angle (RCA), degrees	Advancing contact angle(ACA), degrees
Water	144.3°±3°	146.3°±3°
Tween 20	130.6°±3°	144.3°±3°
Cubosomes	106.7°±3°	133°±3°

Table 6.1: Table shows the receding (RCA) and advancing contact angle (ACA) for the drops of water, tween 20, and lipid nanoparticle dispersions on the lotus leaf inclined at angle 15° with the horizontal. The lotus leaf was supported with the help of a glass slide.

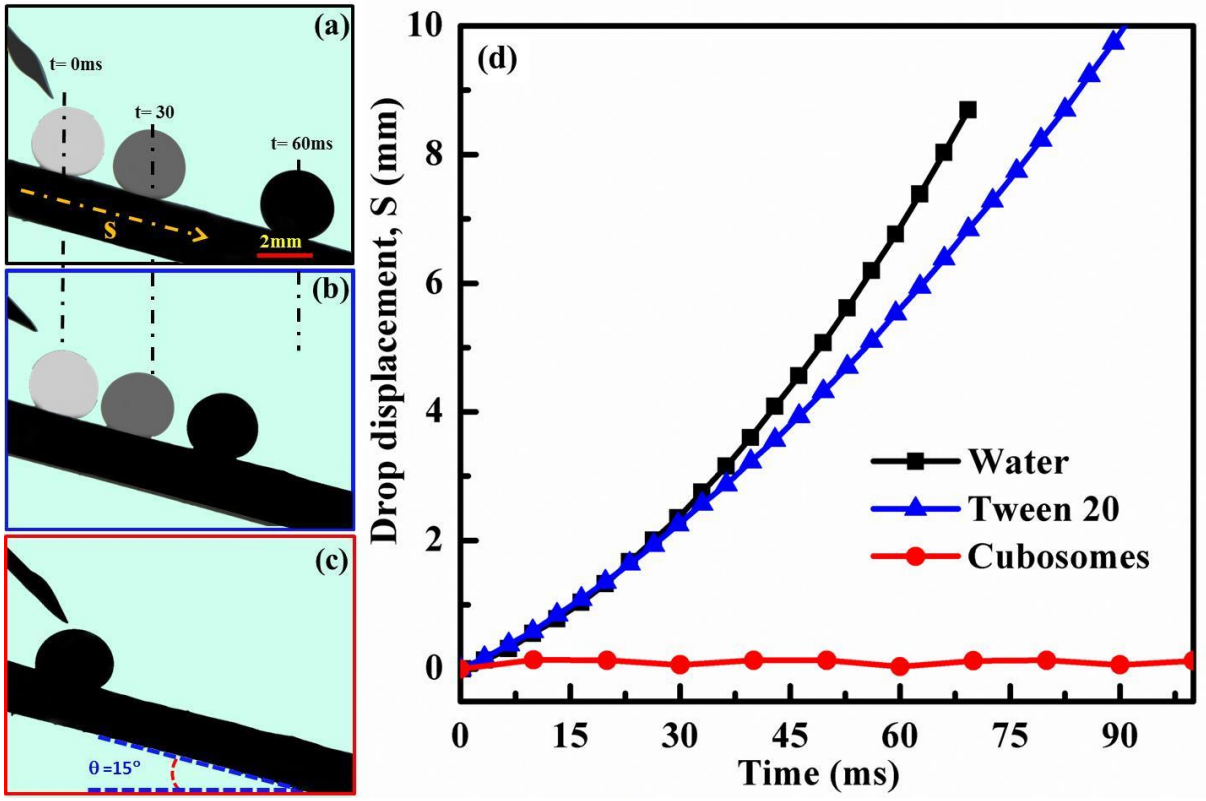

Figure 6.13: Motion along an inclined lotus leaf (as described in the main text) of a drop of (a) water; (b) 1% aqueous Tween 20 and (c) 1% aqueous cubosomes. We show the position of the drop as soon as it is placed on the leaf surface (t = 0 ms), and after approximately 30 and 60 ms. (d) The displacement of the center of the drop along the inclined leaf surface is plotted for water, 1% Tween 20 and 1% cubosome drops.

-nonlinearly with time, t (Figure 6.13 a, d). When a drop of aqueous 1% Tween 20 is placed on the inclined lotus leaf, it too rolls off. However, there is distinct hysteresis between ACA (144±3^o) and RCA (130±3^o) and the drop displacement along the surface is slower than for the water drop ($S = 0.03\ t^{1.2}$, Figure 6.13 b, d). In contrast, a drop of 1% cubosome dispersion adheres strongly to the inclined lotus leaf surface (Figure 6.13 c, d). Further, there is a pronounced CAH with an ACA = 133±3^o and an RCA = 106.7±3^o. Remarkably, the cubosome dispersion adheres so strongly to the lotus leaf so that further addition of drops is unable to displace the drop along the leaf surface.

6.5.3 Drop Impact on Horizontal Lotus Leaf:

We now examine rapid drop impact on horizontal lotus leaf surfaces, and impinge ≈ 2.2 mm diameter drops at velocities of 2.42 m/s (Figure 6.14). For water, 1% Tween 20 and 1% cubosome dispersions, the spreading of drops is similar and they reach a comparable maximum diameter. After spreading, the water drop breaks up into smaller droplets that rebound off the surface. We observe that one of the larger sub-droplets bounces several times on the leaf surface -while smaller satellite droplets bounce and move out of the field of view (Figure 6.14, top panel). Similar to the case of water, the drop of 1% Tween 20 also breaks up into multiple droplets. However, we find that some droplets stay pinned to the leaf surface while the others pinch off and bounce multiple times on the leaf surface (Figure 6.14, middle panel). The 1% cubosome drop also breaks up after spreading. However, all the droplets adhere to the surface and do not bounce off it (Figure 6.14, bottom panel).

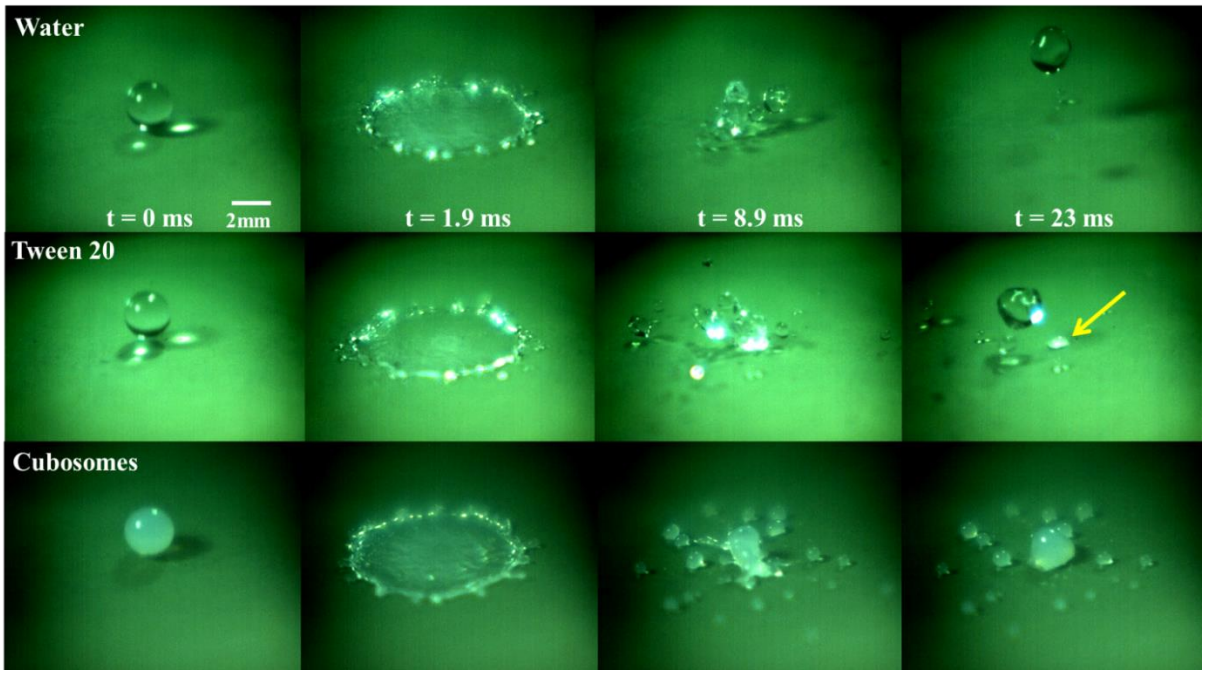

Figure 6.14: Sequence of images shows the spreading of a drop of water (top layer), 1% Tween 20 (middle layer), and 1% cubosomes (lipid nanoparticle dispersion) when impinged on a lotus leaf. The images show the behaviour of the drop before impact (first panel, t = 0; $D_o = 2.20 \pm 0.02$ mm) and at t= 1.9, 8.9 and 23 ms (after impact). The arrow in the middle panel indicates a pinned droplet.

6.5.4 Spray on Inclined Lotus Leaf:

Finally, we investigate spraying of aqueous dispersions on inclined lotus leaf surfaces, an operation characterized by multi drop impact. We use a commercially available spray and subject lotus leaves inclined at 15^o to a spray of either water, 1% Tween 20 or 1% cubosome dispersion. We spray the leaves for 5 seconds with the sprayer held at a distance of approximately 30 cm from the leaf surface. We have examined the drop size distribution for the spray issuing from the nozzle and note that there is no significant difference between the three liquids (Figure 6.3).

When the lotus leaf is sprayed with water (Figure 6.15 A), the superhydrophobic leaf surface is not wetted by the spray. Water droplets bounce and roll off the surface leaving the leaf dry. In the case of 1% Tween 20, a majority of the droplets that issue from the spray nozzle bounce off the leaf surface (Figure 6.15 B). However, a few droplets splinter

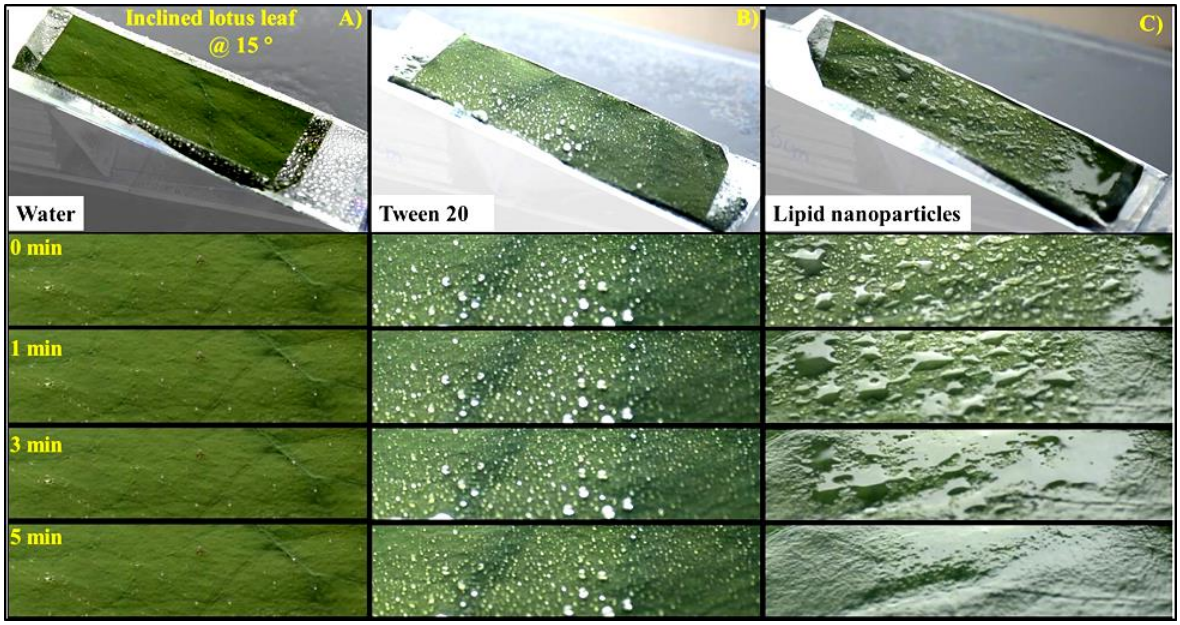

Figure 6.15: Photographs showing the surface of an inclined lotus leaf that is sprayed with water (left panel); 1% aqueous Tween 20 (middle panel) and 1% cubosome dispersion (right panel). Data is presented as a function of time after spraying.

-and stay on the surface and facilitate the retention of subsequent drops that impinge on them. These coalesce and form larger drops. However, most of the spray is lost as mist as the drops break up on impact and no liquid film forms. When 1% cubosome dispersion is sprayed, the droplets are retained on the surface and rapidly coalesce on the leaf surface to form a continuous wetting film (Figure 6.15 c). Thus, we observe qualitatively different wetting behaviour for cubosome dispersions, both for slow and fast drop deposition, on horizontal as well as inclined superhydrophobic surfaces. The adhesion of cubosome dispersions allows film formation on spraying even on inclined superhydrophobic lotus leaf surfaces.

Finally, we examine the effect of non-ionic surfactants on the lotus leaf surface. We examine lotus leaves sprayed with a commercial adjuvant (1% APSA-80), an aqueous 1% solution of Tween 20 and 1% cubosomes (Figure 6.16). We note that the commercial product, APSA-80 wets the lotus leaf when sprayed as a 1% solution (Figure 6.16, left panel). However, leaves sprayed with APSA-80 develop a brown texture when observed 12 hours after spraying (left panel, Figure 6.16). Spraying with 1% Tween 20 results in the deposition of small droplets on the leaf surface (Figure 6.16, middle panel). When the leaf is observed 12 hours after spraying, we notice that brown spots develop at the regions where the spray droplets were deposited. For 1% cubosomes, we observe that the leaf surface is uniformly wetted (Figure 6.16, right panel). Remarkably, unlike the case with non-ionic surfactant

sprays, there is no discolouration or degradation of the leaf surface. Our results are consistent with literature reports that lipids similar to GMO exhibit significantly lower phytotoxicity compared with commercial non-ionic surfactant adjuvants.[32]

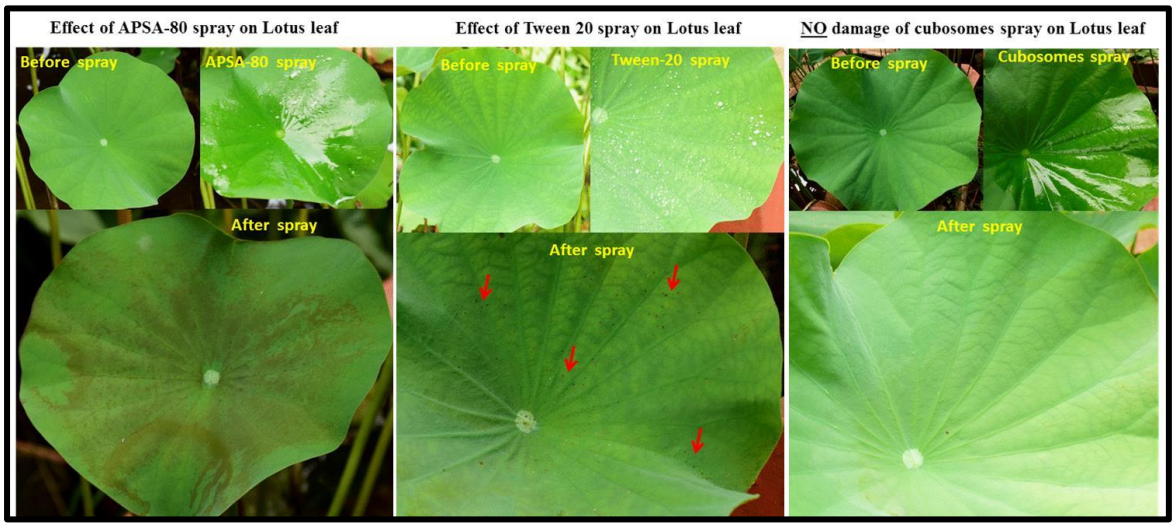

Figure 6.16: Photographs showing the lotus leaf that is sprayed with APSA-80 commercial surfactant (left panel); 1% aqueous Tween 20 (middle panel) and 1% cubosome dispersion (right panel). We observed the effect of spray before and after the spray.

6.6 Summary

In summary, our work demonstrates the remarkable wetting behaviour of aqueous nanoparticle dispersions of glycerol monooleate lipid, called cubosomes. The wetting of cubosome dispersions cannot be attributed to nonlinear rheological effects or due to a change in surface tension. At the low, ~O(1%) concentrations used here, cubosome dispersions exhibit water-like rheology. The ~O(100 nm) size of the cubosomes also precludes their rapid diffusion to the air-water interface. Remarkably, they diffuse to hydrophobic surfaces and reorganize to form a thin wetting film very rapidly, on the millisecond time scales of drop impact experiments. It is possible that the strong hydrophobicity of glycerol monooleate (with an HLB value of 3.8) drives the rapid coating of hydrophobic surfaces by the cubosomes. This change in surface wettability allows the cubosome drops to adhere to the surface. Drops of cubosome dispersions also adhere to superhydrophobic lotus leaf surfaces, even when the leaf surface is inclined. The lipid that comprises cubosomes, glycerol monooleate is a bioderived, commercially available molecule and has been established to

have low phytotoxicity. Thus, our results have important implications for improved crop protection by more efficient delivery of aqueous pesticide sprays.

6.7 References:

1. De Gans, B. J.; Duineveld, P. C.; Schubert, U. S., Inkjet Printing of Polymers: State of the Art and Future Developments. *Adv. Mater.* **2004**, *16*, 203-213.

2. Aziz, S. D.; Chandra, S., Impact, Recoil and Splashing of Molten Metal Droplets. *Int. J. Heat Mass Transf.* **2000**, *43*, 2841-2857

3. Varanasi, K. K.; Deng, T.; Smith, J. D.; Hsu, M.; Bhate, N., Frost Formation and Ice Adhesion on Superhydrophobic Surfaces. *Appl. Phys. Lett.* **2010**, *97*, 234102.

4. Stone, H. A., Icephobic Surfaces that are Wet. *ACS Nano* **2012**, *6*, 6536-6540.

5. Golovin, K.; Kobaku, S. P. R.; Lee, D. H.; DiLoreto, E. T.; Mabry, J. M.; Tuteja, A., Designing Durable Icephobic Surfaces. *Sci. Adv.* **2016**, *2*, e1501496.

6. Kim, P.; Wong, T. S.; Alvarenga, J.; Kreder, M. J.; Adorno-Martinez, W. E.; Aizenberg, J., Liquid-infused Nanostructured Surfaces with Extreme Anti-ice and Anti-frost Performance. *ACS Nano* **2012**, *6*, 6569-6577.

7. Epstein, A. K.; Pokroy, B.; Seminara, A.; Aizenberg, J., Bacterial Biofilm shows Persistent Resistance to Liquid Wetting and Gas Penetration. *Proc. Nat. Acad. Sci.* **2011**, 108, 995-1000

8. Damak, M.; Mahmoudi, S. R.; Hyder, M. N.; Varanasi, K. K., Enhancing Droplet Deposition through in-situ Precipitation. *Nat. Commun.* **2016**, *7*. 12560

9. Song, M.; Ju, J.; Luo, S.; Han, Y.; Dong, Z.; Wang, Y.; Gu, Z.; Zhang, L.; Hao, R.; Jiang, L., Controlling Liquid Splash on Superhydrophobic Surfaces by a Vesicle Surfactant. *Sci. Adv.* **2017**, *3*, e1602188.

10. Taylor, P., Wetting of Leaf Surfaces. *Curr. Opin. Colloid Interface Sci.* **2010**, *16*, 326-334.

11. Sankararamakrishnan, N.; Sharma, A. K.; Sanghi, R., Organochlorine and Organophosphorous Pesticide Residues in Ground Water and Surface Waters of Kanpur, Uttar Pradesh, India. *Environ. Int.* **2005**, *31*, 113-120.

12. Jayashree, R.; Vasudevan, N., Organochlorine Pesticide Residues in Ground Water of Thiruvallur District, India. *Environ*. *Monit. Assess* **2007**, *128*, 209.

13. Bhanti, M.; Taneja, A., Contamination of Vegetables of Different Seasons with Organophosphorous Pesticides and Related Health Risk Assessment in Northern India. *Chemosphere* **2007**, *69*, 63-68.

14. Abhilash, P. C.; Singh, N., Pesticide Use and Application: An Indian Scenario. *J. Hazard. Mater.* **2009**, *165*, 1-12.

15. Stevens, P. J. G.; Gaskin, R. E.; Hong, S. O.; Zabkiewicz, J. A., Contributions of Stomatal Infiltration and Cuticular Penetration to Enhancements of Foliar Uptake by Surfactants. *Pest Manag. Sci.* **1991**, *33*, 371-382.

16. Hess, F. D.; Foy, C. L., Interaction of Surfactants with Plant Cuticles. *Weed Technol.* **2000**, *14*, 807-813.

17. Knoche, M.; Noga, G.; Lenz, F., Surfactant Induced Phytotoxicity: Evidence for Interaction with Epicuticular Wax Fine Structure. *J. Crop Prot.***1992**, *11*, 51-56.

18. Bergeron, V.; Bonn, D.; Martin, J. Y.; Vovelle, L., Controlling Droplet Deposition with Polymer Additives. *Nature* **2000**, *405*, 772-775.

19. Deshpande, S.; Venugopal, E.; Ramagiri, S.; Bellare, J. R.; Kumaraswamy, G.; Singh, N., Enhancing Cubosome Functionality by Coating with a Single Layer of Poly-ε-Lysine. *ACS Appl. Mater. Interface* **2014**, *6*, 17126-17133.

20. Spicer, P. T., Progress in liquid crystalline dispersions: cubosomes. *Curr. Opin. Colloid Interface Sci.* **2005**, *10*, 274-279.

21. Kulkarni, C. V.; Wachter, W.; Iglesias-Salto, G.; Engelskirchen, S.; Ahualli, S., Monoolein: A Magic Lipid? *Phys. Chem. Chem. Phys.* **2011**, *13*, 3004-3021.

22. Briggs, J.; Chung, H.; Caffrey, M., The Temperature-Composition Phase Diagram and Mesophase Structure Characterization of the Monoolein/Water system. *J. De Phys. II* **1996**, *6*, 723-751.

23. Pan, X.; Han, K.; Peng, X.; Yang, Z.; Qin, L.; Zhu, C.; Huang, X.; Shi, X.; Dian, L.; Lu, M., Nanostructed Cubosomes as Advanced Drug Delivery System. *Curr. Pharm. Des.* **2013**, *19*, 6290-6297.

24. Guo, C.; Wang, J.; Cao, F.; Lee, R. J.; Zhai, G., Lyotropic Liquid Crystal Systems in Drug Delivery. *Drug Discov. Today* **2010**, *15*, 1032-1040.

25. Negrini, R.; Mezzenga, R., pH-Responsive Lyotropic Liquid Crystals for Controlled Drug Delivery. *Langmuir* **2011**, *27*, 5296-5303.

26. Negrini, R.; Mezzenga, R., Diffusion, Molecular Separation, and Drug Delivery from Lipid Mesophases with Tunable Water Channels. *Langmuir* **2012**, *28*, 16455-16462.

27. Driever, C. D.; Mulet, X.; Johnston, A. P. R.; Waddington, L. J.; Thissen, H.; Caruso, F.; Drummond, C. J., Converging Layer-by-Layer Polyelectrolyte Microcapsule and Cubic Lyotropic Liquid Crystalline Nanoparticle Approaches for Molecular Encapsulation. *Soft Matter* **2012**, *7*, 4257-4266.

28. Mulet, X.; Boyd, B. J.; Drummond, C. J., Recent Advances in Drug Delivery and Medical Imaging Using Colloidal Nanoparticulate Lyotropic Liquid Crystalline Dispersions. *J. Colloid Interface Sci.* **2012**, *393*, 1-20.

29. Garti, N.; Libster, D.; Aserin, A., Lipid Polymorphism in Lyotropic Liquid Crystals for Triggered Release of Bioactives. *Food Func.* **2012**, *3*, 700-713.

30. Sagalowicz, L.; Leser, M. E.; Watzke, H. J.; Michel, M., Monoglyceride Self-Assembly Structures as Delivery Vehicles. *Trends. Food Sci. Techon.* **2006**, *17*, 204-214.

31. Dong, Y. D.; Larson, I.; Barnes, T. J.; Prestidge, C. A.; Boyd, B. J., Adsorption of Nonlamellar Nanostructured Liquid-Crystalline Particles to Biorelevant Surfaces for Improved Delivery of Bioactive Compounds. *ACS Appl. Mater. Interface* **2011**, *3*, 1771-1780.

32. Nadiminti, P. P.; Dong, Y. D.; Sayer, C.; Hay, P.; Rookes, J. E.; Boyd, B. J.; Cahill, D. M., Nanostructured Liquid Crystalline Particles as an Alternative Delivery Vehicle for Plant Agrochemicals. *ACS Appl. Mater. Interface* **2013**, *5*, 1818-1826.

33. Nadiminti, P. P.; Rookes, J. E.; Dong, Y. D.; Sayer, C.; Boyd, B. J.; Cahill, D. M., Nanostructured Liquid Crystalline Particle Assisted Delivery of 2, 4-Dichlorophenoxyacetic Acid to Weeds, Crops and Model. *Plants. Crop Prot.* **2016**, *82*, 17-29.

34. Rizwan, S. B.; Boyd, B. J.; Rades, T.; Hook, S., Bicontinuous Cubic Liquid Crystals as Sustained Delivery Systems for Peptides and Proteins. *Expert Opin. Drug Deliv.* **2010**, *7*, 1133-1144.

35. Angelov, B.; Angelova, A.; Filippov, S. K.; Drechsler, M.; Štěpánek, P.; Lesieur, S., Multicompartment Lipid Cubic Nanoparticles with High Protein Upload: Millisecond Dynamics of Formation. *ACS Nano* **2014**, *8*, 5216-5226.

36. Yaghmur, A.; Glatter, O., Characterization and Potential Applications of Nanostructured Aqueous Dispersions. *Adv. Colloid Interface Sci.* **2009**, *147*, 333-342.

37. Garti, N.; Aserin, A., Micelles and Microemulsions as Food Ingredient and Nutraceutical Delivery Systems. Woodhead Publishing: Cambridge: UK, **2012**; pp 211-251.

38. Sagalowicz, L.; Leser, M. E., Delivery Systems for Liquid Food Products. *Curr. Opin. Colloid Interface Sci.* **2010**, *15*, 61-72.

39. De Gennes, P. G., Wetting: Statics and Dynamics. *Rev. Modern Phys.* **1985**, *57*, 827.

40. Roisman, I. V.; Rioboo, R.; Tropea, C., In Normal Impact of a Liquid Drop on a Dry surface: Model for Spreading and Receding. *Proc. Math. Phys. Eng. Sci.* **2002**, *458*, 1411-1430.

41. Bartolo, D.; Boudaoud, A.; Narcy, G.; Bonn, D., Dynamics of Non-Newtonian Droplets. *Phys. Rev. Lett.* **2007**, *99*, 174502.

42. Smith, M. I.; Bertola, V., Effect of Polymer Additives on the Wetting of Impacting Droplets. *Phys. Rev. Lett.* **2010**, *104*, 154502.

43. Vandoolaeghe, P.; Tiberg, F.; Nylander, T., Interfacial Behavior of Cubic Liquid Crystalline Nanoparticles at Hydrophilic and Hydrophobic Surfaces. *Langmuir* **2006**, *22*, 9169-9174.

44. Dong, Y. D.; Larson, I.; Barnes, T. J.; Prestidge, C. A.; Allen, S.; Chen, X.; Roberts, C. J.; Boyd, B. J., Understanding the Interfacial Properties of Nanostructured Liquid Crystalline Materials for Surface-Specific Delivery Applications. *Langmuir* **2012**, *28*, 13485-13495.

45. Bartolo, D.; Bouamrirene, F.; Verneuil, É.; Buguin, A.; Silberzan, P.; Moulinet, S., Bouncing or Sticky Droplets: Impalement Transitions on Superhydrophobic Micropatterned Surfaces. *Europhys. Lett.* **2006**, *74*, 299.

46. Lafuma, A.; Quéré, D., Superhydrophobic States. *Nat. Mater.* **2003**, *2*, 457-460.

47. Wagner, P.; Fürstner, R.; Barthlott, W.; Neinhuis, C., Quantitative Assessment to the Structural Basis of Water Repellency in Natural and Technical Surfaces. *J. Exp. Bot.* **2003**, *54*, 1295-1303.

48. Patankar, N. A., Mimicking the Lotus Effect: Influence of Double Roughness Structures and Slender Pillars. *Langmuir* **2004**, *20*, 8209-8213.

49. Balu, B.; Breedveld, V.; Hess, D. W., Fabrication of "Roll-off" and "Sticky" Superhydrophobic Cellulose Surfaces via Plasma Processing. *Langmuir* **2008**, *24*, 4785-4790.

50. Richard, D.; Quéré, D., Viscous Drops Rolling on a Tilted Non-Wettable Solid. *Europhys. Lett.* **1999**, *48*, 286.

51. Kumar, M.; Kumaraswamy, G., Phase Behaviour of the Ternary System: Monoolein–Water–Branched Polyethylenimine. *Soft Matter* **2015**, *11*, 5705-5711.

Chapter 7

Future Work

This thesis is focused on the structure and properties of liquid crystalline mesophases of glycerol monooleate. We studied the phase behaviour of ternary glycerol-monooleate–water–polymer systems and uncovered novel routes to highly curved inverse mesophases. We also demonstrated that aqueous dispersions of lipid nanoparticles, when sprayed on hydrophobic surfaces retard drop retraction. This result has important implications for a wide variety of applications, including the delivery of agrochemicals. My thesis opens up the possibilities of exploiting liquid crystalline mesophases and lipid nanoparticle formulations in a wide range of applications/fields. We have summarised the possible areas of interest below:

1) Liquid crystalline mesophases for vaccine stability and delivery:

Vaccine stability and their effective delivery is a problem of great importance. All vaccines need to be stored at low temperature (2-8 °C) to maintain their efficacy and stability. However, especially in developing countries, it is hard to maintain a cold chain due to inconsistent power supply and improper refrigeration during transportation. Maintaining the appropriate temperature range is critical for vaccine stability. Storage below freezing temperature can also damage the vaccine due to the formation of ice crystals. Therefore, formulations that preserve the vaccine activity in the absence of a quality cold chain would have important implications in resource poor settings.

In solution state, instability of protein vaccines can be attributed due to various chemical and physical processes such as protein unfolding (that result in aggregation due to change in the secondary and ternary protein structure), hydrolysis, formation of disulphide bonds, oxidation, etc. All these destabilising processes are accelerated at elevated temperature.[1,2]

We suggest the encapsulation of the vaccines inside liquid crystalline mesophase matrices for enhanced thermal stability. Valentile et al. have studied the effect of confinement of protein inside a silica matrix on its stability.[3] Protein confinement enhances thermal stability and preserves the native conformations on heating. Winter et al. have shown that incorporation of insulin into cubic mesophases of monoolein enhances stability against aggregation and at elevated temperatures.[4] It has been observed that the lipid mesophase

matrix greatly enhances the protein stability compared to bulk solutions by inhibiting protein aggregation at increased temperature.[5] Thus, we suggest that the use of cubic mesophases of GMO to encapsulate vaccine might enhance its thermal stability. Moreover, the glycerol head group of GMO can interact with functional groups present on the vaccine to preserve their conformation.

2) Lipid nanoparticle formulations for patterning the super-hydrophobic surfaces: Harvesting water from dew/humid environment:

The habitability of arid areas of the world is deteremined by access to water. Fetching water from the humid air is an alternative resource of water for regions which receive very low rain fall though moderate moisture content is present in the environment. We are interested to prepare micro-sized hydrophilic patterns on superhydrophobic surfaces for harvesting the water from dew/moisture present in the air.[7] This work is inspired by the Stenocara beetles in the Namib Desert that are known for their water harvesting from the fog-loaded wind. Such beetles are capable of surviving even in the driest regions of the earth. Careful observations of such beetles show a unique array of hydrophilic bumps on the wax coated superhydrophobic back of the beetle. Wang et al. have used inkjet printing[8] of microdroplets of dopamine solution to create hydrophilic bumps on a superhydrophobic surface.

Recently, we have shown that lipid nanoparticle dispersions (called cubosomes) can render superhydrophobic lotus leaf surfaces hydrophilic in nature. When a drop containing lipid nanoparticle is delivered on a superhydrophobic surface, the lipid particles diffuse and reorganise to create a thin ~2 nm wetting layer. We propose that lipid nanoparticle formulations can be used as inks for inkjet printing on superhydrophobic surfaces to readily create patterns for moisture harvesting. In preliminary studies, we have observed the formation of the hydrophilic patches using cubosomes on hydrophobic surface. These hydrophilic patches help the tiny water droplets to condense into bigger droplets that subsequently roll off the surface.

3) Cubosomes can assist killing of biofilm

Bacteria, at high concentrations, generate an extracellular polymeric matrix known as a biofilm. These bacterial communities are protected by the biofilm structure and are resistant to challenge by antimicrobial agents, resulting in chronic bacterial infections.[9] Biofilms also contaminate medical devices as well as pipes and oil wells in the chemical industry. Microbial infections resulted into 100,000 nosocomial deaths per annum in the US. In order to kill these biofilms, biocide must penetrate into the extracellular matrix (ECM). The ECM of biofilms provides protection for bacteria against environmental threats and also act as a diffusion barrier for certain antibiotics.[9]

In literature, Aizerberg et al. have reported the superhydrophobic nature of Bacillus subtilis biofilm colonies.[10] Their study also showed that the non-wetting property of biofilms persists even for organic solvents such as ethanol at concentrations of up to 80% (clinical concentration range). This non-wetting property of biofilms inhibits their penetration by aqueous antimicrobial formulations. We propose to use lipid nanoparticle formulations encapsulated with antibiotics for the killing of biofilms. In Chapter 6, we have shown that cubosome aqueous dispersions are able to wet superhydrophobic lotus leaf surface. Therefore, we suggest that the antibiotic-loaded cubosome dispersions might be effective formulations to wet biofilms and to enhance diffusion of antimicrobials into them.

4) Spray formulations for painting and printing

We also propose that the wetting ability of lipid cubic nanoparticles (cubosomes) can allow them to be used in inkjet printing and painting technology. We also anticipate the lipid nanoparticle can be used in perfume formulations. The cubosomes can stick on hydrophobic fabrics to slowly release encapsulated ingredients to enhance the durability of perfumes on the fabrics.

References:

1. Chen, D.; Kristensen, D., *Expert Rev. Vaccines* **2009**, *8*, 547-557.
2. Wang, W., Instability, stabilization, and formulation of liquid protein pharmaceuticals. *Int. J. Pharm.* **1999**, *185*, 129-188.
3. Eggers, D. K.; Valentine, J. S., Molecular confinement influences protein structure and enhances thermal protein stability. *Prot. Sci.* **2001**, *10*, 250-261.
4. Kraineva, J.; Smirnovas, V.; Winter, R., Effects of lipid confinement on insulin stability and amyloid formation. *Langmuir* **2007**, *23*, 7118-7126.
5. Mishraki, T.; Libster, D.; Aserin, A.; Garti, N., Temperature-dependent behavior of lysozyme within the reverse hexagonal mesophases (H_{II}). *Colloids Surf. B Biointerfaces* **2010**, *75*, 391-397.
6. Amar-Yuli, I.; Azulay, D.; Mishraki, T.; Aserin, A.; Garti, N., The role of glycerol and phosphatidylcholine in solubilizing and enhancing insulin stability in reverse hexagonal mesophases. *J. Colloid Interface Sci.***2011**, *364*, 379-387.
7. White, B.; Sarkar, A.; Kietzig, A. M., *Appl. Surface Sci.* **2013**, *284*, 826-836.
8. Bai, H.; Wang, L.; Ju, J.; Sun, R.; Zheng, Y.; Jiang, L., Efficient water collection on integrative bioinspired surfaces with star–shaped wettability patterns. *Adv.Mater.***2014**, *26*, 5025-5030.
9. Costerton, J. W.; Stewart, P. S.; Greenberg, E. P., Bacterial biofilms: a common cause of persistent infections. *Science* **1999**, *284*, 1318-1322.
10. Epstein, A. K.; Pokroy, B.; Seminara, A.; Aizenberg, J., Bacterial biofilm shows persistent resistance to liquid wetting and gas penetration. *Proc. Natl. Acad. Sci.* **2011**, 108, 995-1000.

List of Research Credential, Awards and Conferences

Publications and Patents:

1. **M. Kumar**, N. G. Patil, C. K. Choudhury, S. Roy, A. V. Ambade, and G. Kumaraswamy, "Compact polar moieties induce lipid–water systems to form discontinuous reverse micellar phase", ***Soft Matter,*** vol. 11, pp 5417, 2015 (**Inner Cover Page**)

2. **M. Kumar**, and G. Kumaraswamy, "Phase behaviour of the ternary system: monoolein–water–branched polyethylenimine", ***Soft Matter***, vol. 11, pp. 5705-5711, 2015.
3. **M. Kumar**, P. Makkar, A. Sharma, P. Sastri, and G. Kumaraswamy, "Effect of Mesophase Domain Structure on Drug Release from Glycerol Monooleate Mesophases" (Manuscript Prepared)

4. **M. Kumar**, M. A. Kulkarni, C. G. Narendiran, A. Banpurkar, and G. Kumaraswamy, "Aqueous dispersions of lipid nanoparticles wet superhydrophobic Lotus leaf surface" (Manuscript Submitted)

5. **M. Kumar**, and G. Kumaraswamy, "Inclusion of 5^{th} generation PAMAM Dendron in Lipid/Water System Induces Formation of unusual $P4_332$ Mesophase" (Manuscript Prepared)

6. G. Kumaraswamy, **M. Kumar**, and A. V. Ambade,"A discontinuous reverse micellar composition in cubic Fd3m phase for sustained release of therapeutic drugs", **Patent** WO2016092569 A1, 2015.

7. G. Kumaraswamy, **M. Kumar**, and M. A. Kulkarni, "Surfactant combination applied through aqueous dispersion that allows effective staining of hydrophobic surfaces", **Patent** IN 201611023934, 2016.

Awards:

1. NCL RF-Keerthi Sangoram Memorial Endowment Award (2016) for "**best Research Scholar in Chemical Engineering**".

2. Fellowship (two months) for visiting McGill University in Montreal, Quebec, as part of collaborative research programme supported under the "**Indo-Canadian collaborative programme in Nano Science and Technology".**

3. **Awarded Junior Research Fellowship(JRF)** by University Grant Commission (UGC).

Conferences:

1. Attended "National Fluorescence Workshop: FCS Satellite hands-on workshop on total internal reflection fluorescence microscopy (TIRFM), and FCS-2013 conference" organised by IISc Bangalore, India during November 2013.

2. Attended "SERB school on Rheology of Complex fluids: Advanced computational Methods & Symposium on Rheology of Complex Fluids-2013", organised by IIT Delhi, December 2013.

3. Poster presentation in National Florescence Conference, FCS-2013.

4. Poster presentation in Complex Fluids CompFlue-2016, held at Pune, India.